



University of
Massachusetts
Amherst


QUANTITATIVE IMAGING OF TENSILE FORCES AT CELL-CELL JUNCTION WITH DNA-BASED PROBES

Item Type	Dissertation (Open Access)
Authors	Keshri, Puspam
DOI	10.7275/26592780
Rights	Attribution-NonCommercial 4.0 International
Download date	2026-03-13 01:44:41
Item License	http://creativecommons.org/licenses/by-nc/4.0/
Link to Item	https://hdl.handle.net/20.500.14394/18754

QUANTITATIVE IMAGING OF TENSILE FORCES AT CELL-CELL JUNCTION WITH DNA-BASED PROBES

Puspam Keshri

Follow this and additional works at: https://scholarworks.umass.edu/dissertations_2

 Part of the [Analytical Chemistry Commons](#), [Biochemistry Commons](#), [Biophysics Commons](#), and the [Molecular Biology Commons](#)

**QUANTITATIVE IMAGING OF TENSILE FORCES AT CELL-CELL
JUNCTION WITH DNA-BASED PROBES**

A Dissertation Presented

by

PUSPAM KESHRI

Submitted to the Graduate School of the
University of Massachusetts Amherst in partial fulfillment
of the requirements for the degree of

DOCTOR OF PHILOSOPHY

February 2022

Chemistry

© Copyright by Puspam Keshri 2022

All Rights Reserved

**QUANTITATIVE IMAGING OF TENSILE FORCES AT CELL-CELL
JUNCTION WITH DNA-BASED PROBES**

A Dissertation Presented

by

PUSPAM KESHRI

Approved as to style and content by:

Mingxu You, Chair

Min Chen

Michael Knapp

Barbara A. Osborne

Ricardo Metz, Department Head
Department of Chemistry

DEDICATION

To my parents, sister, and beloved wife

To my teachers and professors,

To my friends,

and

To my research advisor, Mingxu

ACKNOWLEDGMENTS

I would like to thank everyone for playing an important role in my Ph.D. and making my efforts a success. I would thank all the people who supported me and inspired me throughout the journey.

With a deep sense of gratitude, I express my profound and sincere thanks to my research supervisor Prof. Mingxu You, for his expert guidance, continuous encouragement, constant support, and motivation throughout the course of my investigation. He made me think independently and efficiently in order to tackle multidisciplinary projects. I also found a great mentor in him since he would guide me through the challenging times. His engaging mentality provided me the correct platform to express my thoughts. I am very grateful that I found not only a great supervisor but a mentor in him.

I would sincerely thank to my thesis committee members, Prof. Min Chen, Prof. Michael Knapp and Prof. Barbara A. Osborne. Their valuable insight and guidance during my Ph.D. were very helpful and shaped me as a scientist.

I would like to thank Dr. James Chamber for his support in microscope facility and always providing his input for the imaging. I am grateful for all the collaborations with Prof. Yubing Sun, Prof. Barbara A. Osborne, Prof. Thomas J. Maresca, Prof. Cheng Zhu, and Prof. Michael B. Elowitz.

I also thank all my lab mates who were always helpful and created a joyous environment for working. Thank you, Dr. Bin Zhao, Dr. Kewei Ren, Dr. Qikun Yu, Dr. Yousef Bagheri, Aruni Karunanayake, Rigumula Wu, Jennings Sun, Fatemeh (Ida) Shafiei, Qian Tian, Ru Zheng, Ahsan Ali, Zhaolin Xue, and Lan Mi. I am very thankful to Dr. Bin Zhao, Dr.

Yousef Bagheri and Qian Tian for all the meaningful scientific conversations during my Ph.D. I also want to thank all the members of 7th & 8th floor of LGRT for sharing instruments and helping me in my studies.

I would also like to thank Prof. Dhandapani Venkataraman, for being a wonderful graduate program director, who thinks from the perspective of a student. To all the staffs in Chemistry department, especially Robert Sabola for assisting with the instruments.

Last but not the least, I would like to thank all my family members, and friends for constantly supporting me in this journey. My parents, Ganesh Keshri & Poonam Keshri always believed me, and their fighting spirit in their personal life always ignited me and gave me the motivation to go beyond. I also want to thank my teachers, especially Pijush Kanti Majumdar, my chemistry teacher, who trusted my ability to achieve my dreams and mentored me. I would also like to thank my beloved wife, Shaily for staying there during the tough times, and playing the ideal role of friend, philosopher, and guide. They equally deserve my degree. I also like to thank all my friends, Anjan, Asish, Soham, Xianzhi, who supported me during this journey.

ABSTRACT

QUANTITATIVE IMAGING OF TENSILE FORCES AT CELL-CELL JUNCTION WITH DNA-BASED PROBES

FEBRUARY 2022

PUSPAM KESHRI

B.Sc., JADAVPUR UNIVERSITY

M.S., INDIAN INSTITUTE OF SCIENCE

Ph.D., UNIVERSITY OF MASSACHUSETTS AMHERST

Directed by: Professor Mingxu You

Mechanical forces are an integral part in biology, they regulate several cellular properties, such as morphology, proliferation, migration. These forces are also involved in receptor signaling and the differentiation of different cell types. Different proteins and biomolecules such as cadherin, integrin, notch proteins are essential elements of these processes. Measuring these intercellular forces are challenging considering the minimal intensity (piconewton-level) of these molecular forces. In our lab, we have developed a membrane DNA tension probe (MDTP) that uses a DNA hairpin module to sense tensile forces and has a lipid anchor to modify onto live-cell membranes. The programmability of DNA and the dynamic insertion capability of lipids provides us a simple tool to visualize the forces. We believe these probes will be a widely useful tool for investigating the mechanical forces. In this thesis, we have used MDTP as a tool to visualize and measure the mechanical forces involved in different receptor-ligand interaction at the cell-cell junctions.

In the first part of the thesis, we have designed a fluorescence lifetime-based membrane DNA tension probe named as FLIM-MDTP, which uses fluorescence lifetime as a read-out. We used this probe to quantitatively image the E-cadherin-mediated tensile forces at the cell-cell junction. Furthermore, we demonstrated the multiplexed imaging capability of the probe to monitor the mechanical dynamics of the epithelial-to-mesenchymal transition. In the second part, we have used the DNA-based probe to visualize the tensile force involved in Notch activation. Our initial results showed low unfolding efficiency of the probe indicating a weak mechanical force involved in the activation of Notch. To potentially image these low levels of forces, we have further designed a MDTP that uses a lower force threshold hairpin (2.2 pN vs. 4.4 pN) as a force module. Finally, we used these DNA-based probes to measure CD40-induced pulling forces at B cell-T cell junction. Our results indicated that the extent of forces involved in this interaction is also quite small and transient in nature. In short summary, our data indicated that DNA-based probes can be used to measure tensile forces within a diverse type of mechanotransduction at cell-cell junction. Our results also demonstrated that the extent of pulling forces differ largely depending on the type of ligand-receptor pairs.

TABLE OF CONTENT

ACKNOWLEDGMENT.....	v
ABSTRACT.....	vii
LIST OF TABLES	xii
LIST OF FIGURES.....	xiii
CHAPTER	
1. INTRODUCTION.....	15
1.1 Biological importance of mechanical forces.....	15
1.2 Current methods for detecting the intercellular tensile forces	16
1.3 Using DNA as a versatile tool for designing force probe.....	18
1.4 Lipid-mediated anchoring on the cell membranes.....	19
1.5 Visualize tensile forces at cell-cell junctions with membrane DNA tension probe (MDTP).....	20
1.6 Quantify intercellular tensile forces with DNAMeter	22
1.7 Objective of the study.....	23
1.8 References	25
2. QUANTITATIVE AND MULTIPLEXED FLUORESCENCE LIFETIME IMAGING (FLIM) OF INTERCELLULAR TENSILE FORCES AT CELL-CELL JUNCTIONS	30
2.1 Introduction	30
2.2 Results and Discussion.....	32
2.2.1 Design and characterization of the FLIM-MDTP.....	32
2.2.2 Quantification of intercellular tensions with the FLIM-MDTP.....	37
2.2.3 Multiplexed imaging of molecular tensions with FLIM-MDTP.....	41
2.2.4 Mechanical features of epithelial-mesenchymal transition.....	49
2.3 Conclusion.....	53
2.4 Materials and Methods.....	54
2.4.1 Reagents.....	54
2.4.2 <i>In vitro</i> fluorescence characterization.....	55

2.4.3 Cell culture, imaging, and data analysis.....	55
2.4.4 Synthesis of protein G-modified DNA strands.....	56
2.4.5 Preparation of the FLIM-MDTP.....	57
2.4.6 Imaging of intercellular tensile forces.....	57
2.4.7 Preparation of the supported lipid bilayer (SLB).....	58
2.4.8 Calibration of the FLIM-MDTP on SLB.....	58
2.4.9 Immunostaining experiment.....	59
2.5 References	61
3. VISUALIZING FORCE-INDUCED NOTCH SIGNALING WITH THE HELP OF DNA-BASED MEMBRANE TENSION RATIOMETRIC PROBE (DNAMETER)	65
3.1 Introduction	65
3.2 Results and Discussion.....	68
3.2.1 Design and characterization the probe.....	68
3.2.2 Quantifying the molecular tension at the cell-cell junction.....	69
3.2.3 Designing a lower force threshold probe for studying Notch activation.....	73
3.2.4 Quantifying Notch molecular tension with low-force-threshold design.....	74
3.2.5 Studying receptor-induced Notch activation.....	75
3.3 Conclusion	77
3.4 Materials and Methods.....	78
3.4.1 Reagents.....	78
3.4.2 Cell culture, imaging, and data analysis.....	79
3.4.3 Synthesis of Protein G-modified DNA strands.....	79
3.4.4 Preparation of the N1-FLIM-MDTP (N1-DNAMeter).....	80
3.4.5 Imaging of intercellular tensile forces.....	80
3.5 References.....	81
4. MEASURING CD40 INDUCED PULLING FORCES IN B CELL WITH DNA- BASED MEMBRANE TENSION RATIOMETRIC PROBE (DNAMETER)	85
4.1 Introduction	85
4.2 Results and Discussion.....	86
4.2.1 Selective labeling of Jurkat cells.....	86

4.2.2 Design and characterization the probe.....	88
4.2.3 Imaging and quantifying molecular tensions at the cell-cell junctions	89
4.3 Conclusion	93
4.4 Materials and Methods.....	93
4.4.1 Reagents.....	93
4.4.2 Cell culture, imaging, and data analysis.....	94
4.4.3 Synthesis of Protein G-modified DNA strands.....	94
4.4.4 Preparation of the CD40L-DNAMeter.....	95
4.4.5 Imaging intercellular tensile forces.....	95
4.5 References.....	96
5. SUMMARY AND FUTURE DIRECTIONS.....	100
5.1 Summary and future directions of DNA-based tension probes.....	100
5.2 References	102
BIBLIOGRAPHY.....	105

LIST OF TABLES

Table 2.1. DNA sequences used for this chapter 2.....	60
Table 2.2. Standard curve equations used for calculating the percentage of unfolded probes based on the fluorescence lifetime.....	61
Table 3.1. Hairpin design and force calculation.....	74
Table 3.2. DNA sequences used for this chapter 3.....	81
Table 4.1. DNA sequences used for this chapter 4.....	96

LIST OF FIGURES

Figure 1.1. Design of membrane DNA tension probes.....	22
Figure 2.1. Design and mechanism of the FLIM-MDTP in measuring tensile forces at cell–cell junctions.....	32
Figure 2.2. <i>In vitro</i> characterization of the FLIM-MDTP quenching efficiency.	33
Figure 2.3. <i>In situ</i> unfolding of FLIM-MDTP on cell membranes by complementary DNA strands	34
Figure 2.4. The effect of membrane probe concentrations on the fluorescence lifetime and emission signals of FLIM-MDTP	35
Figure 2.5. Orthogonality of the FLIM-MDTP (FAM) and FLIM-MDTP (Cy3) for fluorescence lifetime imaging.....	36
Figure 2.6. Calibration and validation of the FLIM-MDTP	38
Figure 2.7. Native polyacrylamide gel (10%) characterization of the EC-FLIM-MDTP assembly.....	39
Figure 2.8. Imaging E-cadherin-mediated tensile forces at the MDCK cell–cell junctions	40
Figure 2.9. Imaging E-cadherin-mediated tensile forces simultaneously with the EC-FLIM-MDTP (FAM) and EC-FLIM-MDTP (Cy3).....	42
Figure 2.10. Imaging different force ranges of E-cadherin-mediated tension at the MDCK cell–cell junctions.....	43
Figure 2.11. Immunostaining of EMT biomarkers including N-cadherin, E-cadherin, and ZO-1 after adding different inducers on MCF7 cells.....	45
Figure 2.12. Multiplexed imaging of E-cadherin- and N-cadherin-mediated tension after adding different types of EMT inducers.....	46
Figure 2.13. Multiplexed imaging of E-cadherin- and N-cadherin-mediated tension after the EMT induction.....	47
Figure 2.14. Validation of the unfolding of FLIM-MDTP during the EMT process is due to E-cadherin and N-cadherin-induced tension.....	48
Figure 2.15. Effect of the EGTA and ML-7 treatment on the lifetime signal of cadherin-free FLIM-MDTP.....	49

Figure 2.16. Correlation of the percentage of unfolded NC-FLIM-MDTP (FAM) and EC-FLIM-MDTP (Cy3) at the same cell–cell junctions.....	51
Figure 2.17. Imaging E-cadherin- and N-cadherin-mediated tension after different time treatment with 30 ng/mL of TGF- β 1.....	52
Figure 2.18. Immunostaining of EMT biomarkers including N-cadherin, E-cadherin, and ZO-1 after different time treatment with 30 ng/mL of TGF- β 1.....	53
Figure 3.1. Mechanism of Notch signaling according to the “lift and cut” model indicating the presence of tensile forces required for Notch activation.....	66
Figure 3.2. Mammalian Notch receptor and ligand families.....	67
Figure 3.3. Design and anchoring of the probe on the cell membrane.....	68
Figure 3.4. Native polyacrylamide gel (10%) characterization of the N1-FLIM-MDTP assembly.....	69
Figure 3.5. Imaging Notch1-mediated tensile forces at the cell-cell junctions with N1-FLIM-MDTP (Cy3).....	71
Figure 3.6. Imaging Notch1-mediated tensile forces at the cell–cell junctions with N1-DNAMeter (Cy3).....	72
Figure 3.7. Imaging Notch1-mediated tensile forces at the cell-cell junctions with N1-FLIM-MDTP (0 % GC, Cy3).....	75
Figure 3.8. Studying Notch signaling with citrine reporter.....	77
Figure 4.1. Key intercellular molecular interactions between follicular lymphoma B cells and follicular helper T cells.....	86
Figure 4.2. Labeling of Jurkat cells with cell tracker solution	88
Figure 4.3. Native polyacrylamide gel (10%) characterization of the CD40L-DNAMeter (FAM) assembly.....	89
Figure 4.4. Imaging CD40-mediated tensile forces at the cell-cell junctions with a CD40L-DNAMeter (FAM) and locking strand	91
Figure 4.5. Imaging CD40-mediated tensile forces at the cell-cell junctions with CD40L-DNAMeter (Cy3).....	92

CHAPTER 1

BACKGROUND AND INTRODUCTION

This chapter is partially adapted with permission from Keshri, P.; Zhao, B.; Xie, T.; Bagheri, Y.; Chambers, J.; Sun, Y.; and You, M. Quantitative and Multiplexed Fluorescence Lifetime Imaging of Intercellular Tensile Forces. *Angew. Chem. Int. Ed.*, 2021, 60, 15548-15555 © Copyright Wiley-VCH on behalf of the German Chemical Society 2021.

1.1 Biological importance of mechanical forces

Communication is a key process, and it is one of the most important factors for human survival. Similarly, in cellular biology, intercellular interactions and signaling play an important role in dictating the fate and function of cells. In these organisms and tissues, the membranes of adjacent cells can form various functional junctions, such as tight junctions, gap junctions, and adherens junctions¹. Various chemical and biological stimuli are known to be capable of controlling these intercellular communications². Mechanical force is one of the key regulators at these junctions, controlling cell morphology, proliferation, and various signaling pathways³. Different kinds of cell adhesion molecules, including integrins, cadherins, selectins, and immunoglobulin superfamilies, are actively involved in these mechano-based junction interactions⁴.

Mechanical force-dependent communication processes in cells can be classified into two major categories, cell-cell communication & cell-ECM communication. Cells communicate with ECM with the help of different ligands such as integrin, which controls the cellular responses to the stiffness of the matrix and consequently the migratory

properties⁵. On the other hand, intercellular forces are dictated by various cell surface receptors such as cadherin, notch, etc., which are key regulators of epithelial-to-mesenchymal transition (EMT), epithelial viscoelasticity, and cell signaling, etc⁶⁻⁸ (ref).

1.2 Current methods for detecting intercellular tensile forces

Measuring the intensity and spatiotemporal distribution of intercellular forces is critical for our understanding of these cellular signaling processes. It can also provide us some potential tools to modulate the cellular downstream electrical and biochemical events. Piconewton (pN)-range tensile forces are the typical mechanical forces involved in these processes⁹. As an example, each cadherin–catenin complex is subjected to a tension of ~5 pN under resting conditions rising to ~50 pN in stressed conditions⁹. On the other hand, integrin-ECM based forces vary widely from 1 pN to 40 pN depending on the state of the complex¹⁰. Different methods have been used to measure the forces between cells and ECM, such as traction force microscopy¹¹, collagen gel¹², tissue pillar¹³, and microneedle¹⁴.

Traction force microscopy (TFM) requires an elastic polymeric substance loaded with fluorescent particles that deforms itself in the presence of forces¹¹. The deformation induced by cells is then mapped quantitatively using this strategy. In case of collagen gel, cells are initially incorporated into the hydrated collagen lattices, and upon contraction, the water molecules are squeezed out¹². For tissue pillars, a microelectromechanical system (MEMS) is used to generate arrays of microtissues¹³. These microtissues consist of cells that are encapsulated within 3D matrices, and the remodeling of these tissues provide information of the forces involved. In case of microneedles, the force is measured using microfabricated arrays of elastomeric, microneedle-like posts¹⁴. After the cells are attached

to the surface, they spread across and deflect the microneedle-like posts and provide us the distribution of traction forces. However, these techniques suffer from a few limitations such as inability to detect forces for specific receptor-ligand pair and the lack of compatibility to study intercellular forces. There is still a great need of specialized biomechanical tools to detect these tiny forces at cell-cell junctions.

Currently, intercellular forces can be studied mainly in three ways. The first method is based on monolayer stress microscopy, which uses the cell-ECM traction force data to deduce the intercellular forces at cell-cell junctions¹⁵. However, extensive image analysis and data processing is required, and it is only suitable for studying a monolayer of cells. The second method utilizes microfabricated cantilever beams to deduce tugging forces between a pair of cells on bowtie-shaped micropatterns¹⁶. This approach is also based on the measurement of cell-ECM traction forces, while it can only be applied to a pair of cells in an artificial pattern. The method also relies on the availability of advanced microfabrication facilities. Both methods cannot be used to measure forces at the molecular level. Some of these challenges were alleviated by using Fluidic probe force microscopy (FluidFM)¹⁷. The technique is based on measuring the force required to retract a nanofluidic cantilever that binds to the cells. Attachment of the cantilever to the cells can be achieved via target-ligand interactions¹⁸ or by generating a small pressure difference¹⁹. However, the method lacks the biological compatibility since the physical contact impacts the cell membrane and works only with monolayer of cells.

In another strategy, a pair of fluorescent proteins is genetically encoded within certain target cell adhesion molecules²⁰⁻²². A mechanosensitive distance change between the fluorescent protein pair induces an observable Förster resonance energy transfer

(FRET) signal. Molecular level mechanotransduction can be studied using this method. However, the sensitivity and brightness of these fluorescent protein probes are limited, and they can only detect a small range of forces (normally <12 pN)²³. More importantly, the insertion of large fluorescent protein conjugates (~500 amino acids) may disrupt the natural functions of junction proteins. An advanced and simple approach is still highly demanded to measure intercellular forces.

1.3 DNA as a versatile tool for designing force probes

DNA has emerged as a versatile material beyond its natural function in the storage of information. The biocompatibility, precise nanoscale geometry, and molecular recognition property of DNA makes it a promising choice to study the biological microenvironment²⁴. Indeed, DNA-based tools have been recently developed for measuring mechanical forces between cells and ECM^{5, 25-27} (ref). Several designs of DNA-based force sensors have been achieved, including for example DNA hairpin probes²⁵, tension gauge tethers²⁸, and nano yoyo system²⁹.

DNA-based molecular tension force microscopy (MTFM) method uses three ssDNA for assembling the probe,²⁵ an anchor strand containing a quencher and functional group that allows the DNA for anchoring onto the surface, a ligand strand that contains the ligand and a fluorophore molecule, and finally a hairpin strand that acts as a force module. This simple design can be easily modulated based on the “threshold force” (force at which the hairpin strand is 50% opened - $F_{1/2}$), the choice of fluorophore and quencher, and the ligand for studying different mechanically active events. In the resting state, the proximity of the fluorophore-quencher pair quenched the fluorescence of the probe. In contrast, in the

presence of mechanical forces higher than $F_{1/2}$, the DNA hairpin unfolds and results in separation of the fluorophore from the quencher and thus increases the fluorescence signal.

The tension gauge tether (TGT) probe was designed for studying the interactions of cell surface receptors and surface bound ligands²⁸. The TGT probes are designed based on a DNA duplex consisting of a tethered ligand in one DNA and a surface-binding biotin unit on the other strand. The DNA duplex is ruptured in the presence of tensile force higher than its “tension tolerance” (T_{tol}). The T_{tol} of the DNA duplex is controlled by attaching the biotin at different positions of the DNA, resulting in different modes of mechanical interaction, including the unzipping mode, intermediate mode, and shear mode. In nano yoyo, an *E. coli* ssDNA-binding protein is used to bind with a long poly-T DNA²⁹. In the event of mechanical interaction, this specific binding process is ruptured, resulting in peeling of the DNA from the protein. However, these existing DNA-based sensors only function at the cell-ECM interface and cannot be used directly to study intercellular forces.

1.4 Lipid-mediated anchoring on the cell membranes

We and others found that the spontaneous cell membrane anchoring of DNA probes can be achieved based on the hydrophobic interactions between a lipid moiety and the cell membrane³⁰⁻³². The cell plasma membrane is composed of a phospholipid bilayer and a plethora of proteins, carbohydrates, and cholesterol³³. The plasma membrane bilayer is hydrophobic and negatively charged. As a result, it is difficult for negatively charged or hydrophilic molecules, such as DNA, to insert into cell membranes. Thus, the cell membrane applications of functional DNA devices have been largely limited for a long time.

As a natural membrane component, lipids have recently gained popularity as an anchoring agent for the DNA modification on live cell membranes³³⁻³⁴. The insertion of these lipid moieties normally will not interfere with the natural structure and function of the plasma membrane. Lipid-mediated membrane modification of DNA is a simple approach with fast insertion kinetics and stable anchoring capability. Meanwhile, the universal presence of lipids in the membrane of different cell lines also makes it a general strategy for the cell membrane modification. To facilitate the potential usage of lipid-DNA conjugates in studying cell membrane-related phenomena, including intercellular tensile forces, we have recently systematically investigated how different chemical and physical properties of lipid-DNA conjugates will affect their cell membrane insertion and anchoring capability³¹. Several lipid structures with different numbers of unsaturated double bonds, lipid arms, and fatty acid lengths were used. Each lipid was chemically attached to a 20-nucleotide-long single-stranded DNA, which was pre-labelled with a 6-FAM fluorophore to monitor their cellular location. The membrane insertion on Madin-Darby Canine Kidney (MDCK) cells indicated that it took only 2–9 min to reach half-maximum membrane signal of each lipid-DNA probe, 90% maximum signal was obtained in 7–31 min. Interestingly, less hydrophobic cholesterol- and 18:0-based lipid-DNA probes achieved the fastest MDCK cell membrane insertion. Similar high membrane modification efficiency was also observed in other cell lines, such as HeLa, HEK293T, and Jurkat.

1.5 Visualize tensile forces at cell-cell junctions with membrane DNA tension probe (MDTP)

We have recently developed a type of membrane DNA tension probe (MDTP) to image tensile forces at cell-cell junctions (Figure 1.1a)³⁵. The MDTP can spontaneously

insert onto cell membranes through a lipid moiety and is capable of sensing small pN-range forces. It contains a DNA hairpin that unfolds upon molecular tension between neighboring cells, which can further induce the separation of a fluorophore/quencher pair. The force tolerance of the MDTP can be modulated based on the stem length and sequence of the DNA hairpin. The simplicity and modularity of these probes makes them compatible and adaptable for different intercellular mechanotransduction studies.

The membrane DNA tension probe we developed comprises of three DNA oligonucleotides that are self-assembled through DNA hybridization (Figure 1.1a). First, a lipid-modified hairpin strand acts as the force-sensing module. Then, a dye-modified ligand strand is conjugated with a ligand molecule to specifically bind with the target membrane receptor. Finally, a quencher-modified anchor strand facilitates the membrane insertion of the probe while quenches its fluorescence in the absence of mechanical forces. The assembled probe presents a pair of lipid moieties at one end, allowing the probe to be anchored onto live cell membranes. Upon experiencing a tension that is exceeding the threshold unfolding force of the hairpin, it consequently opens the hairpin strand and results in the separation of the fluorophore from the quencher, accompanied by the fluorescence activation. Therefore, we can use the MDTP to image and track forces generated at the cell-cell junctions.

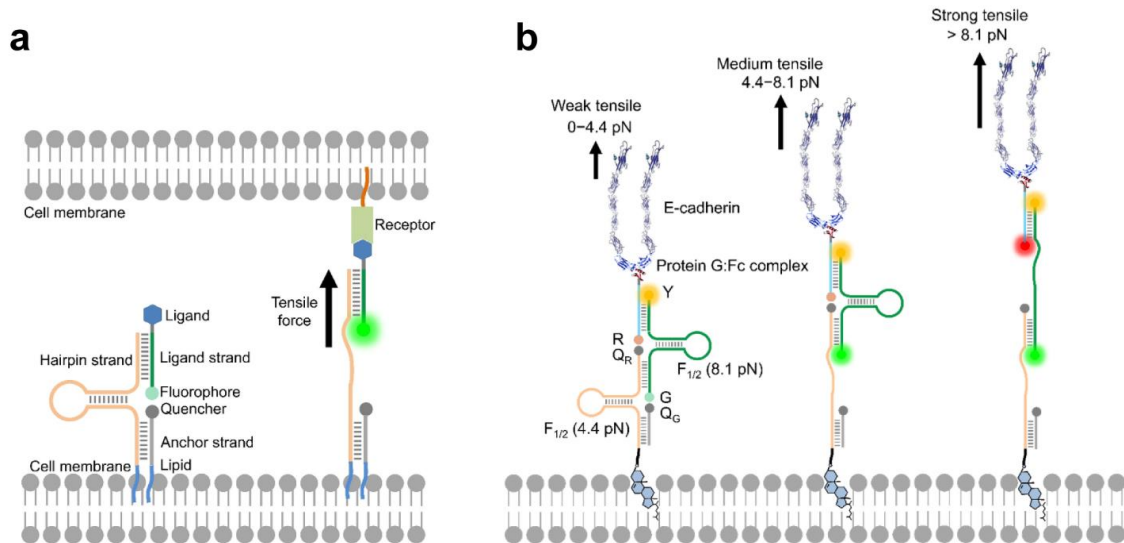


Figure 1.1. Design of membrane DNA tension probes. a) MDTP consists of a hairpin strand (orange), a ligand strand (green) and an anchor strand (grey). The tensile force exerted by the receptor-ligand interaction unfolds the hairpin and results in the separation of fluorophore from quencher. b) DNAMeter is comprised of a 22% GC (orange) and a 66% GC (green) DNA hairpin strand, a ligand strand (light blue) and a helper strand (grey). It is modified with E-cadherin through a Protein G linker. Fluorophore-quencher pairs, FAM (G)-Dabcyl (QG) and Cy5 (R)-QSY21 (QR), are used to report the unfolding of 22% GC and 66% GC hairpin upon experiencing forces. A TAMRA (Y) dye acts as the internal reference for the ratiometric imaging and quantification. Reprinted with permission from ref³⁶.

1.6 Quantify intercellular tensile forces with DNAMeter

MDTP-based visualization of intercellular forces enables us to detect the existence of tensile forces during different biological processes. However, the heterogeneous membrane distributions of the MDTP make it challenging for the real quantitative assessment of the forces. To solve this problem, we have recently engineered the “second-generation” MDTP, termed DNA-based membrane tension ratiometric probe, or in short, the “DNAMeter”³⁶. In our DNAMeter design, a reference fluorophore was added to normalize the variations in the probe distribution on cell membranes. In addition, multiple hairpins were installed in a single DNAMeter to measure a large range of intercellular forces (Figure 1.1b). The precise DNA self-assembly and the modulating capability of DNA hairpins provided a desirable platform for such a design. A typical DNA hairpin can

be made sensitive to forces in the range of about 2–20 pN by simply changing the number of base pairs and GC percentage in the stem region²⁵.

The DNAMeter is composed of four oligonucleotide strands to measure weak (0–4.4 pN), moderate (4.4–8.1 pN), and strong tensile forces (>8.1 pN) based on a 22% GC (threshold unfolding force of 4.4 pN) and a 66% GC hairpin (threshold force of 8.1 pN) (Figure 1.1b) (ref). A FAM (green or G) and Cy5 (red or R) dye was used to report the unfolding of these two hairpins, respectively. A TAMRA (yellow or Y) dye functioned as an internal reference, with constant fluorescence irrespective of the tensile forces. In case of a weak tensile force (0–4.4 pN), the fluorescence of both FAM and Cy5 were quenched by their corresponding quenchers. If the tensile force was stronger than 8.1 pN, both fluorophores were separated from the quencher, resulting in the activated fluorescence. With medium level of tensile forces (4.4–8.1 pN), the 22% GC hairpin was opened but not the 66% GC hairpin, thus only green fluorescence from FAM will be activated. This two-hairpin probe design can be applied for the measurement of different ranges of tensile forces.

1.7 Objective of the study

In this thesis, we aim to highlight some recent breakthrough in the development and applications of these emerging force-sensing probes. Our goal is to use DNA-based probes and design a “plug-and-play” strategy that allows us to study different mechanotransduction processes. In this regard, I will be using MDTP as a tool to visualize the tensile forces at the cell-cell junction in a quantitative manner.

In the second chapter, our goal is to visualize cadherin-mediated interactions at the cell-cell junction in a quantitative and multiplexed imaging pattern. To achieve this goal,

we have developed a fluorescence lifetime-based MDTP (FLIM-MDTP) that uses fluorescence lifetime as a read out instead of typical intensity-based measurements. We used this new probe design to visualize cadherin-mediated mechanical forces at the cell-cell junction. Furthermore, we applied FLIM-MDTP in studying epithelial-to-mesenchymal transition (EMT), which demonstrates the multiplexed imaging application of the FLIM-MDTP. Finally, we also studied the patterns in mechanical interaction of cadherins at different stages of EMT.

In the third chapter, our goal is to develop a DNA-based probe that can help us to visualize mechanical interactions in Notch signaling. In this regard, we designed Notch1-modified probe and the initial results indicated that only weak forces involved in the activation of Notch1 signaling. We have further designed a new low force threshold probe by shortening the stem region of the DNA hairpin. In addition, we have also designed a DLL1 ligand-modified probe that can be used to study receptor-induced mechanical activation of Notch signaling.

In the fourth chapter, our goal is to measure CD40-induced pulling forces involved in B cell-T cell interactions with the help of DNA-based probes. Here, we designed a DNAMeter-based probe for studying the interaction between the B cells (WSU or LY-3) and the Jurkat cells. We first achieved the selective labeling of Jurkat cells in the cell mixture using a cell tracker solution. Our results further indicated that compared to the WSU cells, LY-3 cells exhibited a lower force level. While in both types of cells, only a small portion of DNA probes was activated, indicating the weak mechanical nature of their interactions with Jurkat cells.

1.8 References

1. Alimperti, S.; Andreadis, S. T., CDH2 and CDH11 act as regulators of stem cell fate decisions. *Stem Cell Res* **2015**, *14* (3), 270-82.
2. Artemenko, Y.; Axiotakis, L., Jr.; Borleis, J.; Iglesias, P. A.; Devreotes, P. N., Chemical and mechanical stimuli act on common signal transduction and cytoskeletal networks. *Proc Natl Acad Sci U S A* **2016**, *113* (47), E7500-E7509.
3. Polacheck, W. J.; Chen, C. S., Measuring cell-generated forces: a guide to the available tools. *Nat Methods* **2016**, *13* (5), 415-23.
4. Chen, C. S.; Tan, J.; Tien, J., Mechanotransduction at cell-matrix and cell-cell contacts. *Annu Rev Biomed Eng* **2004**, *6*, 275-302.
5. Liu, Y.; Galior, K.; Ma, V. P.; Salaita, K., Molecular Tension Probes for Imaging Forces at the Cell Surface. *Acc Chem Res* **2017**, *50* (12), 2915-2924.
6. Muhamed, I.; Wu, J.; Sehgal, P.; Kong, X.; Tajik, A.; Wang, N.; Leckband, D. E., E-cadherin-mediated force transduction signals regulate global cell mechanics. *J Cell Sci* **2016**, *129* (9), 1843-54.
7. Kalluri, R.; Weinberg, R. A., The basics of epithelial-mesenchymal transition. *J Clin Invest* **2009**, *119* (6), 1420-8.
8. Iyer, K. V.; Piscitello-Gomez, R.; Paijmans, J.; Julicher, F.; Eaton, S., Epithelial Viscoelasticity Is Regulated by Mechanosensitive E-cadherin Turnover. *Curr Biol* **2019**, *29* (4), 578-591 e5.
9. Charras, G.; Yap, A. S., Tensile Forces and Mechanotransduction at Cell-Cell Junctions. *Curr Biol* **2018**, *28* (8), R445-R457.

10. Sun, Z.; Guo, S. S.; Fassler, R., Integrin-mediated mechanotransduction. *J Cell Biol* **2016**, *215* (4), 445-456.
11. Legant, W. R.; Choi, C. K.; Miller, J. S.; Shao, L.; Gao, L.; Betzig, E.; Chen, C. S., Multidimensional traction force microscopy reveals out-of-plane rotational moments about focal adhesions. *Proc Natl Acad Sci U S A* **2013**, *110* (3), 881-6.
12. Bell, E.; Ivarsson, B.; Merrill, C., Production of a tissue-like structure by contraction of collagen lattices by human fibroblasts of different proliferative potential in vitro. *Proc Natl Acad Sci U S A* **1979**, *76* (3), 1274-8.
13. Legant, W. R.; Pathak, A.; Yang, M. T.; Deshpande, V. S.; McMeeking, R. M.; Chen, C. S., Microfabricated tissue gauges to measure and manipulate forces from 3D microtissues. *Proc Natl Acad Sci U S A* **2009**, *106* (25), 10097-102.
14. Tan, J. L.; Tien, J.; Pirone, D. M.; Gray, D. S.; Bhadriraju, K.; Chen, C. S., Cells lying on a bed of microneedles: an approach to isolate mechanical force. *Proc Natl Acad Sci U S A* **2003**, *100* (4), 1484-9.
15. Tambe, D. T.; Hardin, C. C.; Angelini, T. E.; Rajendran, K.; Park, C. Y.; Serrapicamal, X.; Zhou, E. H.; Zaman, M. H.; Butler, J. P.; Weitz, D. A.; Fredberg, J. J.; Trepats, X., Collective cell guidance by cooperative intercellular forces. *Nat Mater* **2011**, *10* (6), 469-75.
16. Liu, Z.; Tan, J. L.; Cohen, D. M.; Yang, M. T.; Sniadecki, N. J.; Ruiz, S. A.; Nelson, C. M.; Chen, C. S., Mechanical tugging force regulates the size of cell-cell junctions. *Proc Natl Acad Sci U S A* **2010**, *107* (22), 9944-9.

17. Meister, A.; Gabi, M.; Behr, P.; Studer, P.; Voros, J.; Niedermann, P.; Bitterli, J.; Polesel-Maris, J.; Liley, M.; Heinzelmann, H.; Zambelli, T., FluidFM: combining atomic force microscopy and nanofluidics in a universal liquid delivery system for single cell applications and beyond. *Nano Lett* **2009**, *9* (6), 2501-7.
18. Sancho, A.; Vandersmissen, I.; Craps, S.; Lutun, A.; Groll, J., A new strategy to measure intercellular adhesion forces in mature cell-cell contacts. *Sci Rep* **2017**, *7*, 46152.
19. Cohen, N.; Sarkar, S.; Hondroulis, E.; Sabhachandani, P.; Konry, T., Quantification of intercellular adhesion forces measured by fluid force microscopy. *Talanta* **2017**, *174*, 409-413.
20. Borghi, N.; Sorokina, M.; Shcherbakova, O. G.; Weis, W. I.; Pruitt, B. L.; Nelson, W. J.; Dunn, A. R., E-cadherin is under constitutive actomyosin-generated tension that is increased at cell-cell contacts upon externally applied stretch. *Proc Natl Acad Sci U S A* **2012**, *109* (31), 12568-73.
21. Conway, D. E.; Breckenridge, M. T.; Hinde, E.; Gratton, E.; Chen, C. S.; Schwartz, M. A., Fluid shear stress on endothelial cells modulates mechanical tension across VE-cadherin and PECAM-1. *Curr Biol* **2013**, *23* (11), 1024-30.
22. Wang, P.; Liang, J.; Shi, L. Z.; Wang, Y.; Zhang, P.; Ouyang, M.; Preece, D.; Peng, Q.; Shao, L.; Fan, J.; Sun, J.; Li, S. S.; Berns, M. W.; Zhao, H.; Wang, Y., Visualizing Spatiotemporal Dynamics of Intercellular Mechanotransmission upon Wounding. *ACS Photonics* **2018**, *5* (9), 3565-3574.

23. Jurchenko, C.; Salaita, K. S., Lighting Up the Force: Investigating Mechanisms of Mechanotransduction Using Fluorescent Tension Probes. *Mol Cell Biol* **2015**, *35* (15), 2570-82.
24. Yang, D.; Hartman, M. R.; Derrien, T. L.; Hamada, S.; An, D.; Yancey, K. G.; Cheng, R.; Ma, M.; Luo, D., DNA materials: bridging nanotechnology and biotechnology. *Acc Chem Res* **2014**, *47* (6), 1902-11.
25. Zhang, Y.; Ge, C.; Zhu, C.; Salaita, K., DNA-based digital tension probes reveal integrin forces during early cell adhesion. *Nat Commun* **2014**, *5*, 5167.
26. Ma, R.; Kellner, A. V.; Ma, V. P.; Su, H.; Deal, B. R.; Brockman, J. M.; Salaita, K., DNA probes that store mechanical information reveal transient piconewton forces applied by T cells. *Proc Natl Acad Sci U S A* **2019**, *116* (34), 16949-16954.
27. Glazier, R.; Brockman, J. M.; Bartle, E.; Mattheyses, A. L.; Destaing, O.; Salaita, K., DNA mechanotechnology reveals that integrin receptors apply pN forces in podosomes on fluid substrates. *Nat Commun* **2019**, *10* (1), 4507.
28. Wang, X.; Ha, T., Defining single molecular forces required to activate integrin and notch signaling. *Science* **2013**, *340* (6135), 991-4.
29. Chowdhury, F.; Li, I. T.; Ngo, T. T.; Leslie, B. J.; Kim, B. C.; Sokoloski, J. E.; Weiland, E.; Wang, X.; Chemla, Y. R.; Lohman, T. M.; Ha, T., Defining Single Molecular Forces Required for Notch Activation Using Nano Yoyo. *Nano Lett* **2016**, *16* (6), 3892-7.
30. Ohvo-Rekila, H.; Ramstedt, B.; Leppimaki, P.; Slotte, J. P., Cholesterol interactions with phospholipids in membranes. *Prog Lipid Res* **2002**, *41* (1), 66-97.

31. Bagheri, Y.; Chedid, S.; Shafiei, F.; Zhao, B.; You, M., A quantitative assessment of the dynamic modification of lipid-DNA probes on live cell membranes. *Chem Sci* **2019**, *10* (48), 11030-11040.
32. Tian, Q.; Bagheri, Y.; Keshri, P.; Wu, R.; Ren, K.; Yu, Q.; Zhao, B.; You, M., Efficient and selective DNA modification on bacterial membranes. *Chem Sci* **2020**, *12* (7), 2629-2634.
33. You, M.; Lyu, Y.; Han, D.; Qiu, L.; Liu, Q.; Chen, T.; Sam Wu, C.; Peng, L.; Zhang, L.; Bao, G.; Tan, W., DNA probes for monitoring dynamic and transient molecular encounters on live cell membranes. *Nat Nanotechnol* **2017**, *12* (5), 453-459.
34. Zhao, B.; Tian, Q.; Bagheri, Y.; You, M., Lipid-Oligonucleotide Conjugates for Simple and Efficient Cell Membrane Engineering and Bioanalysis. *Curr Opin Biomed Eng* **2020**, *13*, 76-83.
35. Zhao, B.; O'Brien, C.; Mudiyansele, A.; Li, N.; Bagheri, Y.; Wu, R.; Sun, Y.; You, M., Visualizing Intercellular Tensile Forces by DNA-Based Membrane Molecular Probes. *J Am Chem Soc* **2017**, *139* (50), 18182-18185.
36. Zhao, B.; Li, N.; Xie, T.; Bagheri, Y.; Liang, C.; Keshri, P.; Sun, Y.; You, M., Quantifying tensile forces at cell-cell junctions with a DNA-based fluorescent probe. *Chem Sci* **2020**, *11* (32), 8558-8566.

CHAPTER 2

QUANTITATIVE AND MULTIPLEXED FLUORESCENCE LIFETIME IMAGING (FLIM) OF INTERCELLULAR TENSILE FORCES AT CELL-CELL JUNCTIONS

This chapter is partially adapted with permission from Keshri, P.; Zhao, B.; Xie, T.; Bagheri, Y.; Chambers, J.; Sun, Y.; and You, M. Quantitative and Multiplexed Fluorescence Lifetime Imaging of Intercellular Tensile Forces. *Angew. Chem. Int. Ed*, 2021, 60, 15548-15555© Copyright Wiley-VCH on behalf of the German Chemical Society 2021.

2.1 Introduction

Cell adhesion molecules (CAMs) are specific cell surface proteins, which are associated in the binding of cells and extracellular matrix or other cells. Cadherins are a subset of CAM which are involved in the formation of adherens junctions¹. Classical cadherins contain a transmembrane domain, five EC (extracellular cadherin) repeats and an intracellular domain². The extracellular domain contributes to the adhesion of cells while the intracellular domain plays key role in signaling. Two cadherins on the neighboring cells bind in a homophilic manner during the formation of epithelial tissues. Mechanical forces are well known to be involved in the homophilic interactions between the cadherins³⁻⁴. E-cadherin is an important cell adhesion molecule located at the adherens junctions of epithelial cells⁵. Cadherins are also involved in different biological processes, such as cell-cell adhesion, signaling, epithelial to mesenchymal transition (EMT), etc⁶.

Thus, it is important to study the molecular forces involved in cadherin-based interactions to understand these biological processes.

In this study, we report a fluorescence lifetime imaging microscopy (FLIM)-based probe design, named as FLIM-MDTP, which will dramatically improve the capability of MDTP for the multiplexed imaging and quantitative measurement of intercellular forces. Fluorescence lifetime, i.e., the time a fluorophore remains in an excited state, is a concentration-independent intrinsic property of the fluorophore. FLIM has been previously used together with DNA-based probes for imaging in living cells⁷⁻⁹. Fluorescence lifetime is highly sensitive to the existence of a nearby quencher. Based on this phenomenon, we have designed FLIM-MDTP to quantify molecular tensions at cell–cell junctions (Figure 2.1). Using cadherin-mediated adhesions as an example, we demonstrate here the first molecular tension probe that can simultaneously measure multiple intercellular mechanotransduction events.

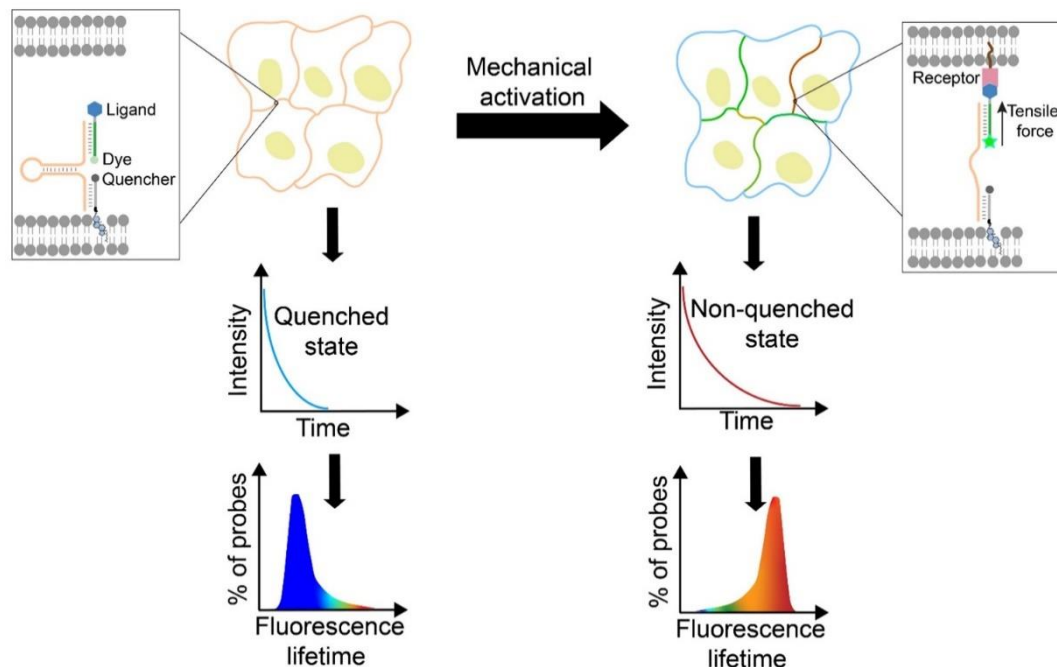


Figure 2.1. Design and mechanism of the FLIM-MDTP in measuring tensile forces at cell–cell junctions. The FLIM-MDTP can anchor onto cell membranes through a lipid moiety. Intercellular ligand-receptor binding induces the unfolding of a DNA hairpin and results in the separation of a fluorophore-quencher pair, which further leads to an increase in the number of probes in the unquenched state, exhibiting a higher fluorescence lifetime.

2.2 Results and Discussion

2.2.1 Design and characterization of the FLIM-MDTP

We first wanted to identify the fluorophore/quencher pairs that can be incorporated with MDTP and used in the fluorescence lifetime measurement. A 6-carboxyfluorescein (FAM)/EclipseTM pair and a Cy3/Black Hole Quencher 2 (BHQ-2) pair were chosen based on their reported large fluorescence lifetime changes upon quenching¹⁰. After incorporating these two fluorophore/quencher pairs into the MDTP, a moderate quenching efficiency (63%) was observed for the FAM/Eclipse pair, while BHQ-2 can efficiently quench (92%) the fluorescence signal of Cy3 (Figure 2.2).

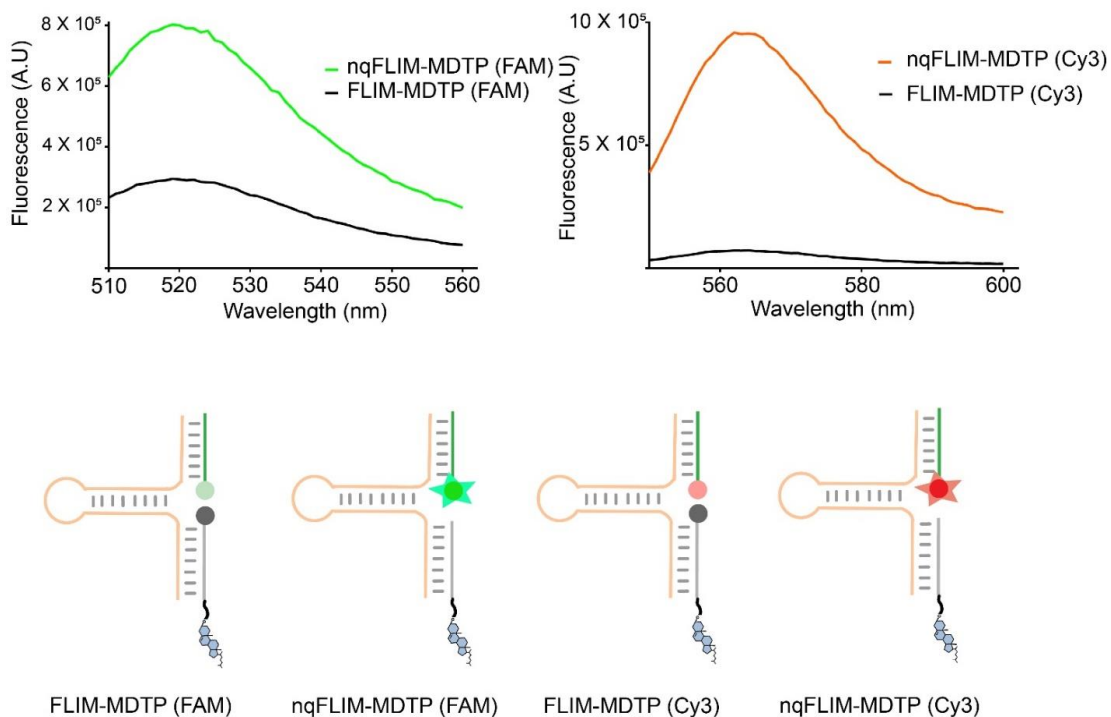


Figure 2.2. *In vitro* characterization of the FLIM-MDTP quenching efficiency. 200 nM of each probe was used including FAM/Eclipse- or Cy3/BHQ2-labeled FLIM-MDTP, and FAM- or Cy3-labeled quencher-free nqFLIM-MDTP. The emission spectra of the a) FAM and b) Cy3 signals were collected after excitation at 488 nm and 540 nm, respectively. The quenching efficiency of FAM- and Cy3-modified probe was found to be 63% and 92%, respectively. The scheme of each FLIM-MDTP is shown.

To further test if these two fluorophore/quencher pairs will exhibit large lifetime changes upon unfolding of the MDTP, we added these probes to the membranes of MCF7 epithelial cells after a brief 20 min incubation. A complementary DNA strand was then added to *in situ* unfold DNA hairpins on the cell membranes. Indeed, a dramatic increase in fluorescence lifetime of both FAM (from 1.2 ± 0.1 ns to 3.2 ± 0.1 ns) and Cy3 (from 1.1 ± 0.1 ns to 1.6 ± 0.1 ns) channels was observed within 30 min (Figure 2.3). These two fluorophore/quencher pairs can thus both be used to measure the activation of the MDTP. We named these FAM/Eclipse- and Cy3/BHQ-2-modified probes as FLIM-MDTP (FAM) and FLIM-MDTP (Cy3), respectively.

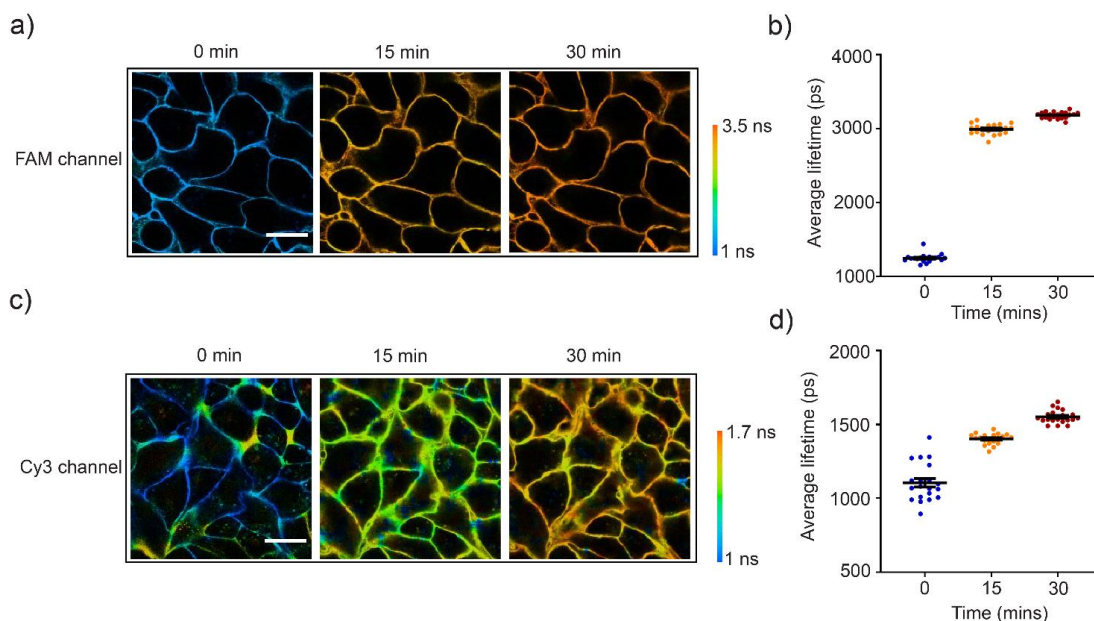


Figure 2.3. *In situ* unfolding of FLIM-MDTP on cell membranes by complementary DNA strands. After incubating 200 nM a) FAM/Eclipse- or c) Cy3/BHQ2-labeled FLIM-MDTP with MCF7 cells for 20 min, 1 μ M complementary strand was added to unfold the DNA hairpin part of FLIM-MDTP. Representative images were shown at different time after adding the complementary strand. Scale bar, 20 μ m. We would like to also point out that, in order to minimize the influence of cell density on the quantification, it would be better to only analyze junctions where clear intercellular contacts can be seen. For example, in panel c), at 0 min, a relatively large variation in lifetime signal was likely due to some loose connective cell regions. Distributions of the cellular lifetime changes were also quantified for the unfolding process of b) FAM/Eclipse- and d) Cy3/BHQ2-labeled FLIM-MDTP. Shown are mean and standard error of the mean (SEM) values from 20 cell–cell junctions in each case.

Next, we asked if the fluorescence lifetime values of the FLIM-MDTP (FAM) and FLIM-MDTP (Cy3) are independent on the membrane probe concentrations. We first added three different initial concentrations (0.2 μ M, 0.5 μ M, and 1.0 μ M) of each probe onto the MCF7 cell membranes. As expected, constant lifetime signals were exhibited in both FAM (<9% variation) and Cy3 (<4% variation) channels at cell–cell junctions (Figure 2.4). To further study if the activated FAM and Cy3 signals are still insensitive to the membrane probe densities, we prepared a quencher-free version of the probe, termed as nqFLIM-MDTP, without adding Eclipse and BHQ-2 (Figure 2.2). Again, on the MCF7 cell membranes, minimal variations (<6%) in the lifetime signals were observed after adding 0.2–1.0 μ M unquenched probes (Figure 2.4). As a control, under the same

experimental condition, clear differences in the membrane probe densities can be visualized based on the largely altered fluorescence emission signals, i.e., over 230% variation in the FAM fluorescence and >300% variation in the Cy3 signal (Figure 2.4-c, d). All these results indicated that the lifetime signals of the FLIM-MDTP (FAM) and FLIM-MDTP (Cy3) are indeed concentration-independent in this range, which will be critical for the potential quantification of intercellular forces.

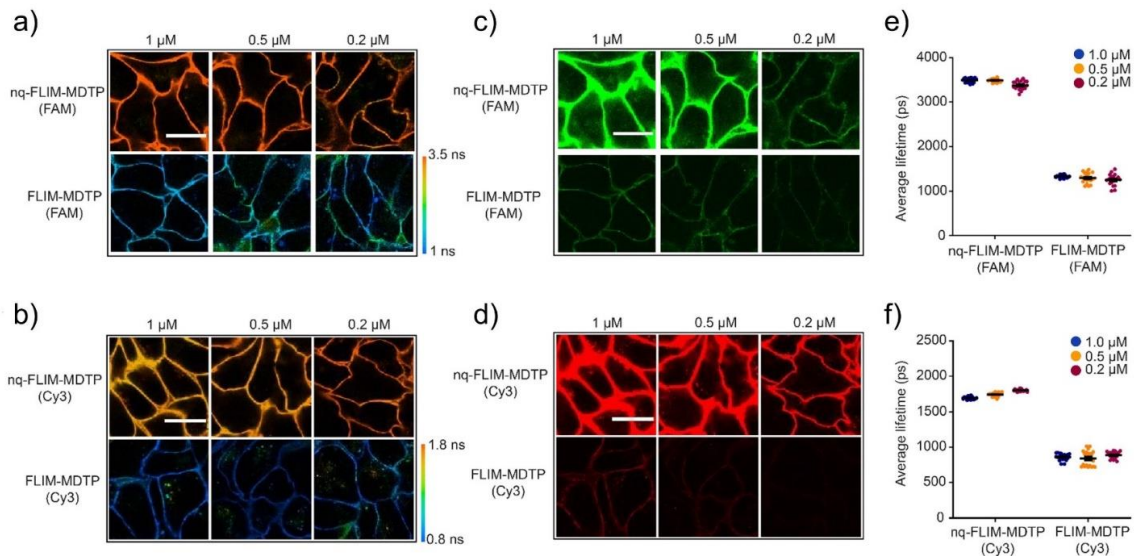


Figure 2.4. The effect of membrane probe concentrations on the fluorescence lifetime and emission signals of FLIM-MDTP. Three different concentrations of FLIM-MDTP (FAM), nqFLIM-MDTP (FAM), FLIM-MDTP (Cy3), and nqFLIM-MDTP (Cy3) were added to the MCF7 cells and imaged after a 30 min incubation. Shown are the representative (a, b) fluorescence lifetime images and (c, d) fluorescence intensity images of the same cell membrane region. Scale bar, 20 μm . Higher probe concentration resulted in obviously higher fluorescence emission intensity, while minimal variation in the lifetime signal was shown. Distributions of cell membrane fluorescence lifetime under each probe concentration were also quantified in the e) FAM and f) Cy3 channels. Shown are mean and standard error of the mean (SEM) values from 20 cell-cell junctions in each case.

We also wondered whether the FLIM-MDTP (FAM) and FLIM-MDTP (Cy3) can function simultaneously on cell membranes for potential multiplexed imaging. For this purpose, we mixed 50% activated FLIM-MDTP (FAM) with either FLIM-MDTP (Cy3) or nqFLIM-MDTP (Cy3) on the MCF7 cell membranes. Indeed, minimal influence (<3%) was observed in the FAM channel (Figure 2.5). Meanwhile, the presence of FLIM-MDTP

(FAM) will also not affect the lifetime values of FLIM-MDTP (Cy3) or nqFLIM-MDTP (Cy3) (<9% variation) (Figure 2.5). The FLIM-MDTP (FAM) and FLIM-MDTP (Cy3) can be orthogonally detected and potentially used for the multiplex imaging of different membrane mechanotransduction events.

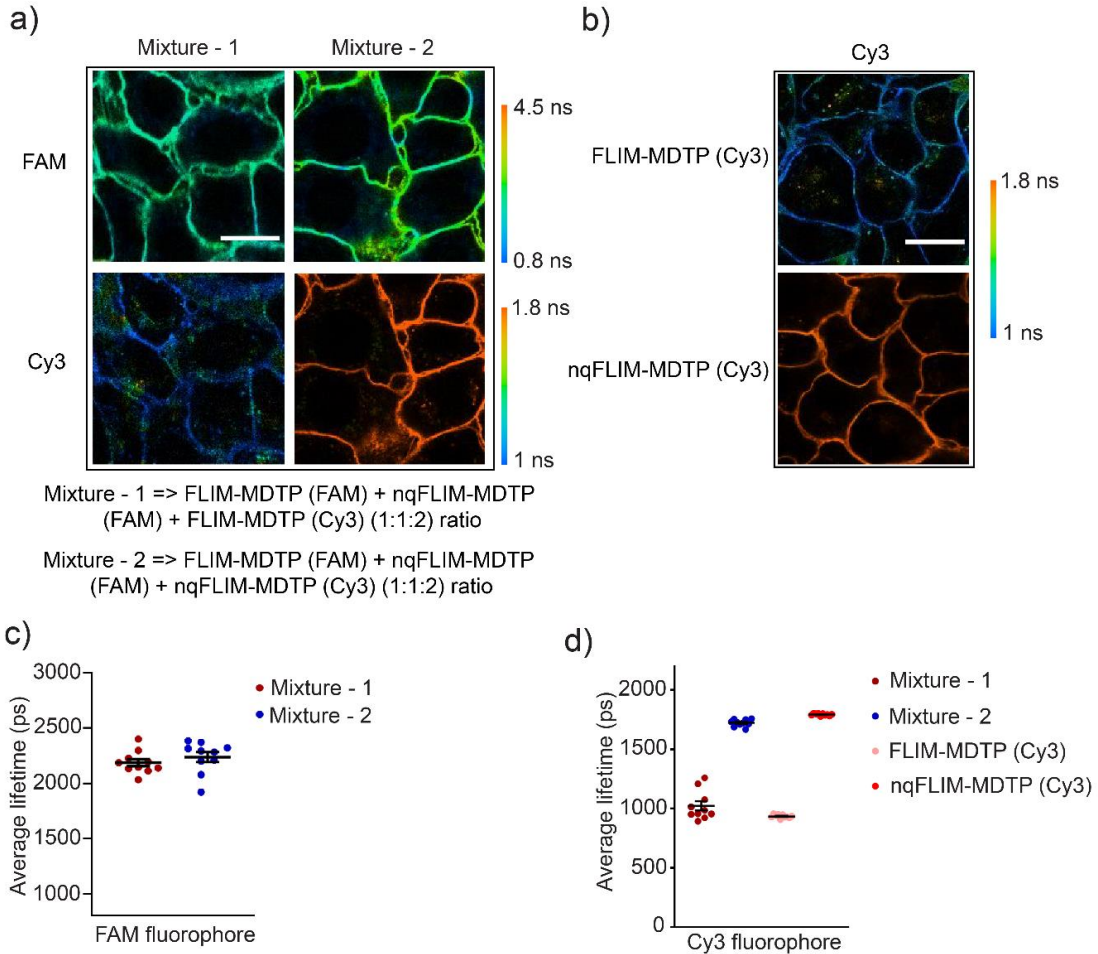


Figure 2.5. Orthogonality of the FLIM-MDTP (FAM) and FLIM-MDTP (Cy3) for fluorescence lifetime imaging. a) Representative images of MCF7 cells after 30 min incubation with mixture-1 consisting of 100 nM FLIM-MDTP (FAM) and nqFLIM-MDTP (FAM) mixture, together with 200 nM FLIM-MDTP (Cy3) or mixture-2 consisting of 100 nM FLIM-MDTP (FAM) and nqFLIM-MDTP (FAM) mixture, together with 200 nM nqFLIM-MDTP (Cy3). b) As a control, without adding FAM-labeled FLIM-MDTP, 200 nM FLIM-MDTP (Cy3) or nqFLIM-MDTP (Cy3) was incubated with the same batch of MCF7 cells for 30 min before imaging. Scale bar, 20 μ m. (c, d) Distributions of cell membrane fluorescence lifetime was also quantified in the c) FAM and d) Cy3 channels. Shown are mean and standard error of the mean (SEM) values from 10 cell-cell junctions in each case. Fluorescence lifetime signals from the FAM and Cy3 channels will not influence each other in the mixture.

2.2.2 Quantification of intercellular tensions with the FLIM-MDTP

Our next goal was to apply the FLIM-MDTP to quantify molecular tensions at cell–cell junctions. We first tried to determine the correlation between the apparent lifetime of each probe and the percentage of unfolded DNA hairpins. In this regard, we prepared a 1,2- dioleoyl-sn-glycero-3-phosphocholine (DOPC) supported lipid bilayer and anchored with different ratios of FLIM-MDTP (0% unfolded) and nq-FLIM-MDTP (100% unfolded) to obtain membranes with standard 0%, 25%, 50%, 75%, and 100% unfolded DNA hairpins (Figure 2.6-a). As expected, the membrane fluorescence lifetime values in both FAM and Cy3 channels gradually increased as the percentage of nqFLIM-MDTP increased (Figure 2.6-b, c). These values were further fit to two first-order exponential growth curves for the FLIM-MDTP (FAM) and FLIM-MDTP (Cy3), respectively, which will be later used for the calibration and quantitative measurement of intercellular forces (Table 2.2).

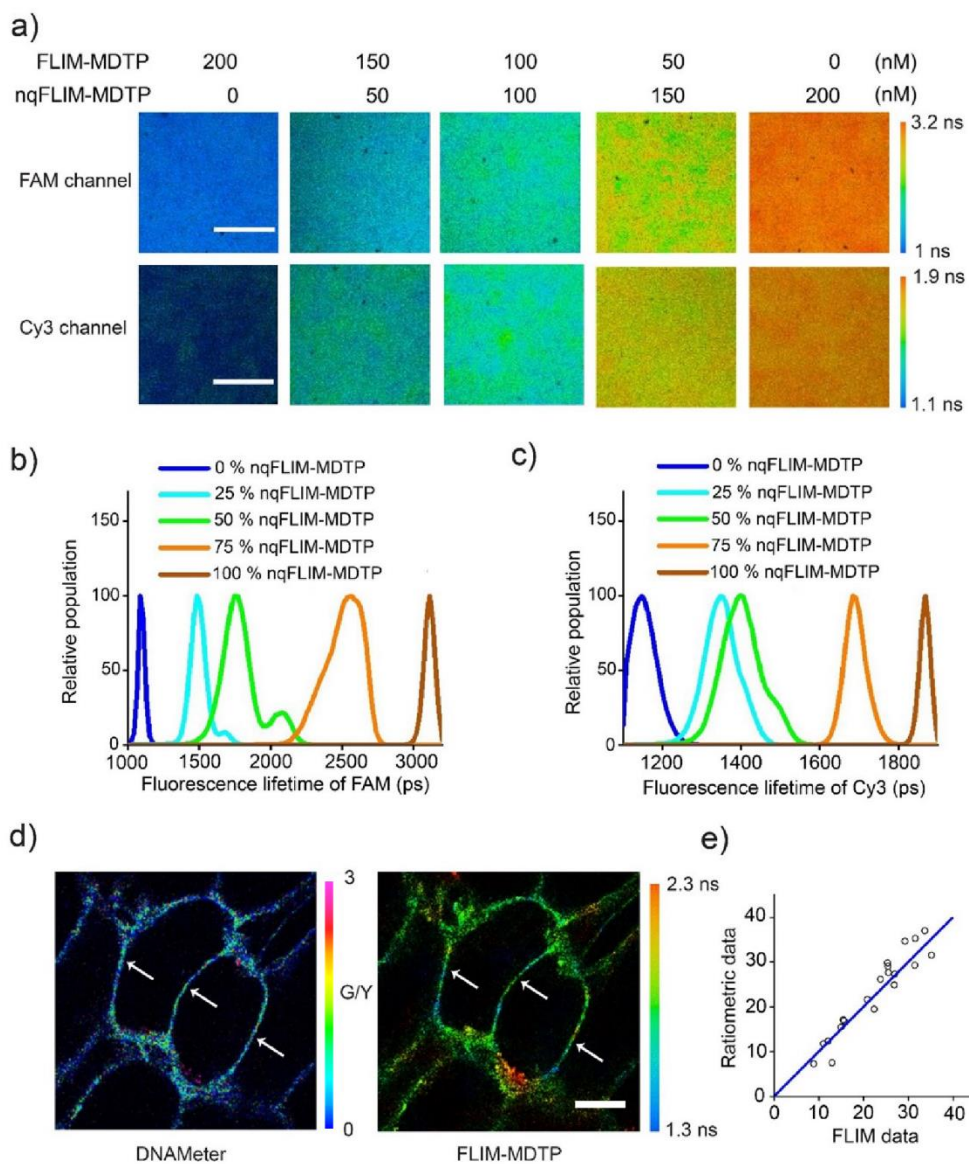


Figure 2.6. Calibration and validation of the FLIM-MDTP. a) Five different ratios of the nqFLIM-MDTP and FLIM-MDTP were mixed at 200/0 nM, 150/50 nM, 100/100 nM, 50/150 nM, and 0/200 nM concentrations including equal amount of FAM- and Cy3-labeled probes. Shown are the representative fluorescence lifetime images in the FAM (top) and Cy3 (bottom) channels after adding each mixture onto a supported lipid bilayer (SLB) membrane. Scale bar, 20 μ m. (b, c) SLB membrane distributions of fluorescence lifetime values were quantified in the b) FAM and c) Cy3 channels for each mixture. d) Representative fluorescence ratiometric (left, FAM/Cy5 signal) and lifetime (right) images of MDCK cells after 30 min incubation with 200 nM of EC-DNAMeter (FAM/Cy5) and EC-FLIM-MDTP (FAM). Scale bar, 10 μ m. e) Correlation of the percentage of unfolded EC-MDTP at the same cell–cell junctions as calculated from the ratiometric or lifetime images. 20 cell–cell junctions were analyzed. Arrows indicated the junctions used for analysis.

We next prepared an E-cadherin-modified FLIM-MDTP (FAM), named as EC-FLIM-MDTP (FAM), to quantify E-cadherin-mediated tensile forces at MDCK cell–cell adhesions. A DNA hairpin with the threshold force value of 4.4 pN was used to construct the probe. We chose this low threshold value probe because cadherin-mediated tension has been estimated to be in a similar range¹¹⁻¹². After confirming the probe assembly and E-cadherin modification in a gel electrophoresis assay (Figure 2.7), we tried to study calcium ion (Ca^{2+})-induced changes in E-cadherin tensions. Ca^{2+} can regulate the homodimerization of cadherins, which is critical for the adhesion formation in epithelia¹³.

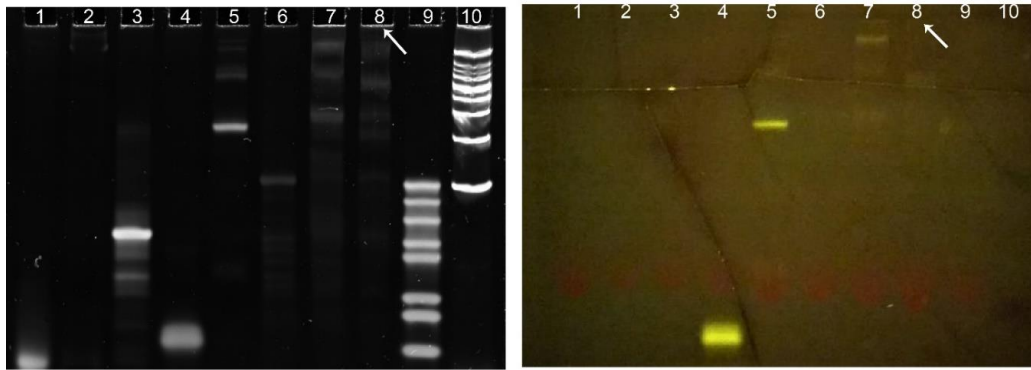


Figure 2.7. Native polyacrylamide gel (10%) characterization of the EC-FLIM-MDTP assembly. The gel was imaged before (right) and after (left) staining with SYBR Gold. Before staining, a blue light was used to visualize FAM-labeled strands. DNA composition in each lane: 1–anchor strand (1 μL , 10 μM), 2–Eclipse quencher-labeled anchor strand (1 μL , 10 μM), 3–hairpin strand (1 μL , 10 μM), 4–FAM-labelled ligand strand (1 μL , 10 μM), 5–Pro G- and FAM-labelled ligand strand (3.33 μL , 3 μM), 6–hairpin strand + Eclipse quencher-labeled anchor strand duplex (1 μL , 10 μM), 7–hairpin strand + Eclipse quencher-labeled anchor strand + Pro G- and FAM-labelled ligand strand (10 μL , 1 μM), 8–EC-FLIM-MDTP (hairpin strand + Eclipse quencher-labeled anchor strand + Pro G- and FAM-labelled ligand strand + Fc-E-cadherin) (10 μL , 1 μM), 9–DNA ladder (20–100 bp, 1 μL , 10 μM), 10–DNA ladder (100–1500 bp, with the 100 bp band of 50 μg). The arrow indicating the probe formation.

As shown in Figure 2.8, after adding 2 mM Ca^{2+} for 15 min, an obvious fluorescence lifetime increase from 1.4 ns to 1.8 ns was observed in the FAM channel. Based on the calibration curve (Table 2.2), this lifetime increase corresponds to 25% more unfolded FLIM-MDTP at cell–cell junctions (Figure 2.8). As a control, without conjugating E-cadherin, a Protein G-modified FLIM-MDTP did not exhibit any Ca^{2+} -

induced changes in the fluorescence lifetime (Figure 2.8). The vast majority of probes (>94%) remained folded even in the presence of Ca^{2+} . The EC-FLIM-MDTP can indeed be used to measure intercellular E-cadherin tensions.

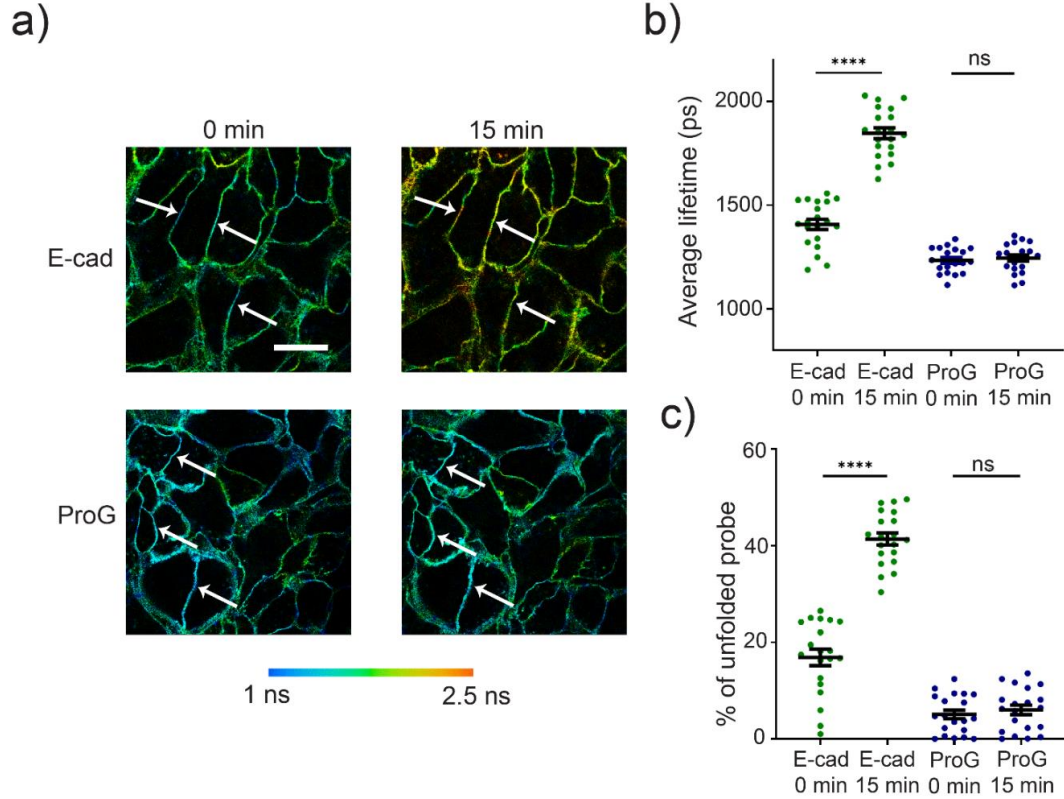


Figure 2.8. Imaging E-cadherin-mediated tensile forces at the MDCK cell–cell junctions. a) MDCK cells were first incubated in the presence of 2 mM EGTA with 200 nM of EC-FLIM-MDTP (E-cad) or Protein G-modified FLIM-MDTP control (Pro G) for 30 min. Representative images were taken before (0 min) and 15 min after adding 2 mM Ca^{2+} ions to induce E-cadherin forces. Scale bar, 20 μm . b) Distributions of cell–cell junction fluorescence lifetime before and after adding Ca^{2+} ions. c) Percentages of the unfolded FLIM-MDTP at each cell–cell junction before and after adding Ca^{2+} ions. Shown are mean and standard error of the mean (SEM) values from 20 junctions in each case. **** $p < 0.0001$ in two-tailed Student’s t-test; ns, not significant. Arrows indicated the junctions used for analysis.

We have recently developed a ratiometric DNA probe, termed DNAMeter, to quantify intercellular tensile forces⁴. To validate the performance of FLIM-MDTP, we wondered how the lifetime measurement-based quantification results can be compared to those obtained from the ratiometric measurement using DNAMeter. We prepared an EC-DNAMeter by modifying an additional Cy5 reference fluorophore at the 3’-end of the hairpin strand in EC-FLIM-MDTP (FAM). As a result, a dual-mode probe was designed

to use either the FAM fluorescence lifetime value or the fluorescence intensity ratio of FAM/Cy5 to measure E-cadherin tensions (Figure 2.6-d). Our results indicated that upon Ca^{2+} -induced force activation, very impressively, an almost identical percentage of unfolded DNA hairpins can be calculated at the same cell–cell junctions based on both ratiometric and lifetime images (Figure 2.6-e). Indeed, the FLIM-MDTP can be used to accurately determine the fraction of tension-induced unfolded probes.

2.2.3 Multiplexed imaging of molecular tensions with FLIM-MDTP

To further test if we can apply FLIM-MDTP for the multiplexed imaging of intercellular tensions, we first asked whether the EC-FLIM-MDTP (FAM) and EC-FLIM-MDTP (Cy3) can be used together to measure E-cadherin tensions. After incubating the MCF7 cells with a mixture of 200 nM EC-FLIM-MDTP (FAM) and EC-FLIM-MDTP (Cy3), we quantified the percentage of unfolded probes in both FAM and Cy3 lifetime imaging channels. As expected, a very similar unfolding percentage was identified at the same cell–cell junctions using either EC-FLIM-MDTP (FAM) or EC-FLIM-MDTP (Cy3) (Figure 2.9). This result demonstrated that both probes can be used simultaneously to quantify E-cadherin tensions.

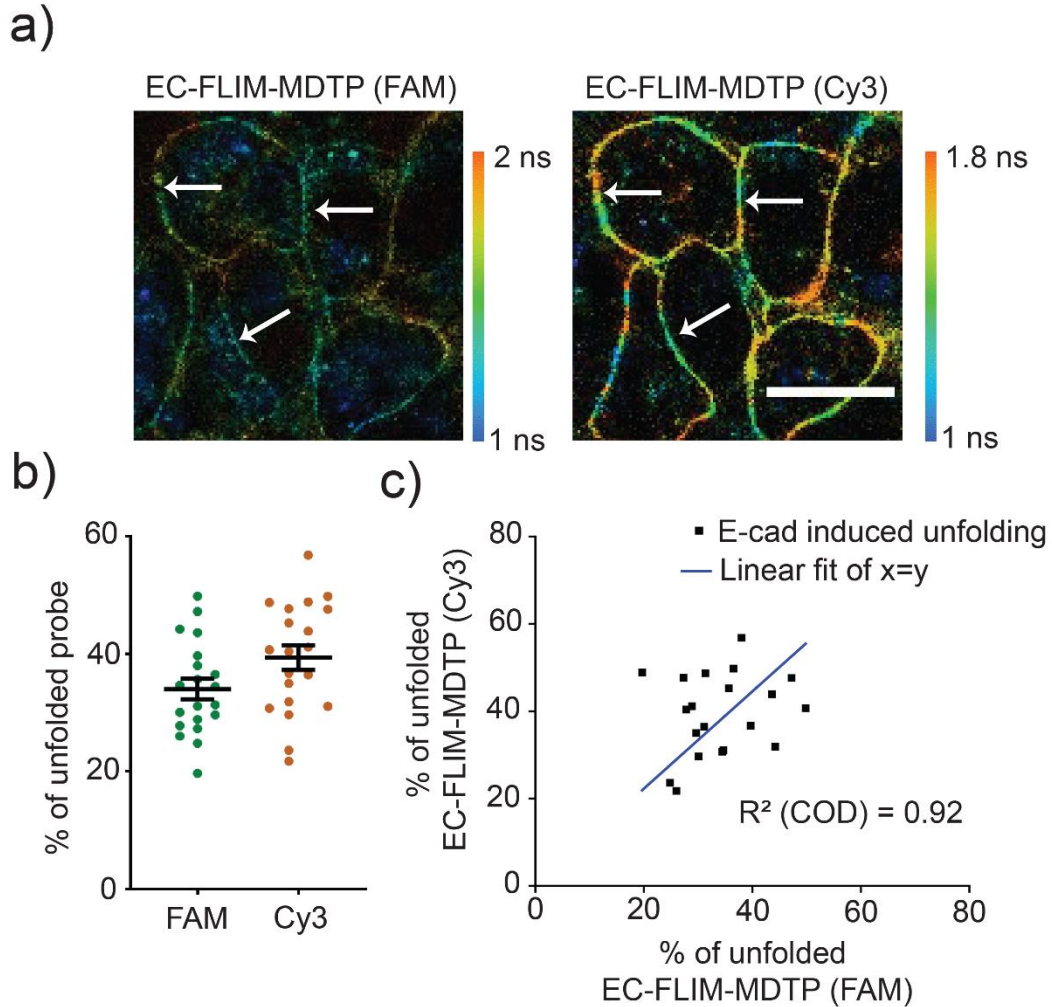


Figure 2.9. Imaging E-cadherin-mediated tensile forces simultaneously with the EC-FLIM-MDTP (FAM) and EC-FLIM-MDTP (Cy3). a) Representative images of MCF7 cells after incubating with a mixture of 200 nM EC-FLIM-MDTP (FAM) and EC-FLIM-MDTP (Cy3) for 30 min. Fluorescence lifetime imaging was taken in both (left) FAM and (right) Cy3 channels. Scale bar, 20 μm . b) Percentages of the unfolded EC-FLIM-MDTP (FAM) and EC-FLIM-MDTP (Cy3) at individual cell-cell junctions. Shown are mean and standard error of the mean (SEM) values from 20 junctions in each case. c) Correlation of the percentage of unfolded EC-FLIM-MDTP (FAM) and EC-FLIM-MDTP (Cy3) at the same cell-cell junctions. These two values are directly proportional to each other with a coefficient of determination (COD) of 0.92. Arrows indicated the junctions used for analysis.

Our next goal was to apply these dual EC-FLIM-MDTPs to study different force ranges of E-cadherin-mediated tension. The EC-FLIM-MDTP (FAM) or EC-FLIM-MDTP (Cy3) used above contains a 25 nt DNA hairpin with 22% G/C base pairs to detect forces around 4.4 pN^4 . To enable the detection of stronger E-cadherin tension, we have replaced the EC-FLIM-MDTP (Cy3) with a DNA hairpin of the same length but contains 66% G/C

base pairs. A threshold force value of 8.1 pN has been determined for this probe construct⁴. To clarify this difference in the DNA hairpin, we just named these two probes as EC-22-FLIM-MDTP (FAM) and EC-66-FLIM-MDTP (Cy3). We incubated a mixture of these two probes with the MDCK cells, and a Ca²⁺-induced increase in the fluorescence lifetime can be observed in both FAM and Cy3 channels. After quantification, 24% and 48% of the EC-22-FLIM-MDTP (FAM) was unfolded before and after the addition of calcium ions (Figure 2.10). Very similarly, 24% more EC-66-FLIM-MDTP (Cy3) was also activated (from 14% to 38%) upon adding Ca²⁺. Multiple force ranges can thus be simultaneously detected using this dual FLIM-MDTP probe design.

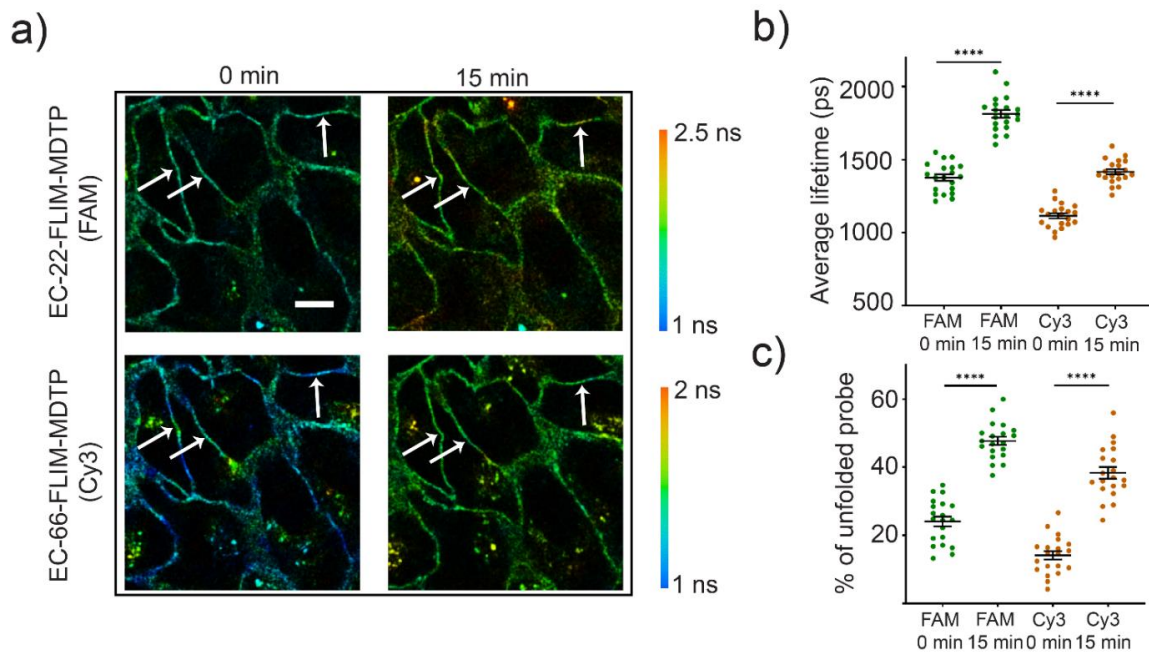


Figure 2.10. Imaging different force ranges of E-cadherin-mediated tension at the MDCK cell-cell junctions. a) Cells were first incubated in the presence of 2 mM EGTA with 200 nM of EC-22-FLIM-MDTP (FAM) and EC-66-FLIM-MDTP (Cy3) for 30 min. Representative images were taken before (0 min) and 15 min after adding 2 mM Ca²⁺ ions to induce E-cadherin forces. Scale bar, 20 μ m. b) Distributions of cell-cell junction fluorescence lifetime before and after adding Ca²⁺ ions. c) Percentages of the unfolded 22% GC (FAM) and 66% GC (Cy3) FLIM-MDTP at each cell-cell junction before and after adding Ca²⁺ ions. Shown are mean and standard error of the mean (SEM) values from 20 junctions in each case. ****p < 0.0001 in two-tailed Student's t-test; ns, not significant. Arrows indicated the junctions used for analysis.

We next wanted to demonstrate the potential of applying the FLIM-MDTP to simultaneously image the molecular tensions among different ligand-receptor pairs. We chose to study an epithelial-mesenchymal transition (EMT) process because multiple signaling events occur during this transition, which also plays a key role in development, wound healing and cancer progression, where cells lose their adhesion and become more invasive¹⁴⁻¹⁵. EMT exhibits a characteristic repression of E-cadherin together with the upregulation of N-cadherin¹⁶. To understand the mechanical features of the EMT, we wondered if the FLIM-MDTP can be used to measure the correlations between E-cadherin- and N-cadherin-mediated tensions during this process.

We thus designed an N-cadherin-modified DNA tension probe, NC-FLIM-MDTP (FAM), and used it together with the EC-FLIM-MDTP (Cy3) to simultaneously image N-cadherin and E-cadherin tensions. Transforming growth factor TGF- β 1, a widely used protein inducer of EMT, was used to induce the EMT of MCF7 cells¹⁷. After a 72 h induction, the successful transition was validated in an immunostaining assay based on the downregulation of two epithelial biomarkers, E-cadherin and ZO-1, and the upregulation of a mesenchymal biomarker, N-cadherin (Figure 2.11). We then added a mixture of NC-FLIM-MDTP (FAM) and EC-FLIM-MDTP (Cy3) to these TGF- β 1-induced MCF7 cells. After a brief 20 min incubation, a dramatic fluorescence lifetime increase in the FAM channel and a decrease in the Cy3 channel were observed, as compared to the control cells without adding TGF- β 1 (Figure 2.12). 32% N-cadherin probes and 19% E-cadherin probes were experiencing more than 4.4 pN forces at the junctions of those induced cells. Without the TGF- β 1 induction, the same batch of cells can instead unfold 16% N-cadherin and 50% E-cadherin probes (Figure 2.13-a, b). Since N-cadherin (or E-cadherin) prefers to interact

with another same type of cadherins on the neighboring cells¹⁸, this result can be indeed expected based on the upregulation of N-cadherin and the repression of E-cadherin during the EMT.

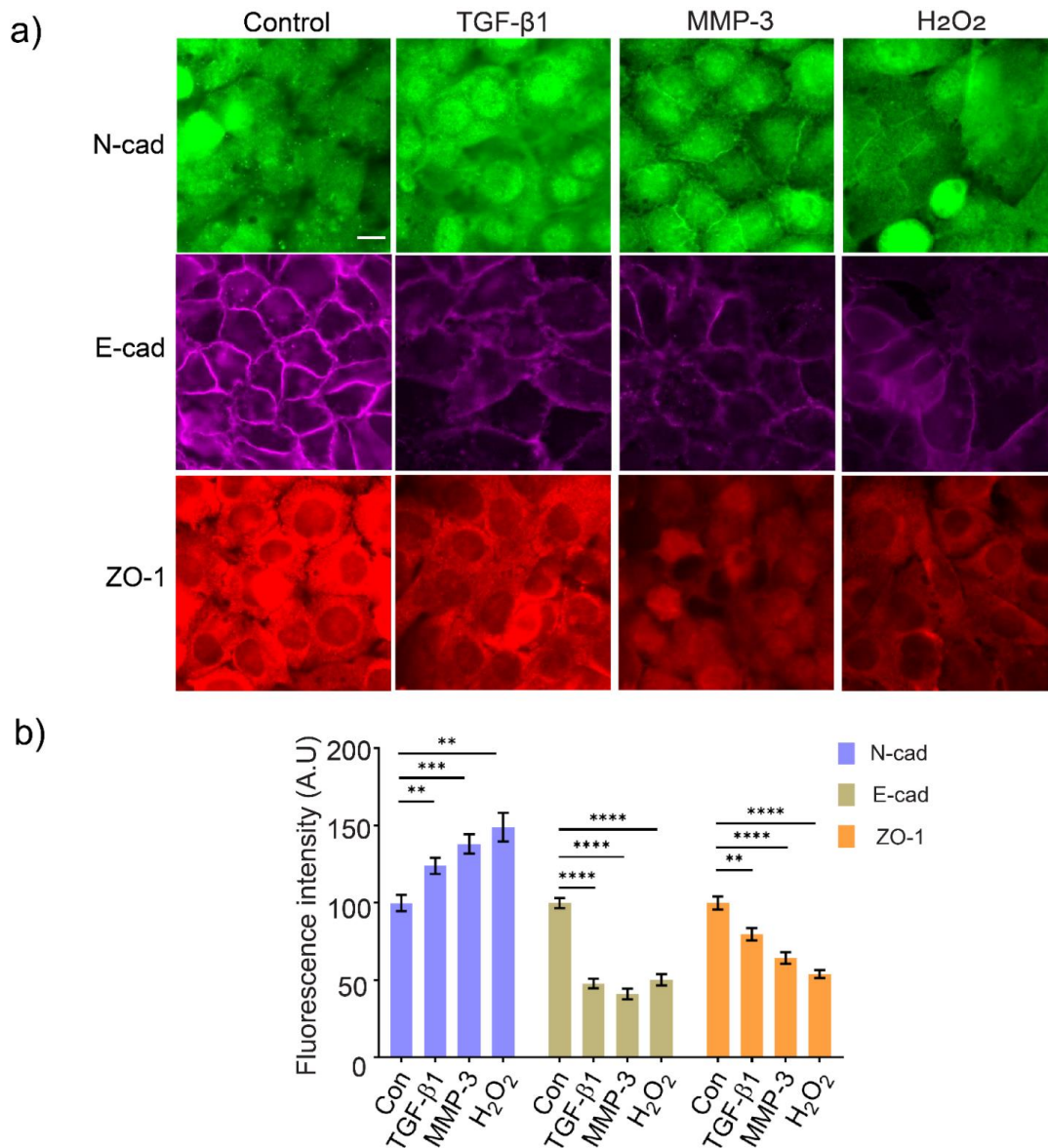


Figure 2.11. Immunostaining of EMT biomarkers including N-cadherin, E-cadherin, and ZO-1 after adding different inducers on MCF7 cells. a) Representative immunostaining images of MCF7 cells after treating with 1% DMSO (control), 30 ng/mL of TGF-β1, 2 μM MMP-3, or 50 μM H₂O₂ for 48–72 h. Scale bar, 20 μm. b) As expected in an EMT process, quantification of cell membrane fluorescence intensities indicated an increase in the N-cadherin expression and a decrease in the E-cadherin and ZO-1 levels after the treatment of each inducer. Shown are mean and standard error of the mean (SEM) values from at least 20 cell–cell junctions in each case. **p < 0.01, ***p < 0.001, ****p < 0.0001 in two-tailed Student’s t-test; ns, not significant.

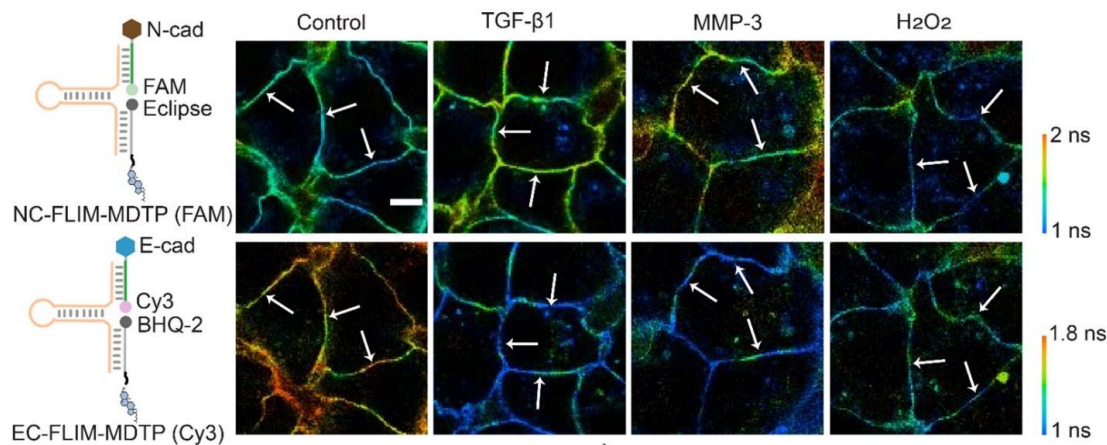


Figure 2.12. Multiplexed imaging of E-cadherin- and N-cadherin-mediated tension after adding different types of EMT inducers. MCF7 cells were first treated with 1% DMSO (control), 30 ng/mL of TGF- β 1, 2 μ M MMP-3, or 50 μ M H₂O₂ for 48–72 h. Representative images were taken after incubating with 200 nM of NC-FLIM-MDTP (FAM) and EC-FLIM-MDTP (Cy3) for 30 min. Scale bar, 10 μ m. Arrows indicated the junctions used for analysis.

To further confirm if the observed fluorescence lifetime changes are indeed due to variations in the E-cadherin and N-cadherin tensions, we first added EGTA to selectively chelate Ca²⁺ and measured its effect on both NC-FLIM-MDTP (FAM) and EC-FLIM-MDTP (Cy3) signals. As expected, a dramatic decrease in the fluorescence lifetime was observed in both FAM and Cy3 channels, regardless of whether the TGF- β 1 was added, (Figure 2.14). As another validation, a myosin light chain kinase inhibitor, ML-7, was used to reduce the local accumulation of cadherins at cell–cell junctions¹⁹. Indeed, after adding 2 mM ML-7, both NC-FLIM-MDTP (FAM) and EC-FLIM-MDTP (Cy3) signals disappeared (Figure 2.13-c, d), which indicated that the cadherin tensions are required for the unfolding of both probes. As a control, without modification of N-cadherin and E-cadherin, no change in the FLIM-MDTP lifetime signal was observed in both FAM and Cy3 channels (Figure 2.15). All these data demonstrated that the FLIM-MDTP can be used to simultaneously measure different molecular tension events at cell–cell junctions.

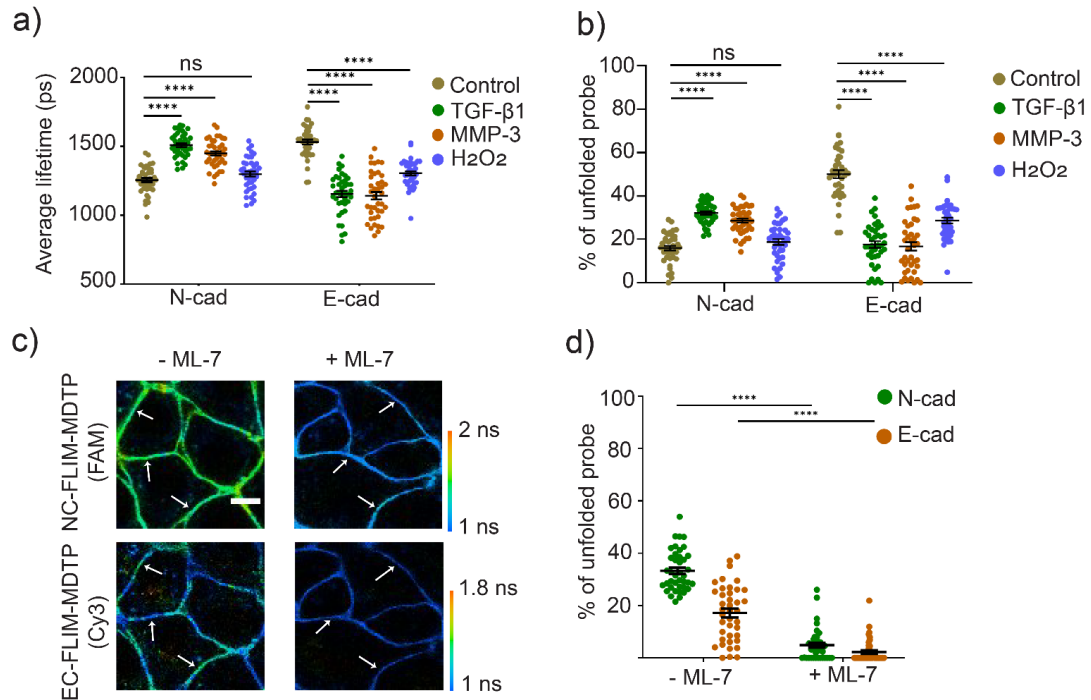


Figure 2.13. Multiplexed imaging of E-cadherin- and N-cadherin-mediated tension after the EMT induction. a) MCF7 cells were first treated with 1% DMSO (control), 30 ng/mL of TGF-β1, 2 μM MMP-3, or 50 μM H2O2 for 48–72 h. Distributions of cell–cell junction fluorescence lifetime after adding different types of EMT inducers. b) Percentages of the unfolded NC-FLIM-MDTP (FAM) and EC-FLIM-MDTP (Cy3) at each cell–cell junction after the treatment with each EMT inducer. c) MCF7 cells were first treated with 30 ng/mL of TGF-β1 for 72 h to induce EMT. A mixture of 200 nM NC-FLIM-MDTP (FAM) and EC-FLIM-MDTP (Cy3) was then added and incubated for 30 min before imaging. Representative images are shown in the presence or absence of 2 mM ML-7. Scale bar, 10 μm. d) Percentages of the unfolded NC-FLIM-MDTP (N-cad) and EC-FLIM-MDTP (E-cad) at each cell–cell junction in the presence or absence of 2 mM ML-7. Shown are mean and standard error of the mean (SEM) values from at least 40 cell–cell junctions in each case. ****p < 0.0001 in two-tailed Student’s t-test; ns, not significant. Arrows indicated the junctions used for analysis.

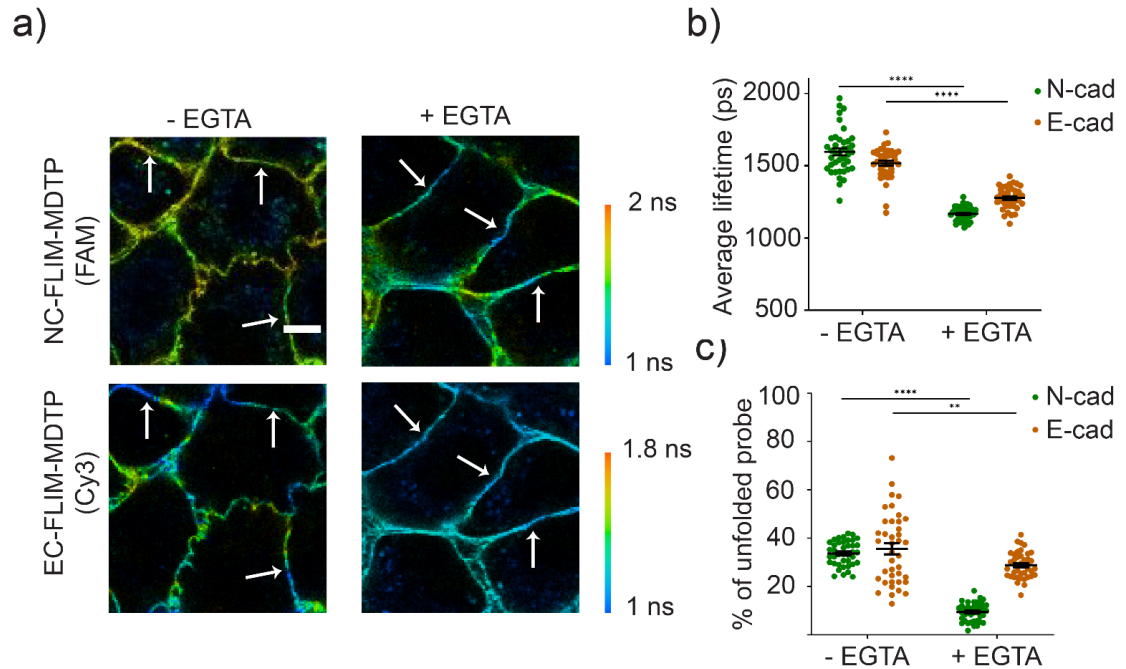


Figure 2.14. Validation of the unfolding of FLIM-MDTP during the EMT process is due to E-cadherin and N-cadherin-induced tension. a) MCF7 cells were first treated with 30 ng/mL of TGF-β1 for 72 h to induce EMT. A mixture of 200 nM NC-FLIM-MDTP (FAM) and EC-FLIM-MDTP (Cy3) was then added and incubated for 30 min before imaging. Representative images are shown in the presence or absence of 2 mM EGTA that can chelate the Ca²⁺ ions and inhibit cadherin tensions. Scale bar, 10 μm. b) Effect of the EGTA treatment on the distributions of cell-cell junction fluorescence lifetime in both FAM (N-cad) and Cy3 (E-cad) channels. c) Percentages of the unfolded NC-FLIM-MDTP (N-cad) and EC-FLIM-MDTP (E-cad) at each cell-cell junction in the presence or absence of 2 mM EGTA. Shown are mean and standard error of the mean (SEM) values from at least 20 cell-cell junctions in each case. **p < 0.01, ****p < 0.0001 in two-tailed Student's t-test. Arrows indicated the junctions used for analysis.

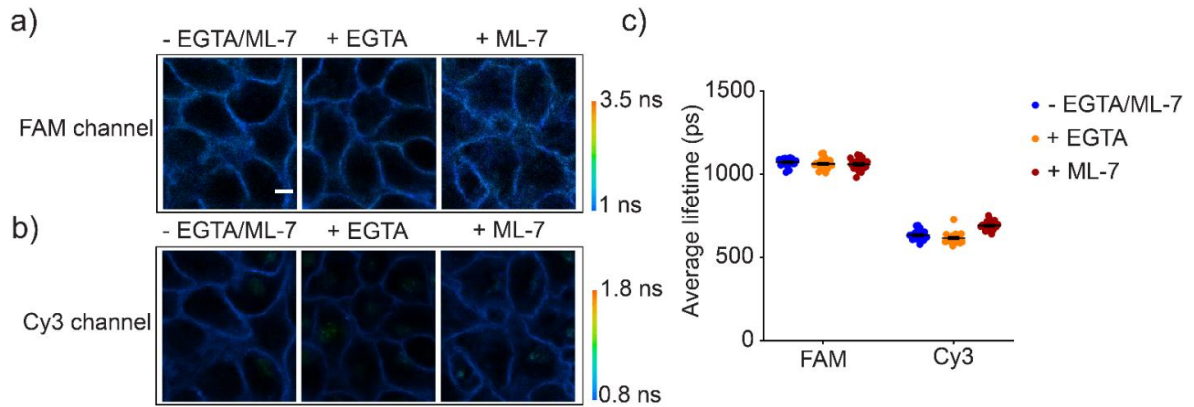


Figure 2.15. Effect of the EGTA and ML-7 treatment on the lifetime signal of cadherin-free FLIM-MDTP. (a, b) A mixture of 200 nM FLIM-MDTP (FAM) and FLIM-MDTP (Cy3), without modification of cadherin, was added and incubated with MCF7 cells for 30 min before imaging. Representative images are shown in the presence or absence of 2 mM EGTA or 2 mM ML-7. Scale bar, 10 μ m. c) Effect of the treatment on the distributions of cell-cell junction fluorescence lifetime in both FAM and Cy3 channels. Shown are mean and standard error of the mean (SEM) values from at least 20 cell-cell junctions in each case.

2.2.4 Mechanical features of epithelial-mesenchymal transition

We wanted to further apply the FLIM-MDTP to provide some mechanical signatures of the EMT. We first asked if cells induced by different types of EMT inducers will exhibit similar mechanical features. In addition to TGF- β 1, we have also tested two other commonly used EMT inducers, matrix metalloproteinase-3 (MMP-3)²⁰ and H₂O₂²¹. After confirming a similar change in the MCF7 cell membrane expression of N-cadherin and E-cadherin using these three inducers (Figure 2.11), we used NC-FLIM-MDTP (FAM) and EC-FLIM-MDTP (Cy3) to measure the effect of different inducers on the cadherin tensions. MMP-3-induced cells exhibited quite similar tensions as that induced by TGF- β 1, with 29% of N-cadherin and 17% of E-cadherin-modified probes being unfolded (Figure 2.12, 2.13-a, and 2.13-b). The small differences (~10%) between MMP-3 and TGF- β 1-induced cadherin tensions are well correlated with their variations in the N/E-cadherin expression levels (Figure 2.11). On the other hand, very interestingly, on H₂O₂-induced

MCF7 cells, the percentage of unfolded N-cadherin probes (19%) was very similar as that on the control non-induced cells (16%). In this case, the higher membrane expression of N-cadherin (Figure 2.11) did not result in the unfolding of more NC-FLIM-MDTP. Meanwhile, even though less E-cadherin probes were unfolded (29%) compared to the control cells (50%), this value is still much larger than that induced by TGF- β 1 (19%) or MMP-3 (17%). These results indicated that while the membrane expression of N/E-cadherins are related with cadherin-mediated tensile forces, it is not the only factor that regulates tensions during EMT at the cell junctions.

We also wondered if there are any strong correlations between the N-cadherin and E-cadherin-mediated tensions. For the purpose, we compared the unfolding percentage of the NC-FLIM-MDTP (FAM) and EC-FLIM-MDTP (Cy3) at each individual MCF7 cell-cell junctions. While a moderate positive correlation was observed in both TGF- β 1-induced cells and control cells, after the induction with MMP-3 or H₂O₂, most MCF7 cells exhibited only a weak correlation of the N/E-cadherin tensions (Figure 2.16)²². These results indicated that the intercellular force distribution across N-cadherin and E-cadherin are independently controlled during the EMT, especially when MMP-3 or H₂O₂ is used as the inducer.

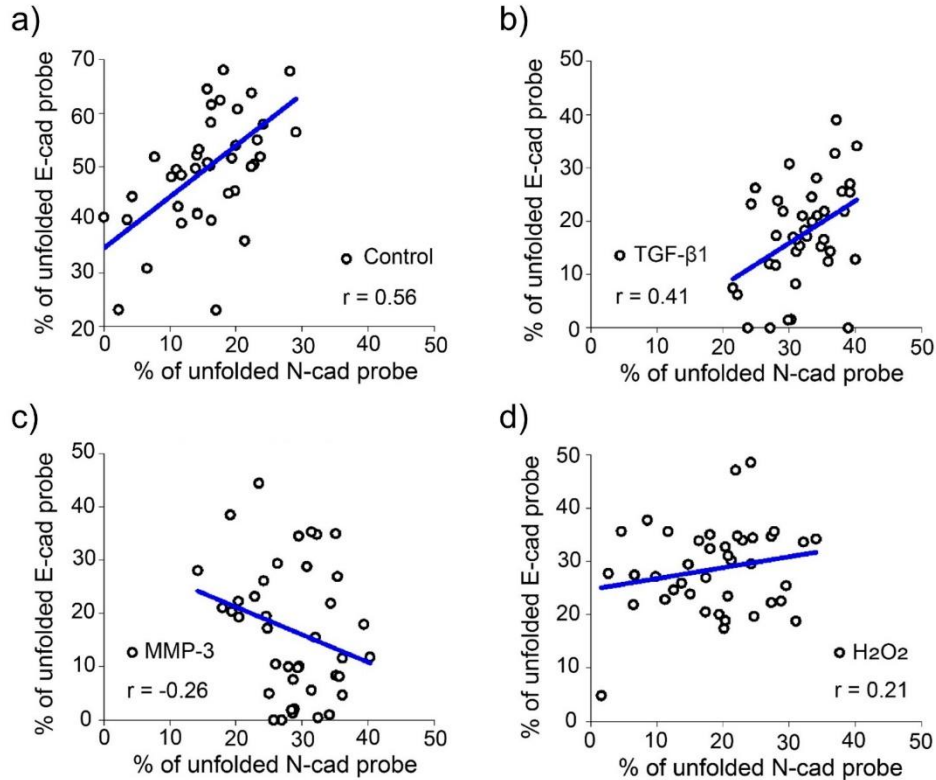


Figure 2.16. Correlation of the percentage of unfolded NC-FLIM-MDTP (FAM) and EC-FLIM-MDTP (Cy3) at the same cell–cell junctions. MCF7 cells were treated with a) 1% DMSO (control), b) 30 ng/mL of TGF- β 1, c) 2 μ M MMP-3, or d) 50 μ M H₂O₂ for 48–72 h. Pearson’s coefficient was determined in each case where a positive (or negative) coefficient value indicates a positive (or negative) correlation between E-cadherin- and N-cadherin-mediated tensile forces. Pearson’s coefficient value between ± 0.70 and ± 1.00 indicates a strong correlation, value between ± 0.30 and ± 0.70 indicates a moderate correlation, value between ± 0.00 and ± 0.30 indicates a weak correlation. At least 40 cell–cell junctions were analyzed in each case.

To study whether the mechanical interaction patterns of cadherins are varied in different stages of the EMT, we added the NC-FLIM-MDTP (FAM) and EC-FLIM-MDTP (Cy3) onto MCF7 cell membranes after 24 h, 48 h, or 72 h of the TGF- β 1 induction. At 24 h, both E-cadherin and N-cadherin tensions were quite similar as that of the control cells (Figure 2.17). A significant increase in the unfolding percentage of the N-cadherin probes was observed at 48 h (50% vs. 29% on the control cells). Correspondingly, the percentage of E-cadherin tension that is larger than 4.4 pN greatly decreased to 25%.

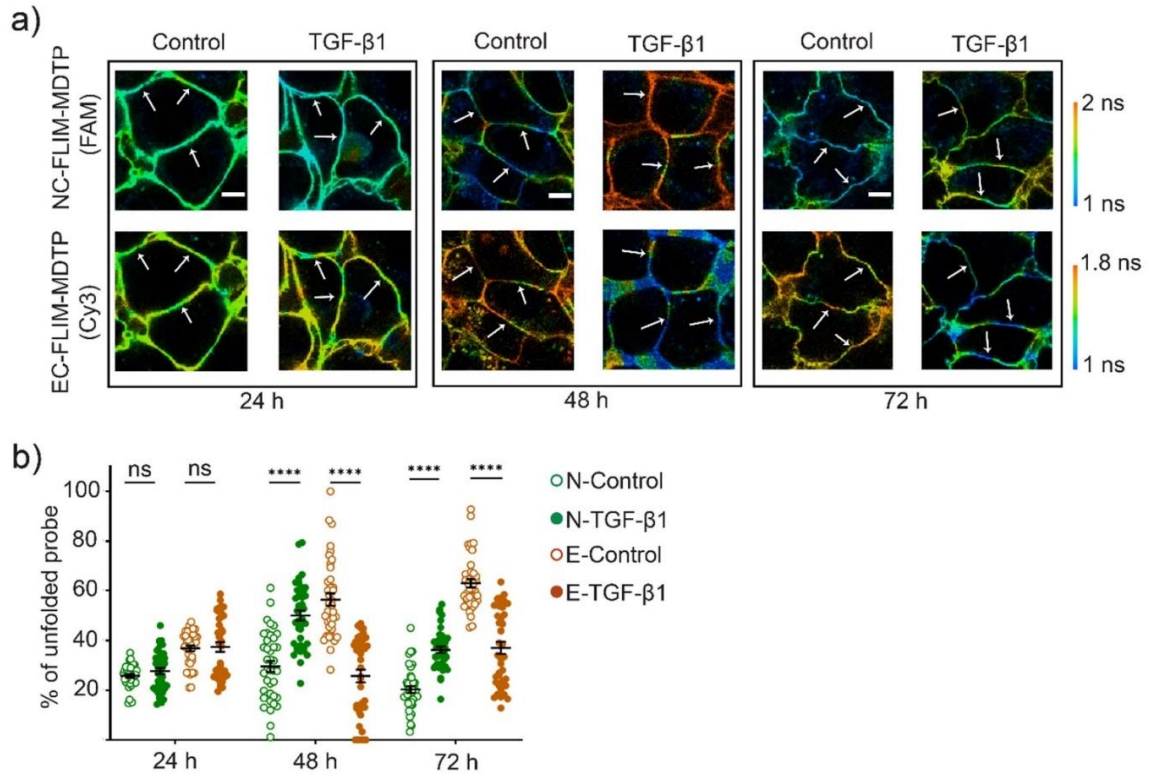


Figure 2.17. Imaging E-cadherin- and N-cadherin-mediated tension after different time treatment with 30 ng/mL of TGF- β 1. (a) MCF7 cells were first treated with 1% DMSO (control) or 30 ng/mL of TGF- β 1 for 24–72 h. Representative images were taken after incubating with 200 nM of NC-FLIM-MDTP (FAM) and EC-FLIM-MDTP (Cy3) for 30 min. Scale bar, 10 μ m. (b) Percentages of the unfolded NC-FLIM-MDTP (FAM) and EC-FLIM-MDTP (Cy3) at each cell–cell junction after 24–72 h treatment with TGF- β 1. Shown are mean and standard error of the mean (SEM) values from at least 40 junctions in each case. **** p < 0.0001 in two-tailed Student’s t -test; ns, not significant. Arrows indicated the junctions used for analysis.

Appealingly at 72 h, the percentage of unfolded N-cadherin probes was actually decreased compared to that at 48 h, while that of E-cadherin was increased. Since the membrane expression levels of both N-cadherin and E-cadherin were quite similar at these two time points (Figure 2.18), the variations in the cadherin tensions could be likely due to the lower cell confluence at 48 h²³. Future studies will be needed to understand the real mechanism of these mechanotransduction process during the EMT, which is beyond the scope of this study.

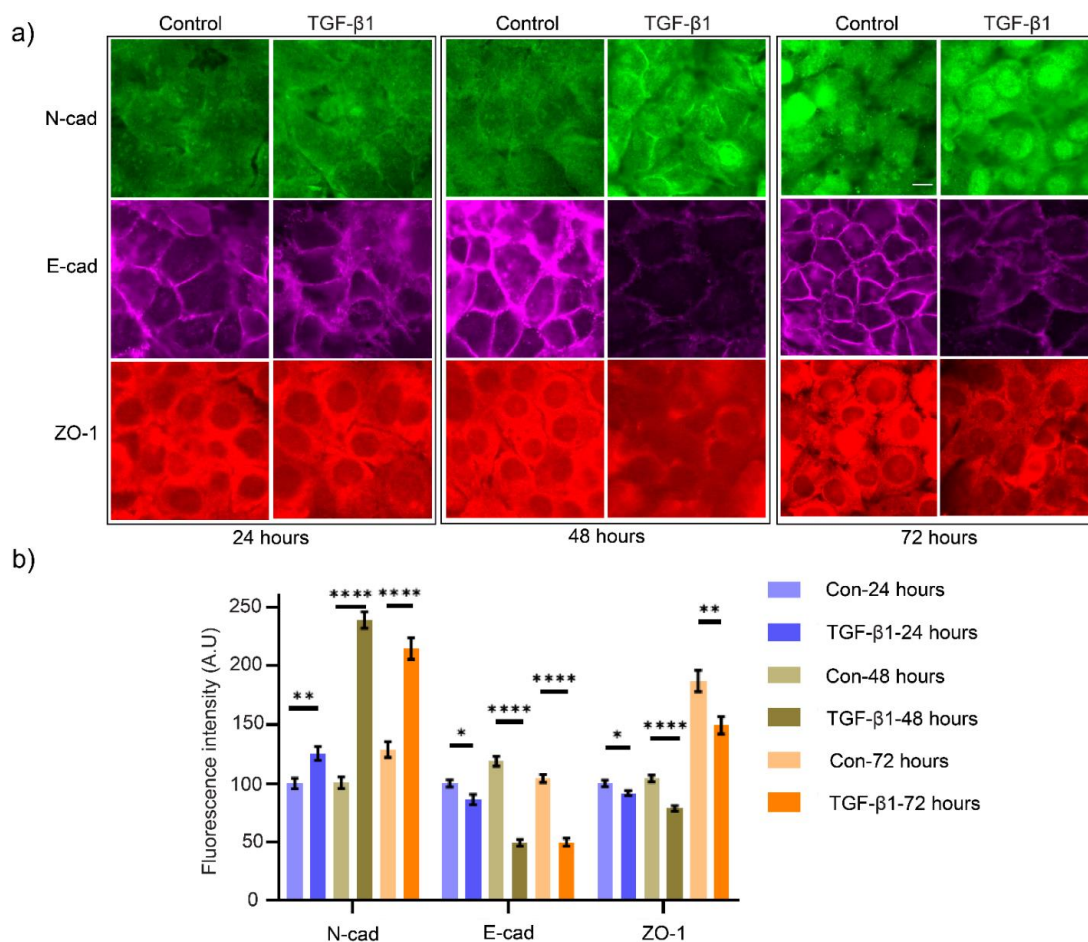


Figure 2.18. Immunostaining of EMT biomarkers including N-cadherin, E-cadherin, and ZO-1 after different time treatment with 30 ng/mL of TGF- β 1. a) Representative immunostaining images of MCF7 cells after treating with 1% DMSO (control) or 30 ng/mL of TGF- β 1 for 24–72 h. Scale bar, 20 μ m. b) As expected in an EMT process, quantification of cell membrane fluorescence intensities indicated an increase in the N-cadherin expression and a decrease in the E-cadherin and ZO-1 levels after the treatment. Maximum differences between control and TGF- β 1 treatment in the expression levels of EMT biomarkers were observed at 48 h. Shown are mean and standard error of the mean (SEM) values from at least 20 cell–cell junctions in each case. * $p < 0.05$, ** $p < 0.01$, **** $p < 0.0001$ in two-tailed Student’s t-test.

2.3 Conclusion

In this project, we developed a fluorescence lifetime imaging-based approach to measure molecular tensions at cell–cell junctions. Compared to the conventional fluorescence intensity-based DNA tension probes (ref), one major advantage of lifetime-based measurement is that its signal is concentration-independent. As a result, the so-called FLIM-MDTP can act as a self-referential system that provides quantitative imaging data

without requiring any additional reference fluorophore for the calibration. This unique feature of lifetime measurement is very critical for membrane-anchored DNA probes since these probes are normally heterogeneously distributed on the cell surfaces. Lifetime-based measurement is also less vulnerable to the light absorption or scattering events that will modulate fluorescence intensities. In addition, the FLIM-MDTP is quite suitable for the multiplexed imaging of forces. Because no reference fluorophore is needed, much less spectral overlap on the membranes can be expected. Meanwhile, fluorophores with similar excitation/emission wavelength can also be potentially distinguished based on their different lifetime values.

Using cadherin-mediated epithelial-mesenchymal transition as an example, we demonstrated, for the first time, that tension applied on different adhesion molecules can be simultaneously studied at the same cell–cell junctions. Our study indicated some intriguing correlations between N-cadherin and E-cadherin tensions during different stages of the EMT process. Simply by changing the conjugated ligand, the FLIM-MDTP can be applied to study various other intercellular mechanotransduction events. A wide choice of fluorophores and quenchers can be potentially incorporated within the FLIM-MDTP to allow even more sensitive and multiplexed imaging of molecular forces. We expect these powerful probes can be broadly used for studying mechanobiology.

2.4 Materials and Methods

2.4.1 Reagents:

Unless specified, all the chemicals were purchased from Sigma or Fisher Scientific and directly used without further purification. Fluorophore-labelled DNA strands were ordered from Integrated DNA Technology and Yale Keck Oligonucleotide Synthesis. The

sequences of DNA strands are listed below in Table 2.1. 1,2-dioleoyl-sn-glycero-3-phosphocholine (DOPC) was purchased from Avanti Polar Lipids. Anti-N-cadherin antibody (ab76057) and recombinant human TGF- β 1 protein (ab50036) were purchased from Abcam. Anti-ZO-1 monoclonal antibody (66452-1-Ig) was purchased from Proteintech Group. Other antibodies were purchased from Thermo Fisher Scientific including anti-E-cadherin monoclonal antibody (14-3249-82), Alexa Fluor 488-labeled goat anti-rabbit IgG secondary antibody (A-11034), Alexa Fluor 647-labeled goat anti-rat IgG secondary antibody (A-21247), and Alexa Fluor 555-labeled goat anti-mouse IgG secondary antibody (A-21424). Recombinant human MMP-3 protein (CF 513-MP-010) was purchased from R&D systems.

2.4.2 *In vitro* fluorescence characterization:

In vitro fluorescence measurements were performed using a PTI fluorimeter (Horiba, New Jersey, NJ). The quenching efficiency of FLIM-MDTP was determined in HEPES buffer (Invitrogen, A14291DJ) consisting of 140 mM NaCl, 20 mM HEPES, 2.5 mM KCl, 1.8 mM CaCl₂, 1.0 mM MgCl₂, at pH=7.4. In these measurements, 200 nM of each probe was used, which was labeled with FAM/Eclipse, FAM only (no quencher), Cy3/BHQ2, and Cy3 only (no quencher), respectively. The emission spectra of the FAM and Cy3 signals were collected in the range of 510–560 nm and 550–600 nm after excitation at 488 nm and 540 nm, respectively.

2.4.3 Cell culture, imaging, and data analysis:

Both MDCK and MCF7 cells were cultured in a DMEM medium supplemented with 10% FBS, 100-unit penicillin, and 0.1 mg/mL streptomycin. These cells were split at 80% confluence and plated at a density of 20% following standard cell culture procedures.

All the images were acquired on a Nikon Eclipse TiE inverted microscope with A1 spectral detector confocal and FLIM/FCS module. A 100x and 60x oil immersion objective was used for imaging MDCK and MCF7 cells, respectively. During imaging, the field of view was first found and focused using the scanning confocal capability of the microscope. The input laser was then changed to the pulsed laser that was synched with the FLIM system and the emitted photons were detected through a Becker-Hickl SPC-152/HPM-100-40 dual detector system (Boston Electronics). The FAM- and Cy3-modified probes were excited at 50 MHz frequency with a 488 nm and 561 nm laser line, respectively. Data acquisition and analysis were performed with a Becker-Hickl TCSPC software package. Raw data was then further processed using the Origin and GraphPad Prism software.

2.4.4 Synthesis of protein G-modified DNA strands:

The Protein G-modified DNA ligand strand was synthesized by mixing 20 μL of DNA ligand strand (200 μM) with 10 μL of 100 mM TCEP in HEPES buffer containing 50 mM EDTA at pH 7.2. After 2 h incubation at room temperature to reduce the disulfide bond, excess TCEP was removed using a Bio-Spin 6 column (Bio-Rad). Then, 1.5 μL of 23 mM freshly prepared sulfo-SMCC was immediately added and incubated at room temperature for 1 min. Afterwards, 10 μL of 5 mg/mL Protein G was added and incubated at 4 $^{\circ}\text{C}$ for overnight. The synthesized Protein G-DNA conjugates were then purified with cobalt-based Dynabeads (Invitrogen, 10103D) through their specific interaction with poly-histidine-tagged proteins. Isolated his-tagged proteins are further eluted from the beads with his elution buffer. After exchanging and concentrating the sample into a HEPES buffer, the concentrations of Protein G-modified DNA strands were quantified with a Nanodrop One UV/Vis spectrometer.

2.4.5 Preparation of the FLIM-MDTP:

To prepare the FLIM-MDTP, 10 μM anchor strand and hairpin strand was first mixed HEPES buffer (Invitrogen, A14291DJ) consisting of 140 mM NaCl, 20 mM HEPES, 2.5 mM KCl, 1.8 mM CaCl_2 , 1.0 mM MgCl_2 , at pH=7.4. The mixture was then denatured for 5 min at 75 $^\circ\text{C}$ and slowly annealed back to the room temperature at a rate of 1.3 $^\circ\text{C}/\text{min}$ in An Eppendorf Thermomixer C. Afterwards, the solution was incubated with the Protein G-modified ligand strand at 1:1 ratio at 4 $^\circ\text{C}$ for overnight. This assembly was then mixed with equimolar of IgG/Fc-fused human E-cadherin (AcroBiosystems, ECDH5250) or N-cadherin (R&D systems, 1388-NC-050) at room temperature for 15 min and kept at 4 $^\circ\text{C}$ for overnight before usage.

2.4.6 Imaging of intercellular tensile forces:

For imaging E-cadherin-mediated tensile forces in MDCK cells, $\sim 10,000$ cells were seeded in an 8-well chamber cover glass system (Cellvis) and grown overnight (16 h). After washing twice with HEPES-buffered saline, 200 nM pre-assembled FLIM-MDTP was added and incubated for 30 min before imaging. For MCF7 cell imaging during the epithelial-mesenchymal transition (EMT), $\sim 25,000$ cells were seeded in each well of the chamber and grown overnight. After washing once with Dulbecco's phosphate-buffered saline, fresh DMEM media was added without FBS. Then 30 ng/mL of TGF- $\beta 1$ or 2 μM of MMP-3 was added and incubated for 72 h to induce the EMT process. In the case of the EMT induction by 50 μM H_2O_2 , only 48 h induction was needed. For all these experiments, the addition of 1% DMSO was used as a control. After the EMT induction, the cells were washed with HEPES-saline buffer for three times, and then 100 μL of 200 nM NC-FLIM-MDTP and EC-FLIM-MDTP was added for 30 min before imaging.

2.4.7 Preparation of the supported lipid bilayer (SLB):

Following a previously reported protocol²⁴, we first prepared lipid vesicles by dissolving 1,2-dioleoyl-sn-glycero-3-phosphocholine (DOPC) in chloroform at 10 mg/mL concentration. Taking 40 μ L of the solution in a clean round-bottom flask, air-dried and kept in vacuum for 1 h to remove the residual chloroform. Such prepared DOPC was then suspended in 1 mL of PBS and vortexed thoroughly. Afterwards, the mixture was frozen in liquid nitrogen and thawed at 37 °C for 3 min. This freeze-thaw cycle was repeated for 5 times to produce the unilamellar vesicles. To obtain uniformly sized lipid vesicles, the above product was further extruded through a 0.1 μ m membrane. The size of these vesicles was then validated based on their dynamic light scattering as measured in a Malvern Zetasizer Nano. To further prepare the SLB, a glass-bottom 96 well-plate was first treated with 2 M NaOH solution and washed thoroughly with de-ionized water for 30 times. Afterwards, 50 μ L of the above-prepared DOPC vesicles were added and incubated at room temperature for 45 min. After washing with PBS buffer for 15 times to remove excess vesicles, 20 μ L of 0.1% BSA was added and incubated for 20 min to block any unmodified surface region. Finally, after washing with PBS for 20 times, different concentrations of lipid-DNA probes were added and incubated for 15 min before imaging. The same conditions as used for cellular imaging were applied here for imaging probes on the SLB.

2.4.8 Calibration of the FLIM-MDTP on SLB:

We used the above-prepared SLB membrane for establishing a calibration curve to correlate the fluorescence lifetime value with the percentage of unfolded DNA probes. In this case, five different ratios of nq-FLIM-MDTP (100% unfolded signal) and FLIM-MDTP (0% unfolded signal) were mixed at 200/0 nM, 150/50 nM, 100/100 nM, 50/150

nM, and 0/200 nM concentrations. After adding these mixtures onto the SLB membrane, an exponential calibration correlation was obtained between the averaged fluorescence lifetime data in the membrane and the percentage of unfolded DNA probes.

2.4.9 Immunostaining experiment:

Before and after the EMT induction, the MCF7 cells were first fixed using 4% paraformaldehyde at room temperature for 20 min. After washing with PBS for three times (each time incubation for 5 min), 0.1% Triton-X was added and incubated for 20 min at room temperature for the cell permeabilization. Afterwards, the cells were washed with PBS for three times, with 5 min incubation each time, and then were incubated with 10% goat serum for 1 h at room temperature to block non-specific interactions. The primary antibody diluted in 10% goat serum at a 1:100 ratio was then added and incubated with the cells at 4 °C for overnight. After washing such-treated cells with PBS for three times (each time incubation for 5 min) at room temperature, fluorophore-labelled secondary antibody was added at a 1:1,000 ratio and incubated at room temperature for 1 h. After washing with PBS for three times (each time incubation for 5 min), cellular images were taken with a Leica DMi8 inverted epifluorescence microscope.

Table 2.1 - DNA sequences used for this chapter

Name	DNA sequence (5' - 3')
Hairpin strand - 1 (22% GC)	CCC GTG AAA TAC CGC ACA GAT GCG TTT <u>GTA TAA ATG TTT TTT TCA TTT ATA CTT TAA GAG CGC CAC GTA GCC CAG C</u>
Ligand strand - 1	HS-TTT GCT GGG CTA CGT GGC GCT CTT-FAM
Anchor strand - 1	Eclipse-CGC ATC TGT GCG GTA TTT CAC CCC-Cholesterol
nqAnchor strand - 1	CGC ATC TGT GCG GTA TTT CAC CCC-Cholesterol
Hairpin strand - 2 (22% GC)	TCG AAG CAA GTG TGA GGA CTC TTT <u>GTA TAA ATG TTT TTT TCA TTT ATA CTT TGC TGG GCT ACG TGG CGC TCT T</u>
Ligand strand - 2	Cy3-GAG TCC TCA CAC TTG CTT CGA TTT-SH
Anchor strand - 2	Cholesterol-CCC AAG AGC GCC ACG TAG CCC AGC-BHQ2
nqAnchor strand - 2	Cholesterol-CCC AAG AGC GCC ACG TAG CCC AGC
Hairpin strand (66% GC)	TCG AAG CAA GTG TGA GGA CTC TTT <u>CTA CGA GCG TTT TTT TCG CTC GTA GTT TGC TGG GCT ACG TGG CGC TCT T</u>
Complementary strand	AAA GTA TAA ATG AAA AAA ACA TTT ATA CAA A

Underlined sequences indicate the stem and loop region of the force-sensing DNA hairpin module.

Table 2.2 - Standard curve equations used for calculating the percentage of unfolded probes (x) based on the fluorescence lifetime (y), as shown in Figure 2.6

Model	Exponential growth order 1
Equation for FAM-labeled probe	$y = A_1 * \exp(x/t_1) + y_0$
Fluorescence lifetime at x = 0 (y ₀)	264.94721 ± 768.00924 ps
Pre-exponential factor (A ₁)	787.85821 ± 650.18657
Exponential factor (t ₁)	70.86895 ± 31.4677
R ² coefficient of determination (COD)	0.99724

Model	Exponential growth order 1
Equation for Cy3-labeled probe	$y = A_1 * \exp(x/t_1) + y_0$
Fluorescence lifetime at x = 0 (y ₀)	2358.67881 ± 442.10055 ps
Pre-exponential factor (A ₁)	-1461.40239 ± 355.44625
Exponential factor (t ₁)	-86.63456 ± 52.25799
R ² coefficient of determination (COD)	0.99798

2.5 References

1. Canel, M.; Serrels, A.; Frame, M. C.; Brunton, V. G., E-cadherin-integrin crosstalk in cancer invasion and metastasis. *J Cell Sci* **2013**, *126* (Pt 2), 393-401.
2. Chappuis-Flament, S.; Wong, E.; Hicks, L. D.; Kay, C. M.; Gumbiner, B. M., Multiple cadherin extracellular repeats mediate homophilic binding and adhesion. *J Cell Biol* **2001**, *154* (1), 231-43.
3. Zhao, B.; O'Brien, C.; Mudiyansele, A.; Li, N.; Bagheri, Y.; Wu, R.; Sun, Y.; You, M., Visualizing Intercellular Tensile Forces by DNA-Based Membrane Molecular Probes. *J Am Chem Soc* **2017**, *139* (50), 18182-18185.

4. Zhao, B.; Li, N.; Xie, T.; Bagheri, Y.; Liang, C.; Keshri, P.; Sun, Y.; You, M., Quantifying tensile forces at cell-cell junctions with a DNA-based fluorescent probe. *Chem Sci* **2020**, *11* (32), 8558-8566.
5. Izaguirre, M. F.; Casco, V. H., E-cadherin roles in animal biology: A perspective on thyroid hormone-influence. *Cell Commun Signal* **2016**, *14* (1), 27.
6. Wheelock, M. J.; Shintani, Y.; Maeda, M.; Fukumoto, Y.; Johnson, K. R., Cadherin switching. *J Cell Sci* **2008**, *121* (Pt 6), 727-35.
7. Dan, K.; Veetil, A. T.; Chakraborty, K.; Krishnan, Y., DNA nanodevices map enzymatic activity in organelles. *Nat Nanotechnol* **2019**, *14* (3), 252-259.
8. Saha, S.; Prakash, V.; Halder, S.; Chakraborty, K.; Krishnan, Y., A pH-independent DNA nanodevice for quantifying chloride transport in organelles of living cells. *Nat Nanotechnol* **2015**, *10* (7), 645-51.
9. Krishnan, Y.; Zou, J.; Jani, M. S., Quantitative Imaging of Biochemistry in Situ and at the Nanoscale. *ACS Cent Sci* **2020**, *6* (11), 1938-1954.
10. Johansson, M. K., Choosing reporter-quencher pairs for efficient quenching through formation of intramolecular dimers. *Methods Mol Biol* **2006**, *335*, 17-29.
11. Borghi, N.; Sorokina, M.; Shcherbakova, O. G.; Weis, W. I.; Pruitt, B. L.; Nelson, W. J.; Dunn, A. R., E-cadherin is under constitutive actomyosin-generated tension that is increased at cell-cell contacts upon externally applied stretch. *Proc Natl Acad Sci U S A* **2012**, *109* (31), 12568-73.

12. Conway, D. E.; Breckenridge, M. T.; Hinde, E.; Gratton, E.; Chen, C. S.; Schwartz, M. A., Fluid shear stress on endothelial cells modulates mechanical tension across VE-cadherin and PECAM-1. *Curr Biol* **2013**, *23* (11), 1024-30.
13. Rothen-Rutishauser, B.; Riesen, F. K.; Braun, A.; Gunthert, M.; Wunderli-Allenspach, H., Dynamics of tight and adherens junctions under EGTA treatment. *J Membr Biol* **2002**, *188* (2), 151-62.
14. Kalluri, R.; Weinberg, R. A., The basics of epithelial-mesenchymal transition. *J Clin Invest* **2009**, *119* (6), 1420-8.
15. Dongre, A.; Rashidian, M.; Reinhardt, F.; Bagnato, A.; Keckesova, Z.; Ploegh, H. L.; Weinberg, R. A., Epithelial-to-Mesenchymal Transition Contributes to Immunosuppression in Breast Carcinomas. *Cancer Res* **2017**, *77* (15), 3982-3989.
16. Loh, C. Y.; Chai, J. Y.; Tang, T. F.; Wong, W. F.; Sethi, G.; Shanmugam, M. K.; Chong, P. P.; Looi, C. Y., The E-Cadherin and N-Cadherin Switch in Epithelial-to-Mesenchymal Transition: Signaling, Therapeutic Implications, and Challenges. *Cells* **2019**, *8* (10).
17. Xu, J.; Lamouille, S.; Derynck, R., TGF-beta-induced epithelial to mesenchymal transition. *Cell Res* **2009**, *19* (2), 156-72.
18. Leckband, D. E.; de Rooij, J., Cadherin adhesion and mechanotransduction. *Annu Rev Cell Dev Biol* **2014**, *30*, 291-315.
19. Shewan, A. M.; Maddugoda, M.; Kraemer, A.; Stehbens, S. J.; Verma, S.; Kovacs, E. M.; Yap, A. S., Myosin 2 is a key Rho kinase target necessary for the local concentration of E-cadherin at cell-cell contacts. *Mol Biol Cell* **2005**, *16* (10), 4531-42.

20. Radisky, E. S.; Radisky, D. C., Matrix metalloproteinase-induced epithelial-mesenchymal transition in breast cancer. *J Mammary Gland Biol Neoplasia* **2010**, *15* (2), 201-12.
21. Kim, M. C.; Cui, F. J.; Kim, Y., Hydrogen peroxide promotes epithelial to mesenchymal transition and stemness in human malignant mesothelioma cells. *Asian Pac J Cancer Prev* **2013**, *14* (6), 3625-30.
22. Ratner, B., The correlation coefficient: Its values range between +1/-1, or do they? *Journal of Targeting, Measurement and Analysis for Marketing* **2009**, *17* (2), 139-142.
23. Maeda, M.; Johnson, K. R.; Wheelock, M. J., Cadherin switching: essential for behavioral but not morphological changes during an epithelium-to-mesenchyme transition. *J Cell Sci* **2005**, *118* (Pt 5), 873-87.
24. Lin, W. C.; Yu, C. H.; Triffo, S.; Groves, J. T., Supported membrane formation, characterization, functionalization, and patterning for application in biological science and technology. *Curr Protoc Chem Biol* **2010**, *2* (4), 235-69.

CHAPTER 3

VISUALIZING FORCE-INDUCED NOTCH SIGNALING WITH THE HELP OF DNA-BASED MEMBRANE TENSION RATIOMETRIC PROBE (DNAMETER)

3.1 Introduction

Notch signaling is one of the most important signaling pathways in molecular and cellular biology¹. It plays crucial role in vascular formation, morphogenesis, cell fate determination and other biological processes². The activity of Notch signaling is also related to different diseases such as cancers and heart diseases³. The Notch pathway is highly conserved and follows a very simple working mechanism⁴. The direct pathway from cell membrane to nucleus gives it few opportunities for the regulation and gives little chance of amplification unlike other signaling pathways. Interestingly, under certain circumstance, Notch signaling is related to cell death and tumor suppression. While in other cases, it is also associated with promotion of tissue growth and cancer⁴. These phenomena show the importance of understanding the mechanism of Notch signaling.

Notch signaling involves a receptor-ligand interaction followed by cascade reactions to regulate certain genes⁵. Initial step of activation is induced by the receptor-ligand interaction, which is then followed by proteolytic cleavages as shown in Figure 3.1. The cleavage releases Notch intracellular domain (NICD), which enters in the nucleus and together with the help of CBF1-suppressor of Hairless-LAG1 (CSL) and co-activator mastermind (MAM) stimulates the transcription process of the target genes. The diverse

outcomes of the signaling process is believed to originate from different ligand-receptor interactions but it could also be due to some other regulatory mechanisms⁶.

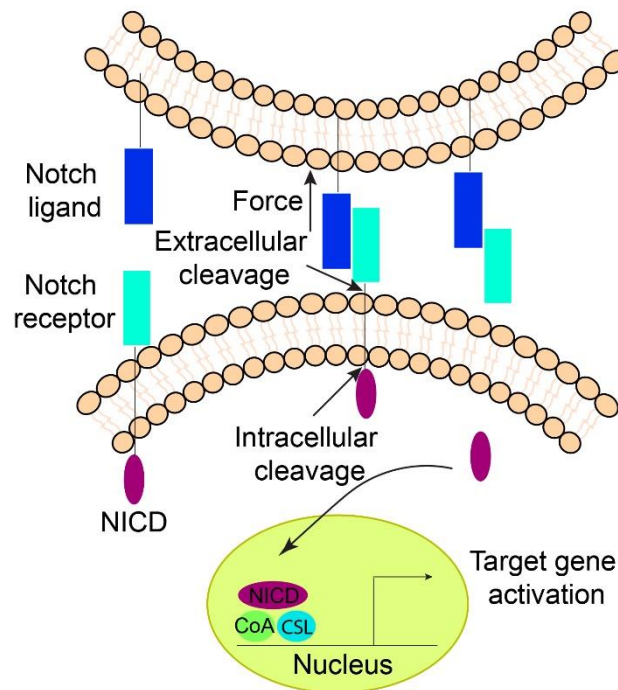


Figure 3.1. Mechanism of Notch signaling according to the “lift and cut” model indicating the presence of tensile forces required for Notch activation.

Notch proteins are large, the extracellular domains contain 29-36 epidermal growth factor (EGF) repeats and negative regulatory domains (Figure 3.2)⁷. There are four different types of mammalian Notch receptors and five different types of mammalian Notch ligands (Figure 3.2). In the case of mammals, two of the four Notch receptors (Notch1 & Notch4) and three of the five ligands (Jagged1, DLL1 & DLL4) are expressed predominantly and play a key role in the signaling process⁷. Dynamic interaction between different receptor-ligand pairs guides the biological processes. For example, DLL1 activates Notch1 discretely while upregulating Notch target genes, however DLL4 activates Notch1 in a sustained manner to activate Hey1 genes⁸. Thus, understanding Notch signaling holds key to study these processes and regulate them.

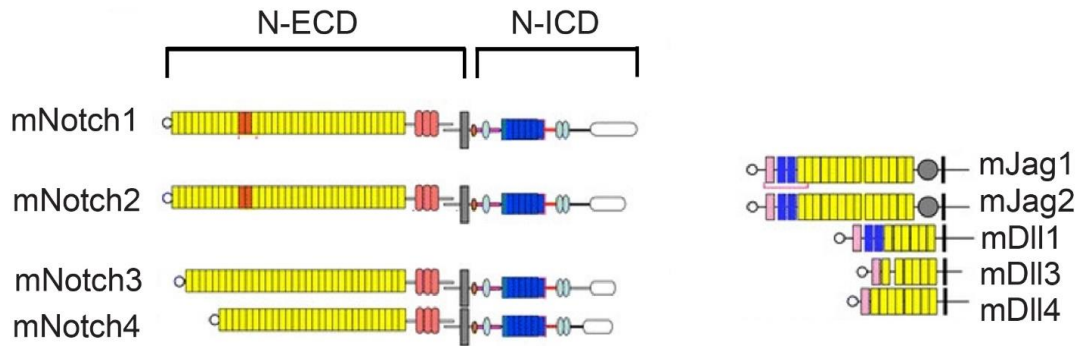


Figure 3.2. Mammalian Notch receptor and ligand families. Notch receptor proteins contain multiple extracellular epidermal growth factor (EGF)-like repeats. Four mammalian Notch receptors differ in the number of repeats. Notch Ligands can be divided into two groups based on their length and subtype of different units. N-ECD – Notch extracellular domain, N-ICD – Notch intracellular domain⁷.

The involvement of mechanical forces is one of the key features of the signaling process. The signaling is initiated by a ligand-receptor interaction followed by the endocytosis of the ligand, this creates a tensile force according to a “lift and cut” model⁵. Thus, mechanical force plays a significant role in the process. One of the first studies on the Notch mechanical force showed that the force involved in the signaling is less than 12 pN⁹. The authors developed a tension gauge tether (TGT) probe, that is irreversibly activated in the presence of molecular tension. Recently, a second generation of TGT probe was designed to detect even lower threshold forces based on nano yoyo¹⁰. The results suggested that the force involved is in the range of 4–12 pN. However, these studies are focused on the interface between the cells and glass surface. Also, the studies are based on the receptor-induced activation of Notch signaling contrary to the belief of “lift and cut” model”. Thus, it is important to quantify the tensile force required at the cell-cell junction and understand the role of ligand in the first step of Notch activation.

3.2 Results and Discussion

3.2.1 Design and characterization the probe

In this study, we have also used FLIM-MDTP (see above section 2.2.1) for studying the Notch activation, which uses fluorescence lifetime of the fluorophores as a read-out. Different CHO (Chinese hamster ovary) cell lines, such as regular CHO cells, CHO-APC cells (expressing green fluorescent protein, GFP), CHO-DLL1 cells (co-expressing GFP & DLL1 ligands) and CHO-JAG1 cells (co-expressing GFP & JAG1 ligand) were used in this project. We first applied the Cy3-modified FLIM-MDTP to test the anchoring efficiency of the probe on to the live cell membrane. We added 100 nM FLIM-MDTP (Cy3) to the CHO cells and significant fluorescence was observed on the membranes after a brief 20 min incubation (Figure 3.3).

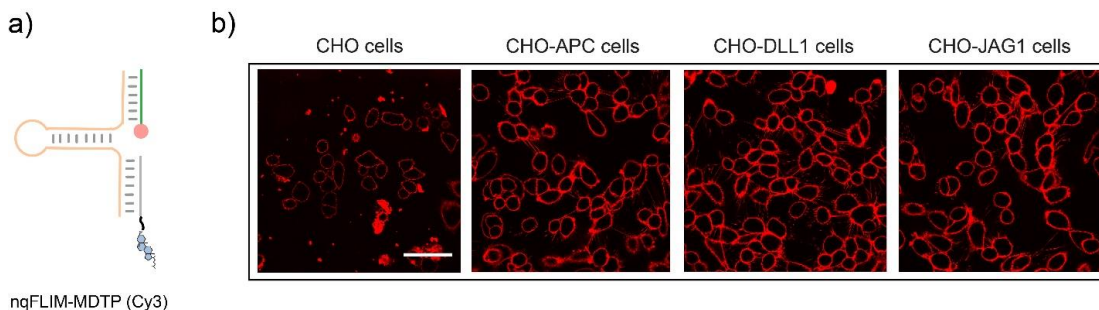


Figure 3.3. Design and anchoring of the probe on the cell membrane. a) Cy3-BHQ2 modified FLIM-based membrane DNA tension probe (MDTP), b) Anchoring of the probe on different CHO cell lines. Scale bar, 50 μm .

After confirming the anchoring of the probe on the cell membrane, our next goal was to use the FLIM-MDTP (Cy3) for quantifying molecular tensions at cell-cell junctions. Thus, we prepared a Notch1-modified FLIM-MDTP (Cy3), named, N1-FLIM-MDTP (Cy3), to quantify Notch1-mediated tensile forces at the cell-cell adhesions. In this regard, a DNA hairpin with 4.4 pN threshold force was used to construct the probe, since

previous data suggested that the force involved in Notch activation is in the range of 4–12 pN (ref). We confirmed the assembly of the probe and Notch-1 modification by a gel electrophoresis assay (Figure 3.4).

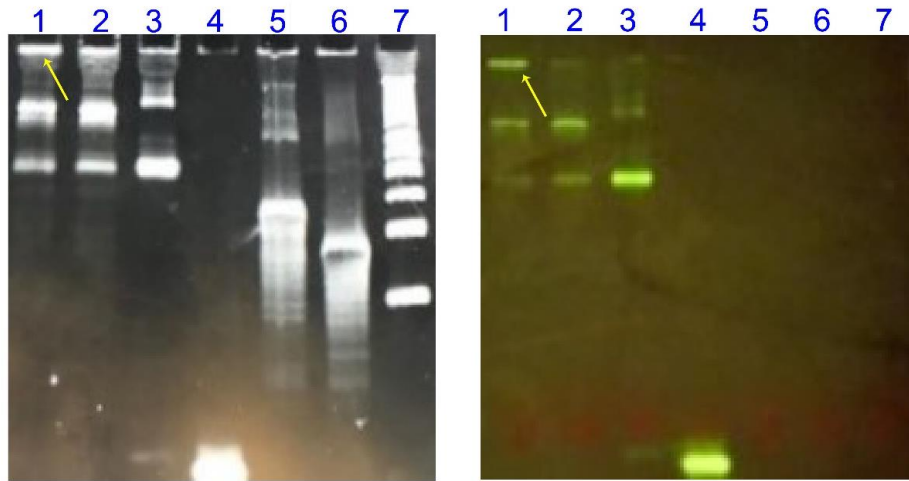


Figure 3.4. Native polyacrylamide gel (10%) characterization of the N1-FLIM-MDTP assembly. The gel was imaged before (right) and after (left) staining with SYBR Gold. Before staining, a blue light was used to visualize Cy3-labeled strands. DNA composition in each lane: 1 - N1-FLIM-MDTP (hairpin strand + anchor strand + Pro G- and Cy3-labelled ligand strand + Fc-Notch1) (10 μ L, 1 μ M), 2 - hairpin strand + anchor strand + Pro G- and Cy3-labelled ligand strand (10 μ L, 1 μ M), 3 - Pro G- and Cy3-labelled ligand strand (2 μ L, 5 μ M), 4 - Cy3-labelled ligand strand (2 μ L, 10 μ M), 5 - hairpin strand (2 μ L, 10 μ M), 6 - anchor strand (2 μ L, 10 μ M), 7 - DNA ladder (20–100 bp, 1 μ L, 10 μ M). The arrow indicating the probe formation.

3.2.2 Quantifying the molecular tension at the cell-cell junction

Our next goal was to visualize the Notch activation at the cell-cell junction. Thus, we created a mixed cell model system for studying the activation. In this case, we have grown the desired cell lines together for overnight, followed by the addition of 100 nM N1-FLIM-MDTP (Cy3). To study the interaction between Notch1 receptor & DLL1 ligand, CHO & CHO-DLL1 cells were mixed together. Accordingly, CHO & CHO-JAG1 cells were mixed to study Notch1-JAG1 forces. As a control, CHO & CHO-APC cells were mixed since CHO-APC cells does not express any Notch ligand. The GFP expression in CHO-DLL1, CHO-JAG1 and CHO-APC cells were used as a marker to locate the desired cell-cell junctions. After the insertion of probes onto cell membranes, we observed a small

change in the lifetime of the probe (0.77 ns to 0.89 ns) for the JAG1 expressing cells, while DLL1 expressing cells showed no significant change in the lifetime (Figure 3.5). To determine the change in the percentage of unfolded probes, we used a previously determined calibration curve¹¹. The results showed that almost 6% of N1-FLIM-MDTP (Cy3) was unfolded for JAG1 expressing cells, while only 1% of the probe was activated for the control APC cells (Figure 3.5). Furthermore, almost no probe unfolding was observed for the DLL1 expressing cells. To further validate the observed experimental results, we performed several trials with the same set-up for the experiments. However, we observed a minimal change in the percentage of unfolded probes in all the trials. We also noted that the variation from day-to-day was significant. This variation in the sample set can be justified by the sensitive behavior of FLIM-based read out when compared to intensity-based measurement. It is known that FLIM is sensitive to the microenvironment of the system, and a minimal change can significantly alter the fluorescence lifetime of the system¹². Thus, we next wanted to design a ratiometric probe, which uses intensity-based measurements as a read-out.

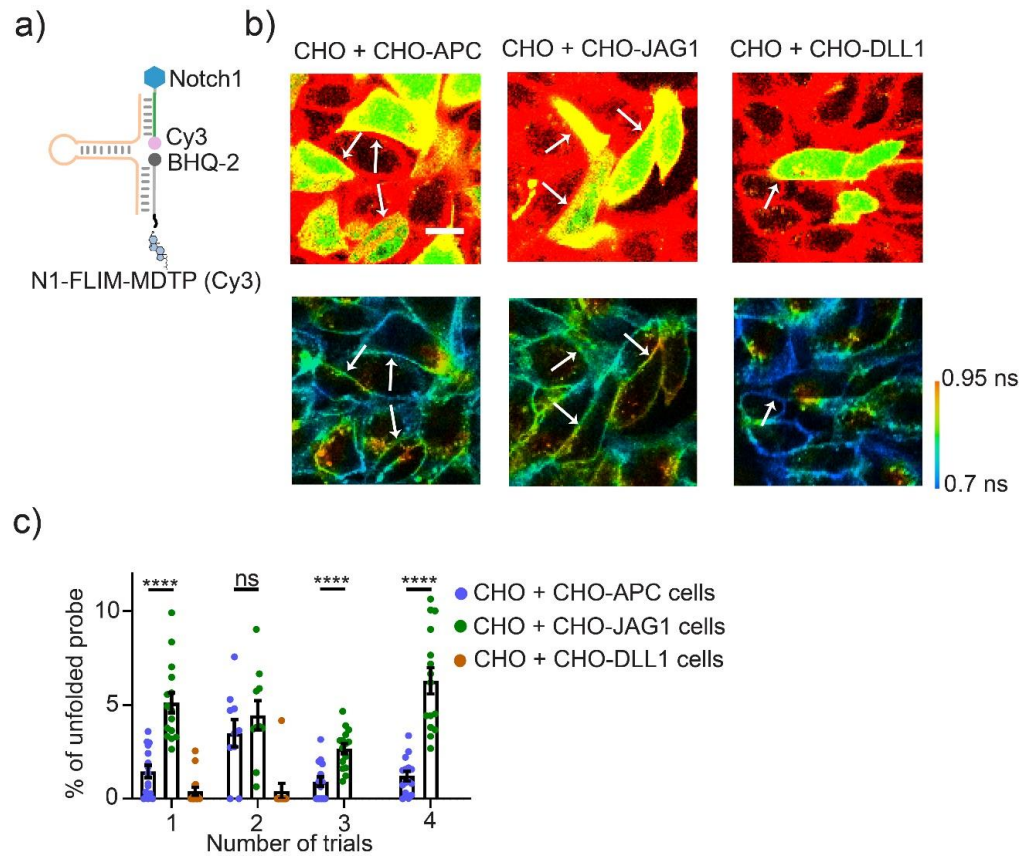


Figure 3.5. Imaging Notch1-mediated tensile forces at the cell-cell junctions with N1-FLIM-MDTP (Cy3). a) Design of N1-FLIM-MDTP (Cy3), b) CHO cells were incubated with control CHO-APC cells or CHO-JAG1 or CHO-DLL1 and 100 nM of N1-FLIM-MDTP (Cy3) was added. Representative images were taken after 30 min of incubation with the probe. Scale bar, 20 μ L. c) Distributions of percentages of the unfolded N1-FLIM-MDTP (Cy3) at each cell-cell junction after different trials. Shown are mean and standard error of the mean (SEM) values from 10–15 junctions in each case. **** $p < 0.0001$ in two-tailed Student's t-test; ns, not significant. Arrows indicated the junctions used for analysis.

In our lab, we have recently developed a DNA-based membrane tension ratiometric probe, named DNAMeter, for quantifying intercellular tensile forces¹³. In this case, two different fluorophores were used together, a reporter fluorophore (Cy3) that reports the mechanical unfolding of the DNA hairpin, and a reference fluorophore (Cy5) that remains non-quenched. The ratio of intensities of these two fluorophores provides a ratiometric read-out and can be used in a quantitative manner since it is concentration independent. Following this design, we engineered a Notch1-modified N1-DNAMeter (Cy3) probe for visualizing Notch1 tension at cell-cell junctions.

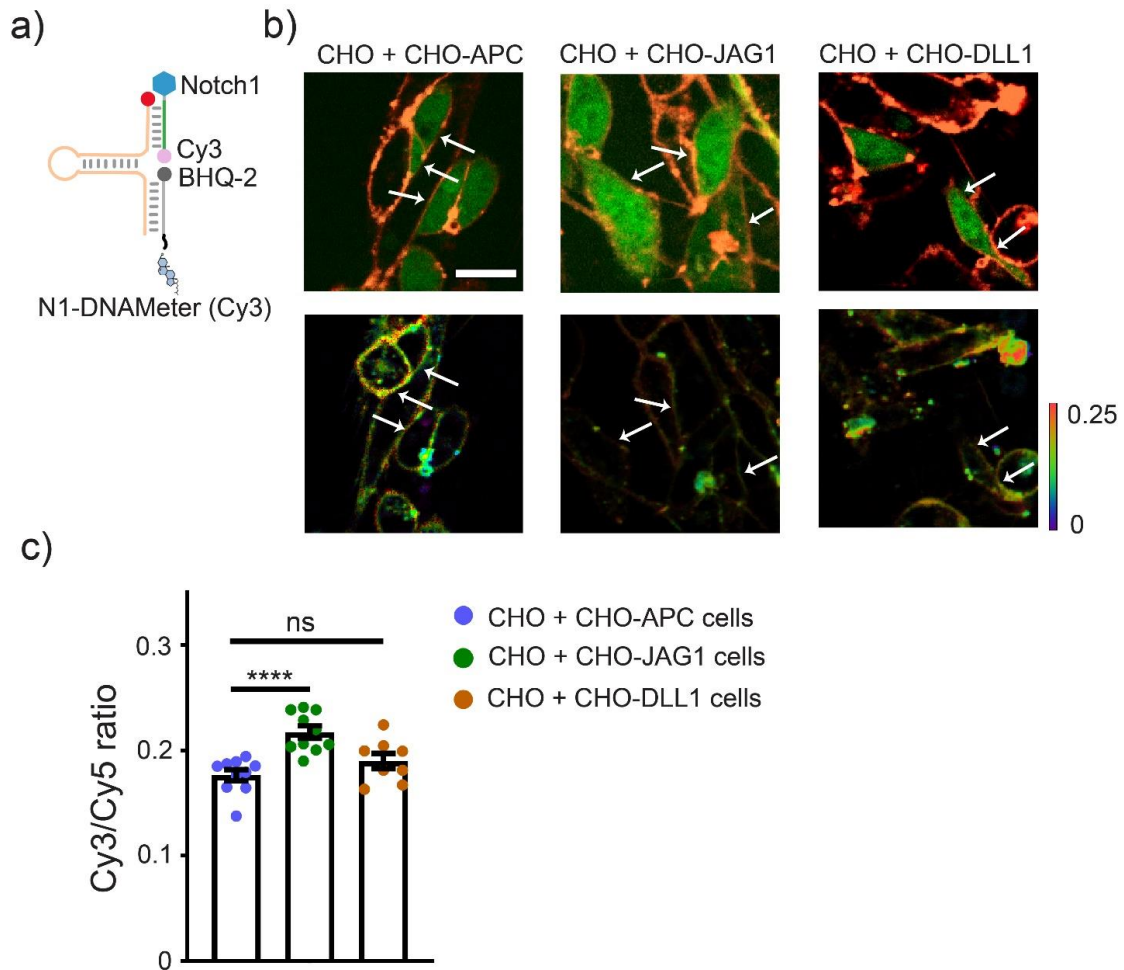


Figure 3.6. Imaging Notch1-mediated tensile forces at the cell–cell junctions with N1-DNAMeter (Cy3). a) Design of N1-DNAMeter (Cy3), b) CHO cells were incubated with control CHO-APC cells or CHO-JAG1 or CHO-DLL1 and 100 nM of N1-DNAMeter (Cy3) was added. Representative images were taken after 30 min of incubation with the probe. Scale bar, 20 μ m. c) Distributions of Cy3/Cy5 ratio at each cell–cell junction after 30 min. Shown are mean and standard error of the mean (SEM) values from 10 junctions in each case. **** $p < 0.0001$ in two-tailed Student’s t-test; ns, not significant. Arrows indicated the junctions used for analysis.

After designing the N1-DNAMeter (Cy3), we incubated 100 nM probe with different CHO cells for 30 min and analyzed the changes in the ratio of Cy3/Cy5. We observed a small change in the ratio for CHO & CHO-JAG1 cells (0.18 to 0.22), compared to the control CHO & CHO-APC cells (Figure 3.6c). Also, CHO & CHO-DLL1 cells did not show any significant change in the ratio. The small change in the ratio indicated a weak activation of N1-DNAMeter (Cy3) by JAG1 ligand compared to the control cell-cell junctions, while no significant activation was observed for DLL1 ligands (Figure 3.6c).

Thus, we hypothesize that the threshold force required for Notch activation was lower than the threshold force of the designed DNA hairpin (4.4 pN) and decided to test a new probe with even lower force threshold.

3.2.3 Designing a low-force-threshold probe for studying Notch activation

To visualize the forces involved in Notch activation, we further designed a new DNA hairpin with a low force threshold. To design this hairpin, the following equations were used to calculate the threshold force¹⁴⁻¹⁵.

$$\Delta G(F, x) = \Delta G_{\text{fold}} + \Delta G_{\text{stretch}} + F \cdot \Delta x \quad (1)$$

Here, $\Delta G(F, x)$ is the overall change in the free energy for the process, ΔG_{fold} is the free energy of unfolding the hairpin at $F=0$, $\Delta G_{\text{stretch}}$ is the free energy of stretching the ssDNA from $F=0$ to $F=F_{1/2}$, F is the externally exerted force, Δx is the hairpin extension.

$$\text{At, } F = F_{1/2}, \Delta G(F, x) = 0, \quad F_{1/2} = -(\Delta G_{\text{fold}} + \Delta G_{\text{stretch}})/\Delta x \quad (2)$$

Using equations (1) & (2), we can obtain the threshold force ($F_{1/2}$) of the DNA hairpin. To design a low-threshold-force probe, we reduced the number of base pairing in the DNA hairpin from 9 to 7 and also eliminated any GC base pairing. The newly designed probe has a $F_{1/2}$ of 2.2 pN (37°C, 140.5 mM Na⁺ and 0.4 mM Mg²⁺), which allows us to detect weaker forces than the previous design (4.4 pN). The Table 3.1 below shows the sequence of the hairpin and its parameters.

Table 3.1 – Hairpin design and force calculation

	DNA sequence (5' - 3')	# of bases in STEM	% GC content	Threshold force ($F_{1/2}$)
Previous design	GTA TAA ATG TTT TTT TCA TTT ATA C	9	22	4.4
New design	AAT AAT TTT TTT TAA TTA TT	7	0	2.2

3.2.4 Quantifying Notch molecular tensions with low-force-threshold design

After designing the new low-threshold-force probe, we wanted to test the probe for visualizing Notch activation. In this regard, we used N1-FLIM-MDTP (0% GC, Cy3) probe (Figure 3.7a). We incubated 100 nM probe with different CHO cells for 30 min and analyzed the changes in the lifetime of Cy3 fluorophore (Figure 3.7b). In this case, we observed a higher probe unfolding since a lower threshold force probe was used (Figure 3.7c). Our analysis of individual junctions showed that the percentage of unfolded probes was indeed higher at CHO/CHO-JAG1 junctions (15.1%) than that at control CHO/CHO-APC cell junctions (10.5%). The new design of low-force-threshold probe can indeed enable more reliable detection of weak tensile forces at cell-cell junctions.

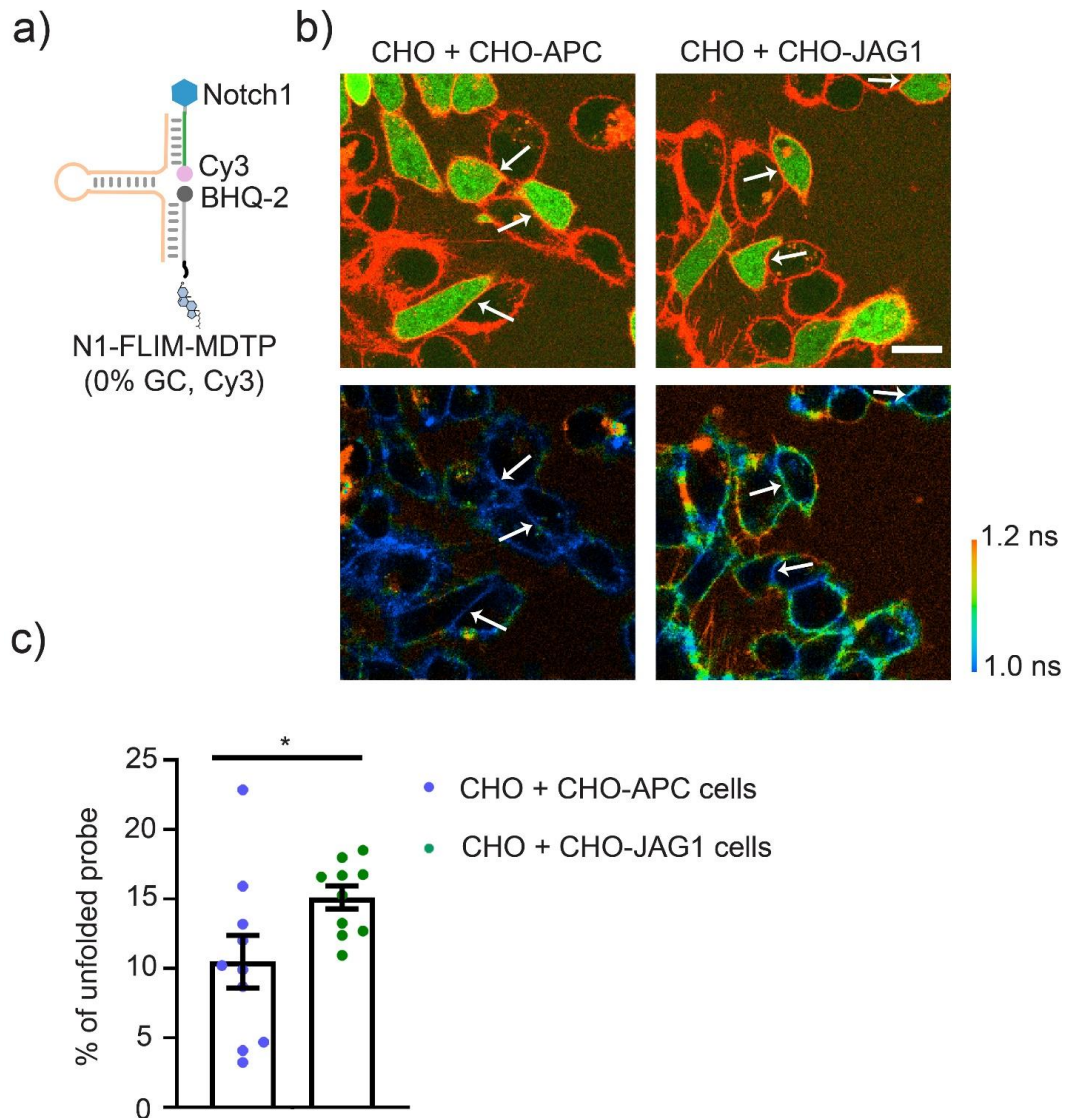


Figure 3.7. Imaging Notch1-mediated tensile forces at cell-cell junctions with N1-FLIM-MDTP (0 % GC, Cy3). a) Design of N1-FLIM-MDTP (0% GC, Cy3), b) CHO cells were incubated with control CHO-APC cells or CHO-JAG1 or CHO-DLL1, and then 100 nM of N1-FLIM-MDTP (0% GC, Cy3) was added. Representative images were taken after 30 min of incubation with the probe. Scale bar, 20 μm. c) Distributions of the percentage of unfolded N1-FLIM-MDTP (0% GC, Cy3) probes at individual cell-cell junction. Shown are mean and standard error of the mean (SEM) values from 10 junctions in each case. * $p < 0.05$ in two-tailed Student's t-test. Arrows indicated the junctions used for analysis.

3.2.5 Studying receptor-induced Notch activation

The “lift and cut” model of Notch signaling is well accepted in the literature⁵. However, there are also other models, which are used to explain each step in the signaling process¹⁶. For example, the origin of forces in the first step of activation is often debated. In this regard, both ligand-induced and receptor-induced forces have been proposed in the

literature¹⁷⁻¹⁸. Previous results have suggested that Notch1-expressing cells can pull on the DLL1 ligands to activate Notch signaling⁹⁻¹⁰. Thus, we wanted to also explore the receptor-mediated mechanical activation of the probes by conjugating DLL1 or JAG1 ligand on the probe and visualizing Notch1-expressing cell-induced forces. In this case, we choose to study CHO-K1 cells, which co-express the Notch1 receptor and mTurq2, a citrine reporter for Notch signaling¹⁹. The citrine reporter allows us to visualize the Notch signaling after the initial step of Notch activation.

We first wanted to validate if we can visualize the Notch signaling after activation. In this regard, we co-incubated Notch1-expressing CHO-K1 cells with JAG1-expressing CHO-JAG1 cells (Figure 3.8a). As a control, we incubated the CHO-K1 cells with CHO cells. After analyzing the fluorescence intensities of the citrine reporter from the CHO-K1 cells, we observed a ~2-fold increase in the fluorescence of the cells co-incubated with CHO-JAG1 cells compared to those with the control cells (Figure 3.8b). These results confirmed that the citrine reporter can be activated in the presence of Notch ligand.

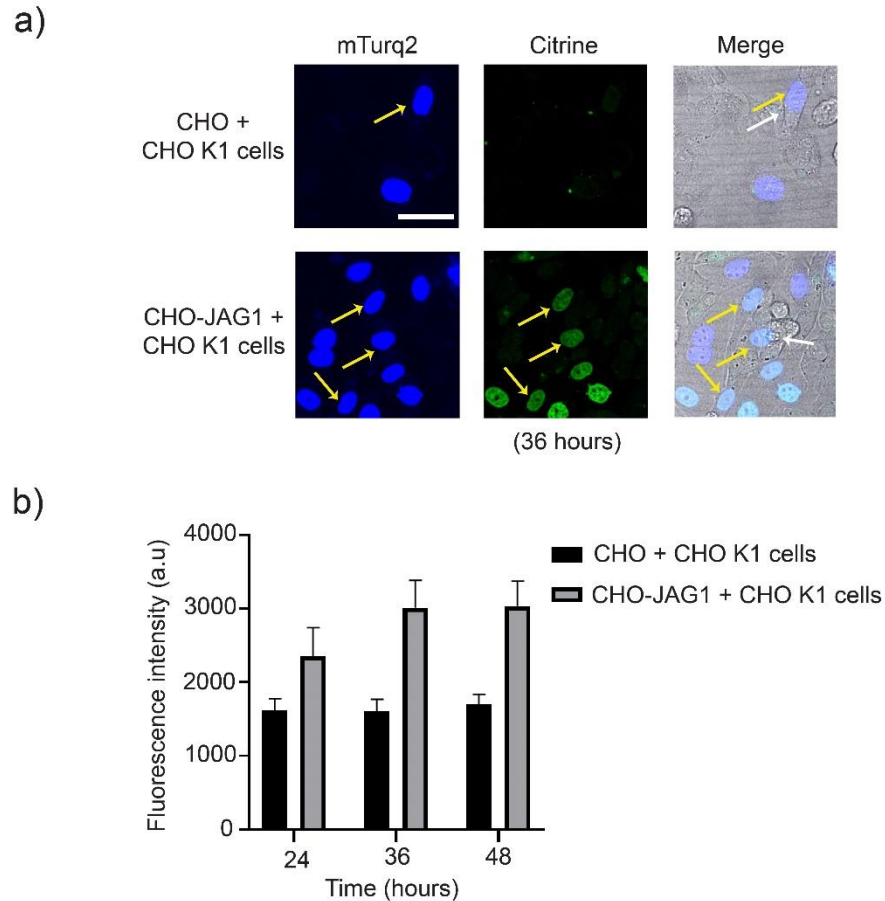


Figure 3.8. Studying Notch signaling with a citrine reporter. a) CHO-K1 and CHO-JAG1 or control CHO cells were incubated together for different period of time. Representative images were taken after 36 h of incubation. Scale bar, 50 μ m. b) Fluorescence intensity of the citrine reporter from CHO-K1 cells are recorded and plotted after different period of time. Shown are mean and standard error of the mean (SEM) values from 20–30 cells in each case. Yellow arrows indicate the CHO-K1 cells and white arrows indicate control CHO cells in the top panel (or CHO-JAG1 cells in the bottom panel).

3.3 Conclusion

Notch signaling plays crucial role in controlling cellular process, and its ability to carry out multiple tasks in a simplified manner makes it interesting. It is known in the literature that mechanical cues can affect cancer cells and decide the fate of the cells²⁰⁻²¹. The tensile force plays a key role in this process, and thus it is important to measure these tensile forces between Notch receptors and ligands. In this study, we have designed a DNA-based probe, which allows us to study the first step of Notch signaling. Finally, with the

current design of low-threshold-force probe, we were able to visualize weak tension in the presence of JAG1 ligands. However, DLL1 ligands did not show any obvious activation of the probe. It is worth mentioning that currently, we still have quite minimal understanding about different mechanical features of different Notch ligand-receptor pairs. These DNA-based probes may potentially allow us to understand the inherent mechanical selectivity of the Notch receptors towards different types of ligands. Our results further suggested that the forces involved in these Notch1-DLL1 and Notch1-JAG1 interaction processes are at a quite low level. Thus, more robust probes need to be developed in the future, which can more reliably detect the small forces required for the Notch activation.

The role of Notch ligands in the Notch signaling process is also currently under debate, especially regarding the generation of forces⁶. Our DNA-based probe can also potentially provide a simple approach to explore the mechanistic aspect of the Notch activation. Equipped with a citrine reporter, our current Notch cell system permits us to visualize and validate the Notch signaling in living cells. We believe soon better understanding of the mechanical mechanism of Notch activation will be potentially solved with the help of these DNA-based probes.

3.4 Materials and Methods

3.4.1 Reagents:

Unless specified, all the chemicals were purchased from Sigma or Fisher Scientific and directly used without further purification. Fluorophore-labelled DNA strands were ordered from Integrated DNA Technology and Yale Keck Oligonucleotide Synthesis. The sequences of DNA strands are listed below in Table 3.2.

3.4.2 Cell culture, imaging, and data analysis:

CHO cells were cultured in a RPMI medium (HyClone, SH3025501) supplemented with 10% FBS, 100-unit penicillin with 0.1 mg/mL streptomycin (Gibco, 15140-122), 1 mM sodium pyruvate, 2 mM L-glutamine (HyClone, SH30034.01), and 1.7 μ L ethanethiol. These cells were split at 80% confluence and plated at a density of 20% following standard cell culture procedures. FLIM-based images were acquired on a Nikon Eclipse TiE inverted microscope with A1 spectral detector confocal and FLIM/FCS module. A 60x oil immersion objective was used for imaging. During imaging, the field of view was first found and focused using the scanning confocal capability of the microscope. The input laser was then changed to the pulsed laser that was synched with the FLIM system and the emitted photons were detected through a Becker-Hickl SPC-152/HPM-100-40 dual detector system (Boston Electronics). The Cy3-modified probes were excited at 50 MHz frequency with a 561 nm laser line, respectively. Data acquisition and analysis were performed with a Becker-Hickl TCSPC software package. Ratiometric images were collected with a NIS-Elements AR software using a Yokogawa spinning disk confocal on a Nikon Eclipse-TI inverted microscope. Cy3 fluorophore was excited with a 561 nm laser line. 60 \times oil immersion objective was used. Raw data was then further processed using the Origin and GraphPad Prism software.

3.4.3 Synthesis of Protein G-modified DNA strands:

The Protein G-modified DNA ligand strand was synthesized by mixing 20 μ L of DNA ligand strand (200 μ M) with 10 μ L of 100 mM TCEP in HEPES buffer containing 50 mM EDTA at pH 7.2. After 2 h incubation at room temperature to reduce the disulfide bond, excess TCEP was removed using a Bio-Spin 6 column (Bio-Rad). Then, 1.5 μ L of

23 mM freshly prepared sulfo-SMCC was immediately added and incubated at room temperature for 1 min. Afterwards, 10 μ L of 5 mg/mL Protein G was added and incubated at 4 °C for overnight. The synthesized Protein G-DNA conjugates were then purified with cobalt-based Dynabeads (Invitrogen, 10103D) through their specific interaction with poly-histidine-tagged proteins. Isolated his-tagged proteins are further eluted from the beads with his elution buffer. After exchanging and concentrating the sample into a DPBS buffer, the concentrations of Protein G-modified DNA strands were quantified with a Nanodrop One UV/Vis spectrometer.

3.4.4 Preparation of the N1-FLIM-MDTP (N1-DNAMeter):

To prepare the N1-FLIM-MDTP (N1-DNAMeter), 10 μ M anchor strand and hairpin strand was first mixed DPBS buffer (Gibco, 14190-144) at pH 7.0–7.3. The mixture was then denatured for 5 min at 75 °C and slowly annealed back to the room temperature at a rate of 1.3 °C/min in an Eppendorf Thermomixer. Afterwards, the solution was incubated with the Protein G-modified ligand strand at 1:1 ratio at 4 °C for overnight. This assembly was then mixed with equimolar of IgG/Fc-fused human Notch1 Protein (Sino Biological, 10954-H02H) at room temperature for 15 min and kept at 4 °C for overnight before usage.

3.4.5 Imaging of intercellular tensile forces:

For imaging Notch-1-mediated tensile forces in CHO cells, ~10,000 cells were seeded with equal proportion of CHO-JAG1 or CHO-DLL1 or control CHO-APC cells in an 8-well chamber cover glass system (Cellvis) and grown overnight (16 h). After washing thrice with DPBS-buffered saline, 100 nM pre-assembled N1-FLIM-MDTP (or N1-DNAMeter) was added and incubated for 30 min before imaging.

Table 3.2 – DNA sequences used for this chapter

Name	DNA sequence (5'-3')
Hairpin strand - 1 (22% GC)	TCG AAG CAA GTG TGA GGA CTC TTT <u>GTA TAA ATG TTT TTT TCA TTT ATA CTT</u> TGC TGG GCT ACG TGG CGC TCT T
Reference hairpin strand - 1 (22% GC)	Cy5-TCG AAG CAA GTG TGA GGA CTC TTT <u>GTA TAA ATG TTT TTT TCA TTT ATA</u> <u>CTT</u> TGC TGG GCT ACG TGG CGC TCT T
Ligand strand	Cy3-GAG TCC TCA CAC TTG CTT CGA TTT-SH
Anchor strand	Cholesterol-CCC AAG AGC GCC ACG TAG CCC AGC-BHQ2
nqAnchor strand	Cholesterol-CCC AAG AGC GCC ACG TAG CCC AGC
Hairpin strand – 2 (0 % GC)	TCG AAG CAA GTG TGA GGA CTC TTT <u>AAT AAT TTT TTT TAA TTA TTT TTG CTG</u> GGC TAC GTG GCG CTC TT

Underlined sequences indicate the stem and loop region of the force-sensing DNA hairpin module.

3.5 References

1. Hori, K.; Sen, A.; Artavanis-Tsakonas, S., Notch signaling at a glance. *J Cell Sci* **2013**, *126* (Pt 10), 2135-40.
2. Shen, W.; Huang, J.; Wang, Y., Biological Significance of NOTCH Signaling Strength. *Front Cell Dev Biol* **2021**, *9*, 652273.
3. Marracino, L.; Fortini, F.; Bouhamida, E.; Camponogara, F.; Severi, P.; Mazzoni, E.; Patergnani, S.; D'Aniello, E.; Campana, R.; Pinton, P.; Martini, F.; Tognon, M.; Campo, G.; Ferrari, R.; Vieceli Dalla Sega, F.; Rizzo, P., Adding a "Notch" to Cardiovascular Disease Therapeutics: A MicroRNA-Based Approach. *Front Cell Dev Biol* **2021**, *9*, 695114.

4. Bray, S. J., Notch signalling in context. *Nat Rev Mol Cell Biol* **2016**, *17* (11), 722-735.
5. Kopan, R.; Ilagan, M. X., The canonical Notch signaling pathway: unfolding the activation mechanism. *Cell* **2009**, *137* (2), 216-33.
6. D'Souza, B.; Miyamoto, A.; Weinmaster, G., The many facets of Notch ligands. *Oncogene* **2008**, *27* (38), 5148-67.
7. Kopan, R.; Chen, S.; Liu, Z., Alagille, Notch, and robustness: why duplicating systems does not ensure redundancy. *Pediatr Nephrol* **2014**, *29* (4), 651-7.
8. Nandagopal, N.; Santat, L. A.; LeBon, L.; Sprinzak, D.; Bronner, M. E.; Elowitz, M. B., Dynamic Ligand Discrimination in the Notch Signaling Pathway. *Cell* **2018**, *172* (4), 869-880 e19.
9. Wang, X.; Ha, T., Defining single molecular forces required to activate integrin and notch signaling. *Science* **2013**, *340* (6135), 991-4.
10. Chowdhury, F.; Li, I. T.; Ngo, T. T.; Leslie, B. J.; Kim, B. C.; Sokoloski, J. E.; Weiland, E.; Wang, X.; Chemla, Y. R.; Lohman, T. M.; Ha, T., Defining Single Molecular Forces Required for Notch Activation Using Nano Yoyo. *Nano Lett* **2016**, *16* (6), 3892-7.
11. Keshri, P.; Zhao, B.; Xie, T.; Bagheri, Y.; Chambers, J.; Sun, Y.; You, M., Quantitative and Multiplexed Fluorescence Lifetime Imaging of Intercellular Tensile Forces. *Angew Chem Int Ed Engl* **2021**, *60* (28), 15548-15555.
12. Datta, R.; Heaster, T. M.; Sharick, J. T.; Gillette, A. A.; Skala, M. C., Fluorescence lifetime imaging microscopy: fundamentals and advances in instrumentation, analysis, and applications. *J Biomed Opt* **2020**, *25* (7), 1-43.

13. Zhao, B.; Li, N.; Xie, T.; Bagheri, Y.; Liang, C.; Keshri, P.; Sun, Y.; You, M., Quantifying tensile forces at cell-cell junctions with a DNA-based fluorescent probe. *Chem Sci* **2020**, *11* (32), 8558-8566.
14. Woodside, M. T.; Behnke-Parks, W. M.; Larizadeh, K.; Travers, K.; Herschlag, D.; Block, S. M., Nanomechanical measurements of the sequence-dependent folding landscapes of single nucleic acid hairpins. *Proc Natl Acad Sci U S A* **2006**, *103* (16), 6190-5.
15. Zhang, Y.; Ge, C.; Zhu, C.; Salaita, K., DNA-based digital tension probes reveal integrin forces during early cell adhesion. *Nat Commun* **2014**, *5*, 5167.
16. Steinbuck, M. P.; Winandy, S., A Review of Notch Processing With New Insights Into Ligand-Independent Notch Signaling in T-Cells. *Front Immunol* **2018**, *9*, 1230.
17. Gordon, W. R.; Zimmerman, B.; He, L.; Miles, L. J.; Huang, J.; Tiyanont, K.; McArthur, D. G.; Aster, J. C.; Perrimon, N.; Loparo, J. J.; Blacklow, S. C., Mechanical Allostery: Evidence for a Force Requirement in the Proteolytic Activation of Notch. *Dev Cell* **2015**, *33* (6), 729-36.
18. Gordon, W. R.; Vardar-Ulu, D.; Histén, G.; Sanchez-Irizarry, C.; Aster, J. C.; Blacklow, S. C., Structural basis for autoinhibition of Notch. *Nat Struct Mol Biol* **2007**, *14* (4), 295-300.
19. Sprinzak, D.; Lakhanpal, A.; Lebon, L.; Santat, L. A.; Fontes, M. E.; Anderson, G. A.; Garcia-Ojalvo, J.; Elowitz, M. B., Cis-interactions between Notch and Delta generate mutually exclusive signalling states. *Nature* **2010**, *465* (7294), 86-90.

20. Jain, R. K.; Martin, J. D.; Stylianopoulos, T., The role of mechanical forces in tumor growth and therapy. *Annu Rev Biomed Eng* **2014**, *16*, 321-46.
21. Northcott, J. M.; Dean, I. S.; Mouw, J. K.; Weaver, V. M., Feeling Stress: The Mechanics of Cancer Progression and Aggression. *Front Cell Dev Biol* **2018**, *6*, 17.

CHAPTER 4

MEASURING CD40-INDUCED PULLING FORCES IN B CELL WITH DNA-BASED MEMBRANE TENSION RATIOMETRIC PROBE (DNAMETER)

4.1 Introduction

B cell lymphomas play a crucial role in the immune system, they take part in triggering antibody responses, and participate in the activation of T cells and B cell receptor signaling¹⁻³. Naive B cells interact with T cells, which is followed by the maturation of antibodies and generation of memory B cells. In germinal centers (GCs), B cells are highly motile, and can form contact with follicular dendritic cells (FDCs) that contain antigens on the surface⁴⁻⁵. The affinity maturation of B cells depends on their ability of extracting antigens from the surface of FDCs. These extraction interactions are known to depend on the conserved biomechanical components and the pulling forces involved⁶⁻⁷. We hypothesize that dysregulations in these mechanical interactions have been shown to impact the downstream B cell signaling, epigenetics, etc. These mechanical dysregulations can also drive the cancerous transformation of B cells by impairing their ability to extinguish pseudo-malignant phenotype of GC B cells. As a result, it is important to understand the mechanical features of B cell immunoreceptors.

CD40 is an important immunoreceptor presented on the B cells, which get involved in the activation of antigen-presenting cells (Figure 4.1)⁸. The CD40 pathway is essential for the survival of different cell types. It also plays a crucial role in mediating a variety of immune and inflammatory responses⁹⁻¹¹. The CD40 ligand (CD40L) on T follicular helper

cells can bind with these CD40 receptors to activate the CD40 signaling¹²⁻¹³. Our hypothesis is, pulling forces exist during the CD40 ligand-receptor interactions, forming a weak catch-slip bond is formed between the CD40 receptor and ligand. Depending on the extent of forces, the mechanical forces involved could either shorten (slip bond) or prolong (catch bond) the bond lifetimes¹⁴. Most of these mechanical measurements were performed at cell-matrix interface, there is limited knowledge about the extent and contribution of mechanical forces involved at the real T cell-B cell junctions. Thus, it is important to measure CD40-induced pulling forces in B cells and to understand their downstream effects in the pathways such as generating pro-apoptotic and anti-apoptotic proteins and activating canonical and non-canonical NF κ B pathways¹⁵.

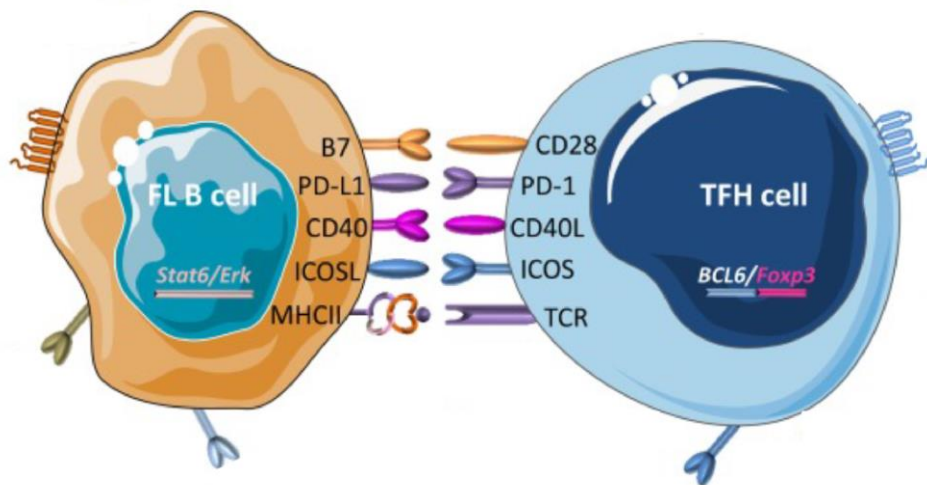


Figure 4.1. Key intercellular molecular interactions between follicular lymphoma B cells and follicular helper T cells. Adapted from ref¹³.

4.2 Results and Discussion

4.2.1 Selective labeling of Jurkat cells

To study if different types of B cell surface CD40 receptors can induce different levels of tensile forces onto T cells, we used two types of B cells, including LY-3 cells

(wild type - early-stage lymphoma) and WSU cells (mutant version - diffused large B cell lymphoma). Jurkat cells were used as a T cell model and were membrane anchored with probes. To measure intercellular forces, Jurkat cells are mixed with LY-3 and WSU cells. In this regard, it is very important to identify the cell junctions where two different cells (B cells and T cells) are interacting with each other. However, the lipid-mediated anchoring of the DNA probe is not specific for a cell type, thus we decided to pre-label Jurkat cells with a cell tracker dye, 7-amino-4-chloromethylcoumarin¹⁶, to distinguish these Jurkat cells from B cells in the cell mixture. In this experiment, Jurkat cells were first incubated with 2.5 μ M cell tracker dye and then washed twice with DPBS buffer to remove the excess dye. Afterwards, 100 nM DNAMeter (FAM) (structure as shown in Figure 4.2a) was added and incubated for 30 min. After removing excess probes by washing twice with DPBS buffer, LY-3 or WSU cells were added. As shown in Figure 4.2b, cell tracker dye can specifically label the Jurkat cells, which can be used for identifying the cell junctions between Jurkat and B cells. These images also showed that following this protocol, minimal amount of the DNAMeter probes was anchored on the B cells as compared to the Jurkat cells.

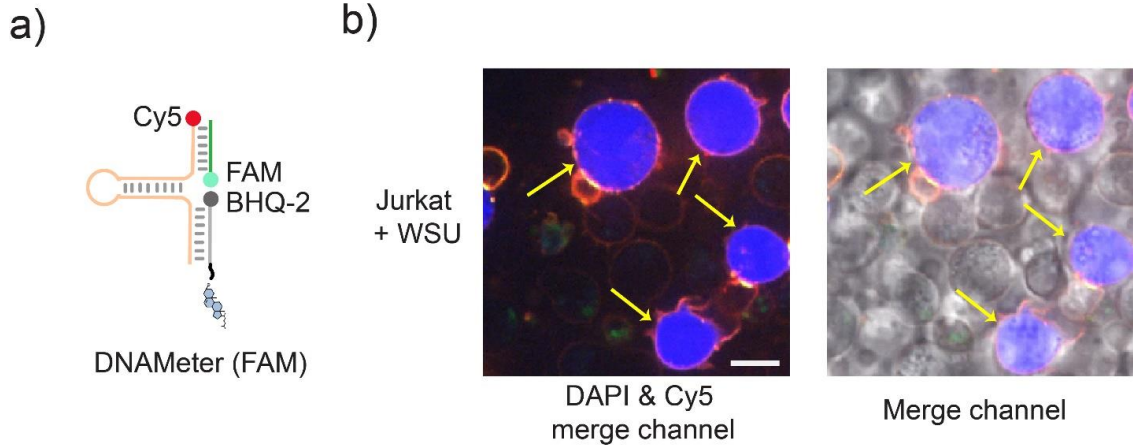


Figure 4.2. Labeling of Jurkat cells with a cell tracker dye. a) Design of the DNAMeter (FAM), b) Selective anchoring of the probe on Jurkat cells, which was labeled with a cell tracker dye (blue). Scale bar, 10 μm . Yellow arrows indicate the Jurkat cells.

4.2.2 Design and characterization the probe

After confirming that Jurkat cells can be labelled with the cell tracker, our next goal was to use the DNAMeter for visualizing and quantifying molecular tensions at cell–cell junctions. Here, we prepared a CD40L-modified DNAMeter probe, named “CD40L-DNAMeter (FAM)”, which has a FAM/BHQ-2 pair as the reporter of forces and a Cy5 dye as the reference to normalize cell membrane probe concentrations. The FAM-to-Cy5 fluorescence ratio can be used to quantify CD40-mediated tensile forces at the T cell–B cell adhesions. In this regard, a DNA hairpin with 4.4 pN threshold force was used to construct the probe. The successful assembly of the CD40L-modified DNAMeter probe was confirmed by a gel electrophoresis assay (Figure 4.3).

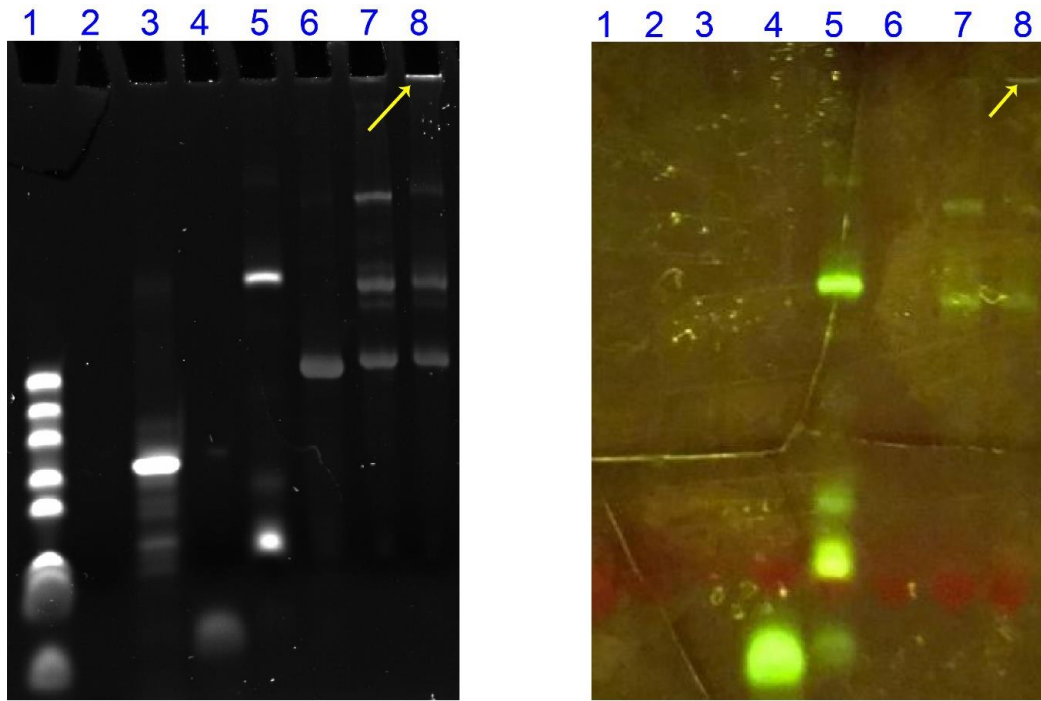


Figure 4.3. Native polyacrylamide gel (10%) characterization of the CD40L-DNAMeter (FAM) assembly. The gel was imaged before (right) and after (left) staining with SYBR Gold. Before staining, a blue light was used to visualize FAM-labeled strands. DNA composition in each lane: 1 - DNA ladder (20-100 bp, 1 μ L, 10 μ M), 2 - anchor strand labelled with eclipse quencher (2 μ L, 10 μ M - Eclipse quencher is quenching the band intensity), 3 - hairpin strand (2 μ L, 10 μ M), 4 - FAM-labelled ligand strand (2 μ L, 10 μ M), 5 - Pro G- and FAM-labelled ligand strand (2 μ L, 5 μ M), 6 - hairpin strand + anchor strand (2 μ L, 10 μ M), 7 - hairpin strand + anchor strand + Pro G- and FAM-labelled ligand strand (10 μ L, 1 μ M), 8 - CD40L-DNAMeter (FAM) (hairpin strand + anchor strand + Pro G- and FAM-labelled ligand strand + Fc-CD40L) (10 μ L, 1 μ M). Arrow indicates the formation of the product.

4.2.3 Imaging and quantifying molecular tensions at the cell-cell junctions

Our next goal was to visualize the mechanical forces at the T cell–B cell junctions. In our system, the WSU and LY-3 cells were respectively mixed with the CD40L-DNAMeter (FAM)-modified Jurkat cells. After the addition of these B cells, both FAM and Cy5 fluorescence was measured on the Jurkat cell membranes at different time points. However, a very low FAM fluorescence intensity and FAM/Cy5 ratiometric signal was observed, which indicated that the DNAMeter probes mostly remained in the folded state. We hypothesized that there may be two main reasons for these weak force signals between

the CD40 ligand and receptor: the duration of the forces is too short, and/or the intensity of the forces are mostly below 4 pN.

We hypothesize that CD40 ligand-receptor interactions are transient in nature, and force-dependent interactions would have a short lifetime. Thus, it is challenging to detect these interactions, especially considering the reversible nature of the DNAMeter-based probes. To overcome this limitation, we decided to apply a locking strand strategy as reported in the literature¹⁷. In this case, an additional DNA strand is added to the cells, which converts the DNAMeter probes into an irreversible state. This additional locking strand can hybridize with tension-induced transiently unfolded probes and lock them in the unfolded state (Figure 4.4a). As a result, it allows the imaging of mechanically activated probes for a longer duration.

A 17-nucleotide-long DNA locking strand was designed here to hybridize with the mechanically unfolded CD40L-DNAMeter (FAM) probes. Again, the WSU/Jurkat and LY-3/Jurkat cell mixture was used respectively to study mechanical forces between B cells and T cells. Indeed, after adding the locking strand, a 2.4-fold and 2.7-fold increase in the FAM/Cy5 ratiometric signals was observed at the WSU/Jurkat and LY-3/Jurkat cellular junctions, respectively, as compared to that on the membranes of non-junction WSU or LY-3 cells (Figure. 4.4). These results indicated that the use of CD40L-DNAMeter (FAM), together with a locking strand, allows the visualization of mechanical forces at T cell-B cell junctions.

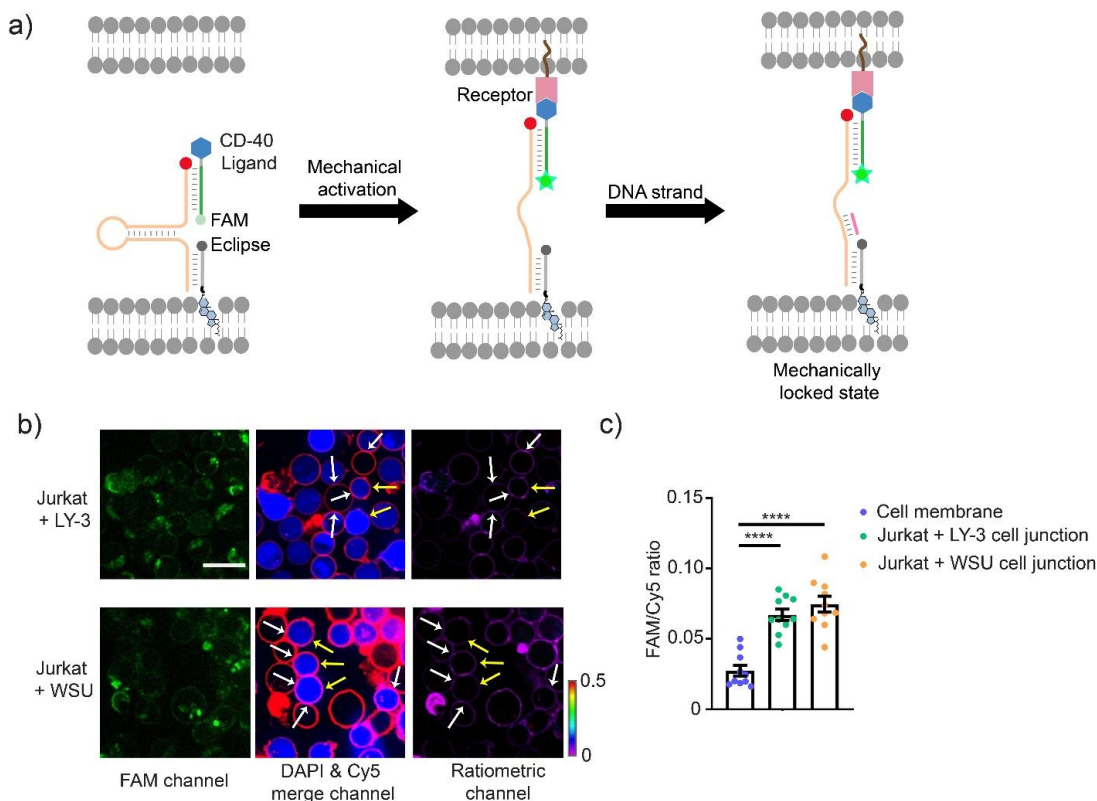


Figure 4.4. Imaging CD40-mediated tensile forces at cell-cell junctions with a CD40L-DNAMeter (FAM) and locking strand. a) Schematic of detecting transient forces with a locking strand and CD40L-DNAMeter (FAM). b) Jurkat cells were first incubated with 100 nM of CD40L-DNAMeter (FAM) and then LY-3 or WSU cells were added, followed by the addition of 1 μ M of locking strands. Representative images were taken after 15 min of incubation with the locking strand. Scale bar, 20 μ m. Yellow arrows indicated the Jurkat cells and white arrows indicated the junctions used for analysis in panel c. c) Distributions of FAM/Cy5 ratiometric signal from CD40L-DNAMeter (FAM) at individual cell-cell junctions. Shown are mean and standard error of the mean (SEM) values from 10 junctions in each case. **** p < 0.0001 in two-tailed Student's t-test.

Even with the help of the locking strand, the low fluorescence intensity in the FAM channel was still a problem, which cannot be solved by simply increasing the laser power of the microscope or using longer exposure time. To test if other reporter fluorophores can result in improved fluorescence intensity, we designed another DNAMeter probe with Cy3/BHQ-2 as a reporter/quencher pair, termed as CD40L-DNAMeter (Cy3). Interestingly, a much higher fluorescence intensity was observed in the Cy3 reporter channel, as well as a higher Cy3/Cy5 ratiometric signal (Figure 4.5b). However, a less significant change in Cy3/Cy5 ratio at both WSU/Jurkat (1.4-fold) and LY-3/Jurkat (1.8-

fold) cell junctions was observed in this case (Figure. 4.5c). These small changes in the ratiometric signal indicated a weak mechanotransduction at these T cell-B cell junctions. While the results from both CD40L-DNAMeter (Cy3) and CD40L-DNAMeter (FAM) showed that a slightly stronger activation of the DNAMeter probe was observed at the LY-3/Jurkat junctions as compared to that in the case of WSU/Jurkat.

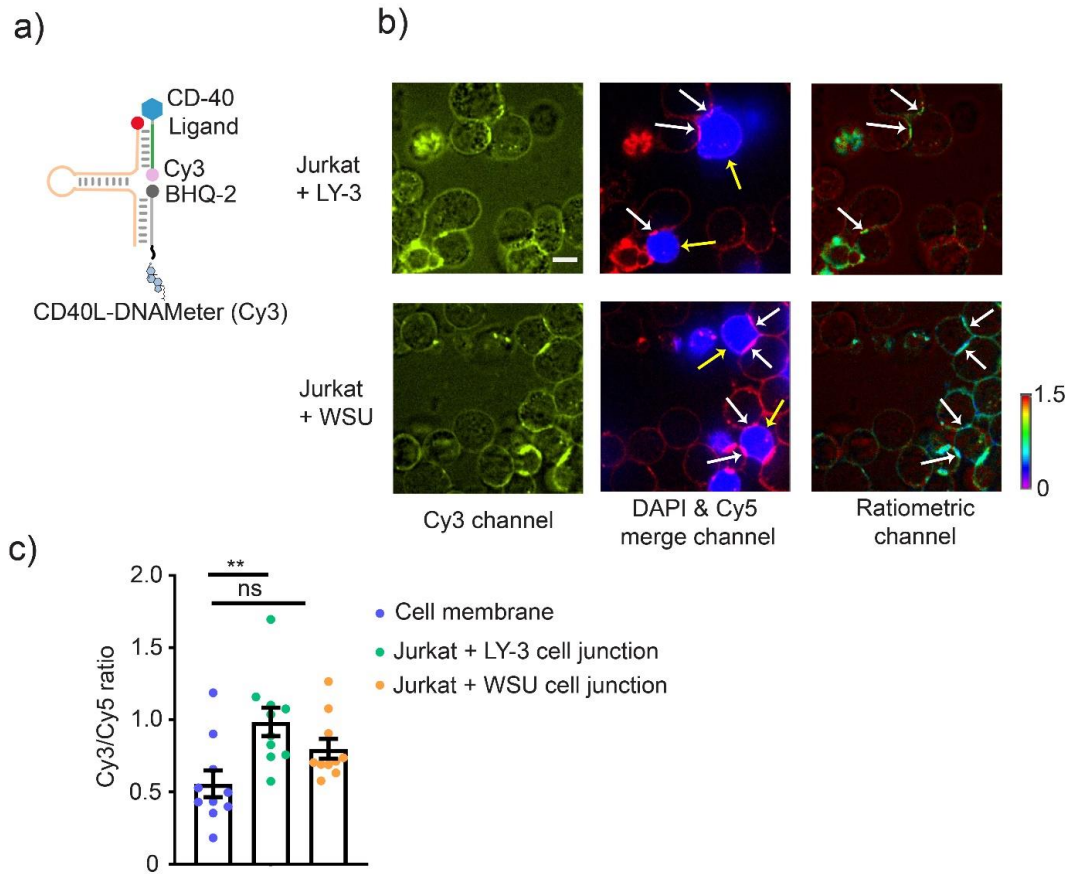


Figure 4.5. Imaging CD40-mediated tensile forces at the cell-cell junctions with CD40L-DNAMeter (Cy3). a) Design of CD40L-DNAMeter (Cy3). b) Jurkat cells were first incubated with 100 nM of CD40L-DNAMeter (Cy3) and then LY-3 or WSU cells were added. Representative images were taken after 15 min of incubation with the cells. Scale bar, 20 μ m. Yellow arrows indicated the Jurkat cells and white arrows indicated the junctions used for analysis in panel c. c) Distributions of Cy3/Cy5 ratiometric signal from CD40L-DNAMeter (Cy3) at individual cell-cell junction. Shown are mean and standard error of the mean (SEM) values from 10 junctions in each case. ** $p < 0.01$ in two-tailed Student's t-test; ns, not significant.

4.3 Conclusion

CD40 signaling is crucial in cell biology, with functions from activating antigen presenting T cells to activating secondary signals of macrophage¹⁸. The role of mechanical forces in these processes is still an open question now. In this work, we have designed DNAMeter-based probes to visualize and quantify the forces involved in CD40 ligand-receptor interactions at T cell-B cell junctions. With the help of a cell tracker dye, a model cell mixture system was optimized for studying these intercellular mechanical events with minimal DNA probe insertion on the B cell membranes. In addition, a locking strand strategy was used to stabilize transient force-induced unfolding of the DNAMeter probes. Our results indicated a weak mechanical interaction via CD40L in both LY-3/Jurkat & WSU/Jurkat cell system, while a relatively stronger mechanical force was shown at LY-3/Jurkat cell junctions than that at WSU/Jurkat junctions.

We expect that a low-threshold-force hairpin design as discussed earlier in Section 3.2.3 can also be potentially useful here to image these low-level mechanical forces. The development of these next-generation probes may allow more reliable detection of the mechanical forces involved in the CD40 receptor-ligand interactions.

4.4 Materials and Methods

4.4.1 Reagents:

Unless specified, all the chemicals were purchased from Sigma or Fisher Scientific and directly used without further purification. Fluorophore-labelled DNA strands were ordered from Integrated DNA Technology and Yale Keck Oligonucleotide Synthesis. The sequences of DNA strands are listed below in Table 4.1.

4.4.2 Cell culture, imaging, and data analysis:

Jurkat, WSU, and LY-3 cells were cultured in a RPMI medium (HyClone, SH3025501) supplemented with 10% FBS, 100-unit penicillin with 0.1 mg/mL streptomycin (Gibco, 15140-122). These cells were split at 80% confluence and plated at a density of 20% following standard cell culture procedures. Ratiometric images were collected with a NIS-Elements AR software using a Yokogawa spinning disk confocal on a Nikon Eclipse-TI inverted microscope. FAM, Cy3, and Cy5 fluorophores were respectively excited with a 488 nm, 561 nm, and 641 laser line. 60× oil immersion objective was used. Raw data was then further processed using the Origin and GraphPad Prism software.

4.4.3 Synthesis of Protein G-modified DNA strands:

The Protein G-modified DNA ligand strand was synthesized by mixing 20 μL of DNA ligand strand (200 μM) with 10 μL of 100 mM TCEP in DPBS buffer containing 50 mM EDTA at pH 7.2. After 2 h incubation at room temperature to reduce the disulfide bond, excess TCEP was removed using a Bio-Spin 6 column (Bio-Rad). Then, 1.5 μL of 23 mM freshly prepared sulfo-SMCC was immediately added and incubated at room temperature for 1 min. Afterwards, 10 μL of 5 mg/mL Protein G was added and incubated at 4 °C for overnight. The synthesized Protein G-DNA conjugates were then purified with cobalt-based Dynabeads (Invitrogen, 10103D) through their specific interaction with poly-histidine-tagged proteins. Isolated his-tagged proteins are further eluted from the beads with histidine elution buffer. After exchanging and concentrating the sample into a DPBS buffer, the concentrations of Protein G-modified DNA strands were quantified with a Nanodrop One UV/Vis spectrometer.

4.4.4 Preparation of the CD40L-DNAMeter:

To prepare the CD40L-DNAMeter, 10 μM anchor strand and hairpin strand was first mixed in a DPBS buffer (Gibco, 14190-144) at pH 7.0–7.3. The mixture was then denatured for 5 min at 75 $^{\circ}\text{C}$ and slowly annealed back to the room temperature at a rate of 1.3 $^{\circ}\text{C}/\text{min}$ in an Eppendorf Thermomixer. Afterwards, the solution was incubated with the Protein G-modified ligand strand at 1:1 ratio at 4 $^{\circ}\text{C}$ for overnight. This assembly was then mixed with equimolar of IgG/Fc-fused human CD40 ligand (Acro biosystems, CDL-H5269) at room temperature for 15 min and kept at 4 $^{\circ}\text{C}$ for overnight before usage.

4.4.5 Imaging intercellular tensile forces:

For imaging CD40-mediated tensile forces, $\sim 20,000$ Jurkat cells were seeded and 2.5 μM of cell tracker (Molecular probes, C2110) was added and incubated for 45 min at room temperature in an 8-well chamber cover glass system (Cellvis). It was then centrifuged at room temperature for 5 min at 300 rpm. This was followed by removal of the dye, and it was washed once more with DPBS. After washing, CD40L-DNAMeter (100 nM) was added to the cells and incubated at room temperature for 30 min, followed by the centrifugation of the cells at room temperature for 5 min at 300 rpm. The cells were again washed with DPBS followed by the centrifugation. Finally, the LY-3 or WSU cells ($\sim 20,000$) in DPBS were added to the Jurkat cells, again centrifuged at room temperature for 5 min at 300 rpm and then the imaging was performed. For the locking strand experiment, 1 μM of locking strand was added after the last centrifugation.

Table 4.1 – DNA sequences used for this chapter

Name	DNA sequence (5' - 3')
Hairpin strand - 1 (22% GC)	CCC GTG AAA TAC CGC ACA GAT GCG TTT <u>GTA TAA ATG TTT TTT TCA TTT ATA CTT TAA</u> GAG CGC CAC GTA GCC CAG C
Reference hairpin strand - 1 (22% GC)	Cy5-TCG AAG CAA GTG TGA GGA CTC TTT <u>GTA TAA ATG TTT TTT TCA TTT ATA CTT TGC</u> TGG GCT ACG TGG CGC TCT T
Ligand strand - 1	HS-TTT GCT GGG CTA CGT GGC GCT CTT-FAM
Anchor strand - 1	Eclipse-CGC ATC TGT GCG GTA TTT CAC CCC- Cholesterol
nqAnchor strand - 1	CGC ATC TGT GCG GTA TTT CAC CCC- Cholesterol
Hairpin strand - 2 (22% GC)	TCG AAG CAA GTG TGA GGA CTC TTT <u>GTA</u> <u>TAA ATG TTT TTT TCA TTT ATA CTT TGC TGG</u> GCT ACG TGG CGC TCT T
Reference hairpin strand - 2 (22% GC)	Cy5-TCG AAG CAA GTG TGA GGA CTC TTT <u>GTA TAA ATG TTT TTT TCA TTT ATA CTT TGC</u> TGG GCT ACG TGG CGC TCT T
Ligand strand - 2	Cy3-GAG TCC TCA CAC TTG CTT CGA TTT-SH
Anchor strand - 2	Cholesterol-CCC AAG AGC GCC ACG TAG CCC AGC-BHQ2
nqAnchor strand - 2	Cholesterol-CCC AAG AGC GCC ACG TAG CCC AGC
Locking strand	GAA AAA AAC ATT TAT AC

Underlined sequences indicate the stem and loop region of the force-sensing DNA hairpin module.

4.5 References

1. Phan, T. G.; Grigorova, I.; Okada, T.; Cyster, J. G., Subcapsular encounter and complement-dependent transport of immune complexes by lymph node B cells. *Nat Immunol* **2007**, 8 (9), 992-1000.
2. Burger, J. A.; Wiestner, A., Targeting B cell receptor signalling in cancer: preclinical and clinical advances. *Nat Rev Cancer* **2018**, 18 (3), 148-167.

3. Woyach, J. A.; Johnson, A. J.; Byrd, J. C., The B-cell receptor signaling pathway as a therapeutic target in CLL. *Blood* **2012**, *120* (6), 1175-84.
4. Hauser, A. E.; Junt, T.; Mempel, T. R.; Sneddon, M. W.; Kleinstein, S. H.; Henrickson, S. E.; von Andrian, U. H.; Shlomchik, M. J.; Haberman, A. M., Definition of germinal-center B cell migration in vivo reveals predominant intrazonal circulation patterns. *Immunity* **2007**, *26* (5), 655-67.
5. Schwickert, T. A.; Lindquist, R. L.; Shakhar, G.; Livshits, G.; Skokos, D.; Kosco-Vilbois, M. H.; Dustin, M. L.; Nussenzweig, M. C., In vivo imaging of germinal centres reveals a dynamic open structure. *Nature* **2007**, *446* (7131), 83-7.
6. Nowosad, C. R.; Spillane, K. M.; Tolar, P., Germinal center B cells recognize antigen through a specialized immune synapse architecture. *Nat Immunol* **2016**, *17* (7), 870-7.
7. Tolar, P., Cytoskeletal control of B cell responses to antigens. *Nat Rev Immunol* **2017**, *17* (10), 621-634.
8. Basso, K.; Klein, U.; Niu, H.; Stolovitzky, G. A.; Tu, Y.; Califano, A.; Cattoretti, G.; Dalla-Favera, R., Tracking CD40 signaling during germinal center development. *Blood* **2004**, *104* (13), 4088-96.
9. Danese, S.; Sans, M.; Fiocchi, C., The CD40/CD40L costimulatory pathway in inflammatory bowel disease. *Gut* **2004**, *53* (7), 1035-43.
10. Senhaji, N.; Kojok, K.; Darif, Y.; Fadainia, C.; Zaid, Y., The Contribution of CD40/CD40L Axis in Inflammatory Bowel Disease: An Update. *Front Immunol* **2015**, *6*, 529.

11. Karnell, J. L.; Rieder, S. A.; Ettinger, R.; Kolbeck, R., Targeting the CD40-CD40L pathway in autoimmune diseases: Humoral immunity and beyond. *Adv Drug Deliv Rev* **2019**, *141*, 92-103.
12. Pype, S.; Declercq, W.; Ibrahimi, A.; Michiels, C.; Van Rietschoten, J. G.; Dewulf, N.; de Boer, M.; Vandenabeele, P.; Huylebroeck, D.; Remacle, J. E., TTRAP, a novel protein that associates with CD40, tumor necrosis factor (TNF) receptor-75 and TNF receptor-associated factors (TRAFs), and that inhibits nuclear factor-kappa B activation. *J Biol Chem* **2000**, *275* (24), 18586-93.
13. Ochando, J.; Braza, M. S., T follicular helper cells: a potential therapeutic target in follicular lymphoma. *Oncotarget* **2017**, *8* (67), 112116-112131.
14. Sokurenko, E. V.; Vogel, V.; Thomas, W. E., Catch-bond mechanism of force-enhanced adhesion: counterintuitive, elusive, but ... widespread? *Cell Host Microbe* **2008**, *4* (4), 314-23.
15. Elgueta, R.; Benson, M. J.; de Vries, V. C.; Wasiuk, A.; Guo, Y.; Noelle, R. J., Molecular mechanism and function of CD40/CD40L engagement in the immune system. *Immunol Rev* **2009**, *229* (1), 152-72.
16. Zha, Y.; Marks, R.; Ho, A. W.; Peterson, A. C.; Janardhan, S.; Brown, I.; Praveen, K.; Stang, S.; Stone, J. C.; Gajewski, T. F., T cell anergy is reversed by active Ras and is regulated by diacylglycerol kinase- α . *Nat Immunol* **2006**, *7* (11), 1166-73.
17. Ma, R.; Kellner, A. V.; Ma, V. P.; Su, H.; Deal, B. R.; Brockman, J. M.; Salaita, K., DNA probes that store mechanical information reveal transient piconewton forces applied by T cells. *Proc Natl Acad Sci U S A* **2019**, *116* (34), 16949-16954.

18. Buhtoiarov, I. N.; Lum, H.; Berke, G.; Paulnock, D. M.; Sondel, P. M.; Rakhmievich, A. L., CD40 ligation activates murine macrophages via an IFN-gamma-dependent mechanism resulting in tumor cell destruction in vitro. *J Immunol* **2005**, *174* (10), 6013-22.

CHAPTER 5

SUMMARY AND FUTURE DIRECTIONS

This chapter is partially adapted with permission from Keshri, P.; Zhao, B.; Xie, T.; Bagheri, Y.; Chambers, J.; Sun, Y.; and You, M. Quantitative and Multiplexed Fluorescence Lifetime Imaging of Intercellular Tensile Forces. *Angew. Chem. Int. Ed.*, 2021, 60, 15548-15555 © Copyright Wiley-VCH on behalf of the German Chemical Society 2021.

5.1 Summary and future directions of DNA-based tension probes

Mechanical forces play important roles in cell biology and their dysregulation is known to be responsible for diseases, such as atherosclerosis, cancer, heart failure, etc¹⁻³. DNA-based membrane tension probes have allowed us to study the involvement of mechanical forces at intercellular junctions in details⁴⁻⁶. The design of the probe is quite simple and can be modulated by selecting the proper ligand moieties, DNA sequences, and fluorophores.

Lipid-mediated cell membrane insertion of the probe is fast and efficient, which can also be used for many different cell lines⁷. The quantitative nature of the DNAMeter probe allows us to easily calculate the extent and distribution of forces in various intercellular signaling processes⁵. On the other hand, FLIM-MDTP provides us a fluorescence lifetime-based approach to image and quantify intercellular molecular tensions as shown in Chapter 2⁶. Meanwhile, using this FLIM-MDTP method, tensile forces among multiple ligand-receptor pairs can be measured simultaneously. In addition,

these lipid-DNA probes are biocompatible and biodegradable, resulting in negligible impact on the natural cellular functions. These advanced features make DNA-based tension probes a great tool to study intercellular mechanotransduction.

Despite the recent advances in this field, there are still a few limitations preventing real broad applications of the probe. Firstly, membrane-anchored lipid-DNA probes are known to be prone to internalization due to endocytosis. As a result, these probes are stable on the membrane for only a few hours. This is a key limitation, for example during our study of the mechanical properties of Notch activation in Chapter 3, we must ensure that all the studies are conducted within a relatively short time ly-window. One of the possible solutions for increasing the membrane persistence of the probe is to fine-tune the hydrophobicity or the number of anchoring lipids⁷. The geometry of DNA nanostructures can also affect the rate of endocytosis and be used to increase the membrane persistence of the probes⁸.

The second challenge is the lack of cell selectivity in the modification of the probes. The universal presence of lipid molecules in different cell membranes makes it less specific in a cell mixture. As a potential solution, with the help of aptamers or antibodies that can target specific cell surface biomarkers, the cell selectivity of the MDTP may be possibly improved. As demonstrated in a recent study, the overexpression of certain enzymes on the cell membranes can also be used to induce specific lipid-DNA probe insertion⁹.

Another current challenge in applying MDTP is to measure forces larger than 20 pN¹⁰. The limited threshold unfolding force of DNA hairpins have constrained the range of potential tensile force measurement¹¹. Our vision is that the use of tension gauge tether design¹² or highly ordered DNA nanostructures, such as G-quadruplex and DNA origami,

can be a potential solution for visualizing forces in the larger range¹³. On the other hand, it is also challenging to visualize weak tensions (forces below 2 pN) with the current design of DNA hairpins. In this regard, we can focus on the structures where elastic linkers can be used and have small energy difference between the closed and the open state. Recently, it has been shown that forces in the range of 1–6 pN can be measured with peptide-based elastic linkers¹⁴. Meanwhile, the future engineering of these membrane-anchored DNA nanostructures may also facilitate the measurement of forces other than tension, such as the compression forces between neighboring cells.

So far, MDTP or DNAMeter has not yet been used to measure forces in a three-dimensional multilayered system such as tissues or organisms. The real world or in vivo applications of these probes will likely face some additional challenges. However, DNA-based tension probes indeed hold great promise for exploring the underlying forces involved in these complicated cell systems. They present us a new picture of intercellular communications where mechanical stimuli function as one of the deciding elements.

5.2 References

1. Salameh, A.; Dhein, S., Effects of mechanical forces and stretch on intercellular gap junction coupling. *Biochim Biophys Acta* **2013**, *1828* (1), 147-56.
2. Granados-Riveron, J. T.; Brook, J. D., The impact of mechanical forces in heart morphogenesis. *Circ Cardiovasc Genet* **2012**, *5* (1), 132-42.
3. Jain, R. K.; Martin, J. D.; Stylianopoulos, T., The role of mechanical forces in tumor growth and therapy. *Annu Rev Biomed Eng* **2014**, *16*, 321-46.

4. Zhao, B.; O'Brien, C.; Mudiyansele, A.; Li, N.; Bagheri, Y.; Wu, R.; Sun, Y.; You, M., Visualizing Intercellular Tensile Forces by DNA-Based Membrane Molecular Probes. *J Am Chem Soc* **2017**, *139* (50), 18182-18185.
5. Zhao, B.; Li, N.; Xie, T.; Bagheri, Y.; Liang, C.; Keshri, P.; Sun, Y.; You, M., Quantifying tensile forces at cell-cell junctions with a DNA-based fluorescent probe. *Chem Sci* **2020**, *11* (32), 8558-8566.
6. Keshri, P.; Zhao, B.; Xie, T.; Bagheri, Y.; Chambers, J.; Sun, Y.; You, M., Quantitative and Multiplexed Fluorescence Lifetime Imaging of Intercellular Tensile Forces. *Angew Chem Int Ed Engl* **2021**, *60* (28), 15548-15555.
7. Bagheri, Y.; Chedid, S.; Shafiei, F.; Zhao, B.; You, M., A quantitative assessment of the dynamic modification of lipid-DNA probes on live cell membranes. *Chem Sci* **2019**, *10* (48), 11030-11040.
8. Li, J.; Xun, K.; Pei, K.; Liu, X.; Peng, X.; Du, Y.; Qiu, L.; Tan, W., Cell-Membrane-Anchored DNA NanoplatforM for Programming Cellular Interactions. *J Am Chem Soc* **2019**, *141* (45), 18013-18020.
9. Jin, C.; He, J.; Zou, J.; Xuan, W.; Fu, T.; Wang, R.; Tan, W., Phosphorylated lipid-conjugated oligonucleotide selectively anchors on cell membranes with high alkaline phosphatase expression. *Nat Commun* **2019**, *10* (1), 2704.
10. Liu, Y.; Galior, K.; Ma, V. P.; Salaita, K., Molecular Tension Probes for Imaging Forces at the Cell Surface. *Acc Chem Res* **2017**, *50* (12), 2915-2924.
11. Ma, V. P.; Salaita, K., DNA Nanotechnology as an Emerging Tool to Study Mechanotransduction in Living Systems. *Small* **2019**, *15* (26), e1900961.

12. Wang, X.; Ha, T., Defining single molecular forces required to activate integrin and notch signaling. *Science* **2013**, *340* (6135), 991-4.
13. Feng, G.; Luo, X.; Lu, X.; Xie, S.; Deng, L.; Kang, W.; He, F.; Zhang, J.; Lei, C.; Lin, B.; Huang, Y.; Nie, Z.; Yao, S., Engineering of Nucleic Acids and Synthetic Cofactors as Holo Sensors for Probing Signaling Molecules in the Cellular Membrane Microenvironment. *Angew Chem Int Ed Engl* **2019**, *58* (20), 6590-6594.
14. Grashoff, C.; Hoffman, B. D.; Brenner, M. D.; Zhou, R.; Parsons, M.; Yang, M. T.; McLean, M. A.; Sliagar, S. G.; Chen, C. S.; Ha, T.; Schwartz, M. A., Measuring mechanical tension across vinculin reveals regulation of focal adhesion dynamics. *Nature* **2010**, *466* (7303), 263-6.

BIBLIOGRAPHY

Alimperti, S.; Andreadis, S. T., CDH2 and CDH11 act as regulators of stem cell fate decisions. *Stem Cell Res* **2015**, *14* (3), 270-82.

Artemenko, Y.; Axiotakis, L., Jr.; Borleis, J.; Iglesias, P. A.; Devreotes, P. N., Chemical and mechanical stimuli act on common signal transduction and cytoskeletal networks. *Proc Natl Acad Sci U S A* **2016**, *113* (47), E7500-E7509.

Bagheri, Y.; Chedid, S.; Shafiei, F.; Zhao, B.; You, M., A quantitative assessment of the dynamic modification of lipid-DNA probes on live cell membranes. *Chem Sci* **2019**, *10* (48), 11030-11040.

Basso, K.; Klein, U.; Niu, H.; Stolovitzky, G. A.; Tu, Y.; Califano, A.; Cattoretti, G.; Dalla-Favera, R., Tracking CD40 signaling during germinal center development. *Blood* **2004**, *104* (13), 4088-96.

Bell, E.; Ivarsson, B.; Merrill, C., Production of a tissue-like structure by contraction of collagen lattices by human fibroblasts of different proliferative potential in vitro. *Proc Natl Acad Sci U S A* **1979**, *76* (3), 1274-8.

Borghini, N.; Sorokina, M.; Shcherbakova, O. G.; Weis, W. I.; Pruitt, B. L.; Nelson, W. J.; Dunn, A. R., E-cadherin is under constitutive actomyosin-generated tension that is increased at cell-cell contacts upon externally applied stretch. *Proc Natl Acad Sci U S A* **2012**, *109* (31), 12568-73.

Bray, S. J., Notch signalling in context. *Nat Rev Mol Cell Biol* **2016**, *17* (11), 722-735.

Buhtoiarov, I. N.; Lum, H.; Berke, G.; Paulnock, D. M.; Sondel, P. M.; Rakhmilevich, A. L., CD40 ligation activates murine macrophages via an IFN-gamma-dependent mechanism resulting in tumor cell destruction in vitro. *J Immunol* **2005**, *174* (10), 6013-22.

Burger, J. A.; Wiestner, A., Targeting B cell receptor signalling in cancer: preclinical and clinical advances. *Nat Rev Cancer* **2018**, *18* (3), 148-167.

Canel, M.; Serrels, A.; Frame, M. C.; Brunton, V. G., E-cadherin-integrin crosstalk in cancer invasion and metastasis. *J Cell Sci* **2013**, *126* (Pt 2), 393-401.

Chappuis-Flament, S.; Wong, E.; Hicks, L. D.; Kay, C. M.; Gumbiner, B. M., Multiple cadherin extracellular repeats mediate homophilic binding and adhesion. *J Cell Biol* **2001**, *154* (1), 231-43

Charras, G.; Yap, A. S., Tensile Forces and Mechanotransduction at Cell-Cell Junctions. *Curr Biol* **2018**, *28* (8), R445-R457.

Chen, C. S.; Tan, J.; Tien, J., Mechanotransduction at cell-matrix and cell-cell contacts. *Annu Rev Biomed Eng* **2004**, *6*, 275-302.

Chowdhury, F.; Li, I. T.; Ngo, T. T.; Leslie, B. J.; Kim, B. C.; Sokoloski, J. E.; Weiland, E.; Wang, X.; Chemla, Y. R.; Lohman, T. M.; Ha, T., Defining Single Molecular Forces Required for Notch Activation Using Nano Yoyo. *Nano Lett* **2016**, *16* (6), 3892-7.

Cohen, N.; Sarkar, S.; Hondroulis, E.; Sabhachandani, P.; Konry, T., Quantification of intercellular adhesion forces measured by fluid force microscopy. *Talanta* **2017**, *174*, 409-413.

Conway, D. E.; Breckenridge, M. T.; Hinde, E.; Gratton, E.; Chen, C. S.; Schwartz, M. A., Fluid shear stress on endothelial cells modulates mechanical tension across VE-cadherin and PECAM-1. *Curr Biol* **2013**, *23* (11), 1024-30.

Dan, K.; Veetil, A. T.; Chakraborty, K.; Krishnan, Y., DNA nanodevices map enzymatic activity in organelles. *Nat Nanotechnol* **2019**, *14* (3), 252-259.

Danese, S.; Sans, M.; Fiocchi, C., The CD40/CD40L costimulatory pathway in inflammatory bowel disease. *Gut* **2004**, *53* (7), 1035-43.

Datta, R.; Heaster, T. M.; Sharick, J. T.; Gillette, A. A.; Skala, M. C., Fluorescence lifetime imaging microscopy: fundamentals and advances in instrumentation, analysis, and applications. *J Biomed Opt* **2020**, *25* (7), 1-43.

Dongre, A.; Rashidian, M.; Reinhardt, F.; Bagnato, A.; Keckesova, Z.; Ploegh, H. L.; Weinberg, R. A., Epithelial-to-Mesenchymal Transition Contributes to Immunosuppression in Breast Carcinomas. *Cancer Res* **2017**, *77* (15), 3982-3989.

D'Souza, B.; Miyamoto, A.; Weinmaster, G., The many facets of Notch ligands. *Oncogene* **2008**, *27* (38), 5148-67

Elgueta, R.; Benson, M. J.; de Vries, V. C.; Wasiuk, A.; Guo, Y.; Noelle, R. J., Molecular mechanism and function of CD40/CD40L engagement in the immune system. *Immunol Rev* **2009**, *229* (1), 152-72.

Feng, G.; Luo, X.; Lu, X.; Xie, S.; Deng, L.; Kang, W.; He, F.; Zhang, J.; Lei, C.; Lin, B.; Huang, Y.; Nie, Z.; Yao, S., Engineering of Nucleic Acids and Synthetic Cofactors as Holo Sensors for Probing Signaling Molecules in the Cellular Membrane Microenvironment. *Angew Chem Int Ed Engl* **2019**, *58* (20), 6590-6594.

Glazier, R.; Brockman, J. M.; Bartle, E.; Mattheyses, A. L.; Destaing, O.; Salaita, K., DNA mechanotechnology reveals that integrin receptors apply pN forces in podosomes on fluid substrates. *Nat Commun* **2019**, *10* (1), 4507.

Gordon, W. R.; Zimmerman, B.; He, L.; Miles, L. J.; Huang, J.; Tiyanont, K.; McArthur, D. G.; Aster, J. C.; Perrimon, N.; Loparo, J. J.; Blacklow, S. C., Mechanical Allostery: Evidence for a Force Requirement in the Proteolytic Activation of Notch. *Dev Cell* **2015**, *33* (6), 729-36.

Gordon, W. R.; Vardar-Ulu, D.; Histen, G.; Sanchez-Irizarry, C.; Aster, J. C.; Blacklow, S. C., Structural basis for autoinhibition of Notch. *Nat Struct Mol Biol* **2007**, *14* (4), 295-300.

Granados-Riveron, J. T.; Brook, J. D., The impact of mechanical forces in heart morphogenesis. *Circ Cardiovasc Genet* **2012**, *5* (1), 132-42.

Grashoff, C.; Hoffman, B. D.; Brenner, M. D.; Zhou, R.; Parsons, M.; Yang, M. T.; McLean, M. A.; Sligar, S. G.; Chen, C. S.; Ha, T.; Schwartz, M. A., Measuring mechanical tension across vinculin reveals regulation of focal adhesion dynamics. *Nature* **2010**, *466* (7303), 263-6.

Hauser, A. E.; Junt, T.; Mempel, T. R.; Sneddon, M. W.; Kleinstein, S. H.; Henrickson, S. E.; von Andrian, U. H.; Shlomchik, M. J.; Haberman, A. M., Definition of germinal-center B cell migration in vivo reveals predominant intrazonal circulation patterns. *Immunity* **2007**, *26* (5), 655-67.

Hori, K.; Sen, A.; Artavanis-Tsakonas, S., Notch signaling at a glance. *J Cell Sci* **2013**, *126* (Pt 10), 2135-40.

Iyer, K. V.; Piscitello-Gomez, R.; Paijmans, J.; Julicher, F.; Eaton, S., Epithelial Viscoelasticity Is Regulated by Mechanosensitive E-cadherin Turnover. *Curr Biol* **2019**, *29* (4), 578-591 e5.

Izaguirre, M. F.; Casco, V. H., E-cadherin roles in animal biology: A perspective on thyroid hormone-influence. *Cell Commun Signal* **2016**, *14* (1), 27.

Jain, R. K.; Martin, J. D.; Stylianopoulos, T., The role of mechanical forces in tumor growth and therapy. *Annu Rev Biomed Eng* **2014**, *16*, 321-46.

Jin, C.; He, J.; Zou, J.; Xuan, W.; Fu, T.; Wang, R.; Tan, W., Phosphorylated lipid-conjugated oligonucleotide selectively anchors on cell membranes with high alkaline phosphatase expression. *Nat Commun* **2019**, *10* (1), 2704.

Johansson, M. K., Choosing reporter-quencher pairs for efficient quenching through formation of intramolecular dimers. *Methods Mol Biol* **2006**, *335*, 17-29.

Jurchenko, C.; Salaita, K. S., Lighting Up the Force: Investigating Mechanisms of Mechanotransduction Using Fluorescent Tension Probes. *Mol Cell Biol* **2015**, *35* (15), 2570-82.

Kalluri, R.; Weinberg, R. A., The basics of epithelial-mesenchymal transition. *J Clin Invest* **2009**, *119* (6), 1420-8.

Karnell, J. L.; Rieder, S. A.; Ettinger, R.; Kolbeck, R., Targeting the CD40-CD40L pathway in autoimmune diseases: Humoral immunity and beyond. *Adv Drug Deliv Rev* **2019**, *141*, 92-103.

Keshri, P.; Zhao, B.; Xie, T.; Bagheri, Y.; Chambers, J.; Sun, Y.; You, M., Quantitative and Multiplexed Fluorescence Lifetime Imaging of Intercellular Tensile Forces. *Angew Chem Int Ed Engl* **2021**, *60* (28), 15548-15555.

Kim, M. C.; Cui, F. J.; Kim, Y., Hydrogen peroxide promotes epithelial to mesenchymal transition and stemness in human malignant mesothelioma cells. *Asian Pac J Cancer Prev* **2013**, *14* (6), 3625-30.

Kopan, R.; Chen, S.; Liu, Z., Alagille, Notch, and robustness: why duplicating systems does not ensure redundancy. *Pediatr Nephrol* **2014**, *29* (4), 651-7.

Kopan, R.; Ilagan, M. X., The canonical Notch signaling pathway: unfolding the activation mechanism. *Cell* **2009**, *137* (2), 216-33.

Krishnan, Y.; Zou, J.; Jani, M. S., Quantitative Imaging of Biochemistry in Situ and at the Nanoscale. *ACS Cent Sci* **2020**, *6* (11), 1938-1954.

Leckband, D. E.; de Rooij, J., Cadherin adhesion and mechanotransduction. *Annu Rev Cell Dev Biol* **2014**, *30*, 291-315.

Legant, W. R.; Choi, C. K.; Miller, J. S.; Shao, L.; Gao, L.; Betzig, E.; Chen, C. S., Multidimensional traction force microscopy reveals out-of-plane rotational moments about focal adhesions. *Proc Natl Acad Sci U S A* **2013**, *110* (3), 881-6.

Legant, W. R.; Pathak, A.; Yang, M. T.; Deshpande, V. S.; McMeeking, R. M.; Chen, C. S., Microfabricated tissue gauges to measure and manipulate forces from 3D microtissues. *Proc Natl Acad Sci U S A* **2009**, *106* (25), 10097-102.

Li, J.; Xun, K.; Pei, K.; Liu, X.; Peng, X.; Du, Y.; Qiu, L.; Tan, W., Cell-Membrane-Anchored DNA Nanoplatfrom for Programming Cellular Interactions. *J Am Chem Soc* **2019**, *141* (45), 18013-18020.

Lin, W. C.; Yu, C. H.; Triffo, S.; Groves, J. T., Supported membrane formation, characterization, functionalization, and patterning for application in biological science and technology. *Curr Protoc Chem Biol* **2010**, *2* (4), 235-69.

Liu, Y.; Galior, K.; Ma, V. P.; Salaita, K., Molecular Tension Probes for Imaging Forces at the Cell Surface. *Acc Chem Res* **2017**, *50* (12), 2915-2924.

Liu, Z.; Tan, J. L.; Cohen, D. M.; Yang, M. T.; Sniadecki, N. J.; Ruiz, S. A.; Nelson, C. M.; Chen, C. S., Mechanical tugging force regulates the size of cell-cell junctions. *Proc Natl Acad Sci U S A* **2010**, *107* (22), 9944-9.

Loh, C. Y.; Chai, J. Y.; Tang, T. F.; Wong, W. F.; Sethi, G.; Shanmugam, M. K.; Chong, P. P.; Looi, C. Y., The E-Cadherin and N-Cadherin Switch in Epithelial-to-Mesenchymal Transition: Signaling, Therapeutic Implications, and Challenges. *Cells* **2019**, *8* (10).

Ma, V. P.; Salaita, K., DNA Nanotechnology as an Emerging Tool to Study Mechanotransduction in Living Systems. *Small* **2019**, *15* (26), e1900961.

Ma, R.; Kellner, A. V.; Ma, V. P.; Su, H.; Deal, B. R.; Brockman, J. M.; Salaita, K., DNA probes that store mechanical information reveal transient piconewton forces applied by T cells. *Proc Natl Acad Sci U S A* **2019**, *116* (34), 16949-16954.

Maeda, M.; Johnson, K. R.; Wheelock, M. J., Cadherin switching: essential for behavioral but not morphological changes during an epithelium-to-mesenchyme transition. *J Cell Sci* **2005**, *118* (Pt 5), 873-87.

Marracino, L.; Fortini, F.; Bouhamida, E.; Camponogara, F.; Severi, P.; Mazzoni, E.; Patergnani, S.; D'Aniello, E.; Campana, R.; Pinton, P.; Martini, F.; Tognon, M.; Campo, G.; Ferrari, R.; Vieceli Dalla Sega, F.; Rizzo, P., Adding a "Notch" to Cardiovascular Disease Therapeutics: A MicroRNA-Based Approach. *Front Cell Dev Biol* **2021**, *9*, 695114.

Meister, A.; Gabi, M.; Behr, P.; Studer, P.; Voros, J.; Niedermann, P.; Bitterli, J.; Polesel-Maris, J.; Liley, M.; Heinzemann, H.; Zambelli, T., FluidFM: combining atomic force microscopy and nanofluidics in a universal liquid delivery system for single cell applications and beyond. *Nano Lett* **2009**, *9* (6), 2501-7.

Muhamed, I.; Wu, J.; Sehgal, P.; Kong, X.; Tajik, A.; Wang, N.; Leckband, D. E., E-cadherin-mediated force transduction signals regulate global cell mechanics. *J Cell Sci* **2016**, *129* (9), 1843-54.

Nandagopal, N.; Santat, L. A.; LeBon, L.; Sprinzak, D.; Bronner, M. E.; Elowitz, M. B., Dynamic Ligand Discrimination in the Notch Signaling Pathway. *Cell* **2018**, *172* (4), 869-880 e19.

Northcott, J. M.; Dean, I. S.; Mouw, J. K.; Weaver, V. M., Feeling Stress: The Mechanics of Cancer Progression and Aggression. *Front Cell Dev Biol* **2018**, *6*, 17

Nowosad, C. R.; Spillane, K. M.; Tolar, P., Germinal center B cells recognize antigen through a specialized immune synapse architecture. *Nat Immunol* **2016**, *17* (7), 870-7.

Ochando, J.; Braza, M. S., T follicular helper cells: a potential therapeutic target in follicular lymphoma. *Oncotarget* **2017**, *8* (67), 112116-112131.

Ohvo-Rekila, H.; Ramstedt, B.; Leppimaki, P.; Slotte, J. P., Cholesterol interactions with phospholipids in membranes. *Prog Lipid Res* **2002**, *41* (1), 66-97.

Phan, T. G.; Grigorova, I.; Okada, T.; Cyster, J. G., Subcapsular encounter and complement-dependent transport of immune complexes by lymph node B cells. *Nat Immunol* **2007**, *8* (9), 992-1000.

Polacheck, W. J.; Chen, C. S., Measuring cell-generated forces: a guide to the available tools. *Nat Methods* **2016**, *13* (5), 415-23.

Pype, S.; Declercq, W.; Ibrahimi, A.; Michiels, C.; Van Rietschoten, J. G.; Dewulf, N.; de Boer, M.; Vandenabeele, P.; Huylebroeck, D.; Remacle, J. E., TTRAP, a novel protein that associates with CD40, tumor necrosis factor (TNF) receptor-75 and TNF receptor-associated factors (TRAFs), and that inhibits nuclear factor-kappa B activation. *J Biol Chem* **2000**, *275* (24), 18586-93.

Radisky, E. S.; Radisky, D. C., Matrix metalloproteinase-induced epithelial-mesenchymal transition in breast cancer. *J Mammary Gland Biol Neoplasia* **2010**, *15* (2), 201-12.

Ratner, B., The correlation coefficient: Its values range between +1/-1, or do they? *Journal of Targeting, Measurement and Analysis for Marketing* **2009**, *17* (2), 139-142.

Rothen-Rutishauser, B.; Riesen, F. K.; Braun, A.; Gunthert, M.; Wunderli-Allenspach, H., Dynamics of tight and adherens junctions under EGTA treatment. *J Membr Biol* **2002**, *188* (2), 151-62.

Saha, S.; Prakash, V.; Halder, S.; Chakraborty, K.; Krishnan, Y., A pH-independent DNA nanodevice for quantifying chloride transport in organelles of living cells. *Nat Nanotechnol* **2015**, *10* (7), 645-51.

Salameh, A.; Dhein, S., Effects of mechanical forces and stretch on intercellular gap junction coupling. *Biochim Biophys Acta* **2013**, *1828* (1), 147-56.

Sancho, A.; Vandersmissen, I.; Craps, S.; Lutun, A.; Groll, J., A new strategy to measure intercellular adhesion forces in mature cell-cell contacts. *Sci Rep* **2017**, *7*, 46152.

Schwickert, T. A.; Lindquist, R. L.; Shakhar, G.; Livshits, G.; Skokos, D.; Kosco-Vilbois, M. H.; Dustin, M. L.; Nussenzweig, M. C., In vivo imaging of germinal centres reveals a dynamic open structure. *Nature* **2007**, *446* (7131), 83-7.

Senhaji, N.; Kojok, K.; Darif, Y.; Fadainia, C.; Zaid, Y., The Contribution of CD40/CD40L Axis in Inflammatory Bowel Disease: An Update. *Front Immunol* **2015**, *6*, 529.

Shen, W.; Huang, J.; Wang, Y., Biological Significance of NOTCH Signaling Strength. *Front Cell Dev Biol* **2021**, *9*, 652273

Shewan, A. M.; Maddugoda, M.; Kraemer, A.; Stehbens, S. J.; Verma, S.; Kovacs, E. M.; Yap, A. S., Myosin 2 is a key Rho kinase target necessary for the local concentration of E-cadherin at cell-cell contacts. *Mol Biol Cell* **2005**, *16* (10), 4531-42.

Sokurenko, E. V.; Vogel, V.; Thomas, W. E., Catch-bond mechanism of force-enhanced adhesion: counterintuitive, elusive, but ... widespread? *Cell Host Microbe* **2008**, *4* (4), 314-23.

Sprinzak, D.; Lakhanpal, A.; Lebon, L.; Santat, L. A.; Fontes, M. E.; Anderson, G. A.; Garcia-Ojalvo, J.; Elowitz, M. B., Cis-interactions between Notch and Delta generate mutually exclusive signalling states. *Nature* **2010**, *465* (7294), 86-90.

Steinbuck, M. P.; Winandy, S., A Review of Notch Processing With New Insights Into Ligand-Independent Notch Signaling in T-Cells. *Front Immunol* **2018**, *9*, 1230.

Sun, Z.; Guo, S. S.; Fassler, R., Integrin-mediated mechanotransduction. *J Cell Biol* **2016**, *215* (4), 445-456.

Tambe, D. T.; Hardin, C. C.; Angelini, T. E.; Rajendran, K.; Park, C. Y.; Serra-Picamal, X.; Zhou, E. H.; Zaman, M. H.; Butler, J. P.; Weitz, D. A.; Fredberg, J. J.; Trepats, X., Collective cell guidance by cooperative intercellular forces. *Nat Mater* **2011**, *10* (6), 469-75.

Tan, J. L.; Tien, J.; Pirone, D. M.; Gray, D. S.; Bhadriraju, K.; Chen, C. S., Cells lying on a bed of microneedles: an approach to isolate mechanical force. *Proc Natl Acad Sci U S A* **2003**, *100* (4), 1484-9.

Tian, Q.; Bagheri, Y.; Keshri, P.; Wu, R.; Ren, K.; Yu, Q.; Zhao, B.; You, M., Efficient and selective DNA modification on bacterial membranes. *Chem Sci* **2020**, *12* (7), 2629-2634.

Tolar, P., Cytoskeletal control of B cell responses to antigens. *Nat Rev Immunol* **2017**, *17* (10), 621-634.

Wang, X.; Ha, T., Defining single molecular forces required to activate integrin and notch signaling. *Science* **2013**, *340* (6135), 991-4.

Wang, P.; Liang, J.; Shi, L. Z.; Wang, Y.; Zhang, P.; Ouyang, M.; Preece, D.; Peng, Q.; Shao, L.; Fan, J.; Sun, J.; Li, S. S.; Berns, M. W.; Zhao, H.; Wang, Y., Visualizing Spatiotemporal Dynamics of Intercellular Mechanotransmission upon Wounding. *ACS Photonics* **2018**, *5* (9), 3565-3574.

Wheelock, M. J.; Shintani, Y.; Maeda, M.; Fukumoto, Y.; Johnson, K. R., Cadherin switching. *J Cell Sci* **2008**, *121* (Pt 6), 727-35.

Woodside, M. T.; Behnke-Parks, W. M.; Larizadeh, K.; Travers, K.; Herschlag, D.; Block, S. M., Nanomechanical measurements of the sequence-dependent folding landscapes of single nucleic acid hairpins. *Proc Natl Acad Sci U S A* **2006**, *103* (16), 6190-5.

Woyach, J. A.; Johnson, A. J.; Byrd, J. C., The B-cell receptor signaling pathway as a therapeutic target in CLL. *Blood* **2012**, *120* (6), 1175-84.

Xu, J.; Lamouille, S.; Derynck, R., TGF-beta-induced epithelial to mesenchymal transition. *Cell Res* **2009**, *19* (2), 156-72.

Yang, D.; Hartman, M. R.; Derrien, T. L.; Hamada, S.; An, D.; Yancey, K. G.; Cheng, R.; Ma, M.; Luo, D., DNA materials: bridging nanotechnology and biotechnology. *Acc Chem Res* **2014**, *47* (6), 1902-11.

You, M.; Lyu, Y.; Han, D.; Qiu, L.; Liu, Q.; Chen, T.; Sam Wu, C.; Peng, L.; Zhang, L.; Bao, G.; Tan, W., DNA probes for monitoring dynamic and transient molecular encounters on live cell membranes. *Nat Nanotechnol* **2017**, *12* (5), 453-459.

Zha, Y.; Marks, R.; Ho, A. W.; Peterson, A. C.; Janardhan, S.; Brown, I.; Praveen, K.; Stang, S.; Stone, J. C.; Gajewski, T. F., T cell anergy is reversed by active Ras and is regulated by diacylglycerol kinase-alpha. *Nat Immunol* **2006**, *7* (11), 1166-73.

Zhang, Y.; Ge, C.; Zhu, C.; Salaita, K., DNA-based digital tension probes reveal integrin forces during early cell adhesion. *Nat Commun* **2014**, *5*, 5167.

Zhao, B.; Tian, Q.; Bagheri, Y.; You, M., Lipid-Oligonucleotide Conjugates for Simple and Efficient Cell Membrane Engineering and Bioanalysis. *Curr Opin Biomed Eng* **2020**, *13*, 76-83.

Zhao, B.; Li, N.; Xie, T.; Bagheri, Y.; Liang, C.; Keshri, P.; Sun, Y.; You, M., Quantifying tensile forces at cell-cell junctions with a DNA-based fluorescent probe. *Chem Sci* **2020**, *11* (32), 8558-8566.

Zhao, B.; O'Brien, C.; Mudiyansele, A.; Li, N.; Bagheri, Y.; Wu, R.; Sun, Y.; You, M., Visualizing Intercellular Tensile Forces by DNA-Based Membrane Molecular Probes. *J Am Chem Soc* **2017**, *139* (50), 18182-18185.